Supplementary Information

Pathogens and host immunity in the ancient human oral cavity

Christina Warinner, João F. Matias Rodrigues, Rounak Vyas, Christian Trachsel, Natallia Shved, Jonas Grossmann, Anita Radini, Y. Hancock, Raul Y. Tito, Sarah Fiddyment, Camilla Speller, Jessica Hendy, Sophy Charlton, Hans Ulrich Luder, Domingo C. Salazar-García, Elisabeth Eppler, Roger Seiler, Lars Hansen, José Alfredo Samaniego Castruita, Simon Barkow-Oesterreicher, Kai Yik Teoh, Christian Kelstrup, Jesper V. Olsen, Paolo Nanni, Toshihisa Kawai, Eske Willerslev, Christian von Mering, Cecil M. Lewis, Jr., Matthew J. Collins, M. Thomas P. Gilbert, Frank Rühli, Enrico Cappellini

SI correspondence to:
twarinner@gmail.com, ecappellini@gmail.com, matthew.collins@york.ac.uk

I. Supplementary Figures

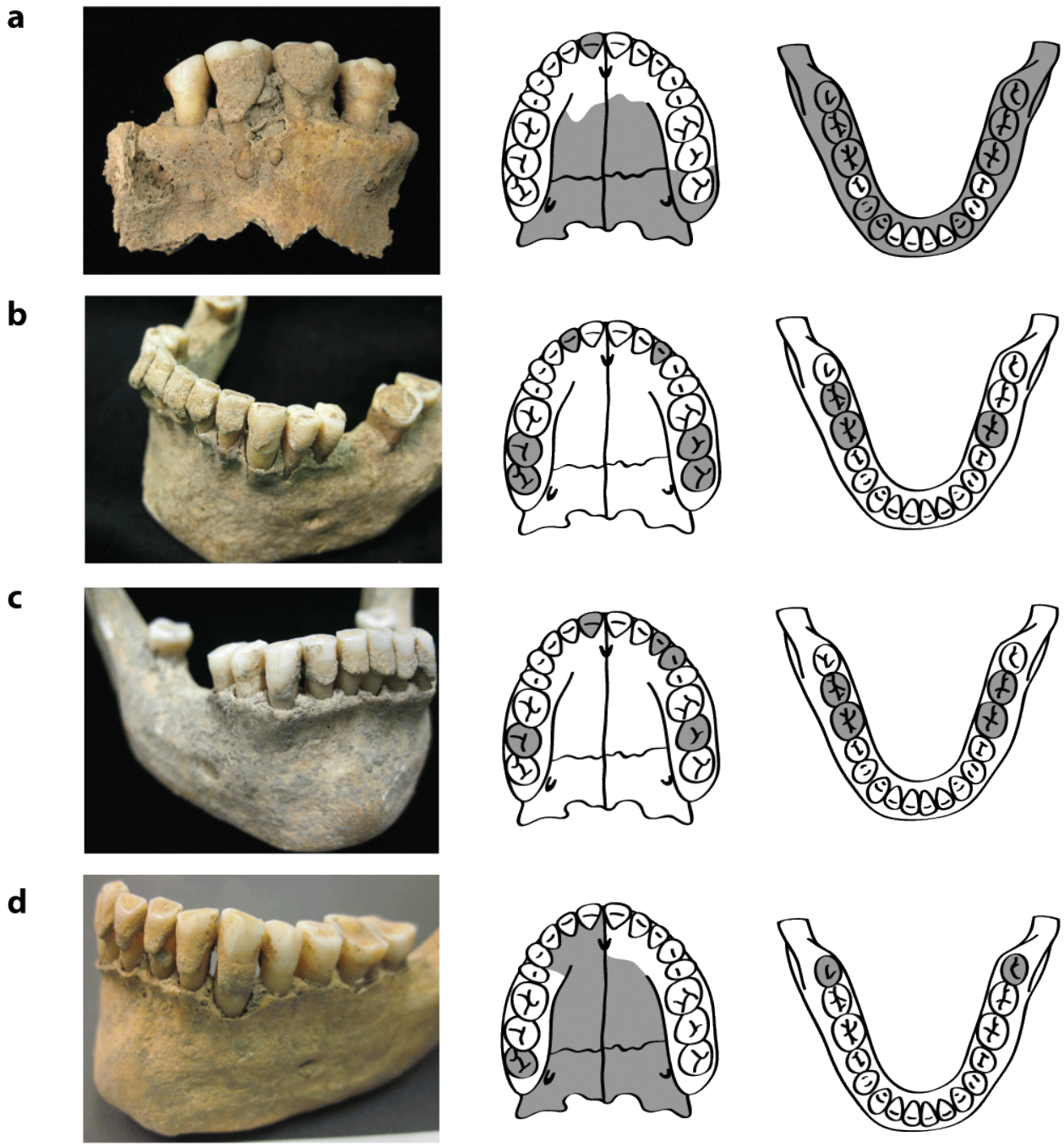

Supplementary Figure 1 | Dalheim human dental material from individuals (**a**) B17, (**b**) B61, (**c**) B78, and (**d**) G12. Gray shading indicates material lost *intra vitam* or which was otherwise not recovered during excavation.

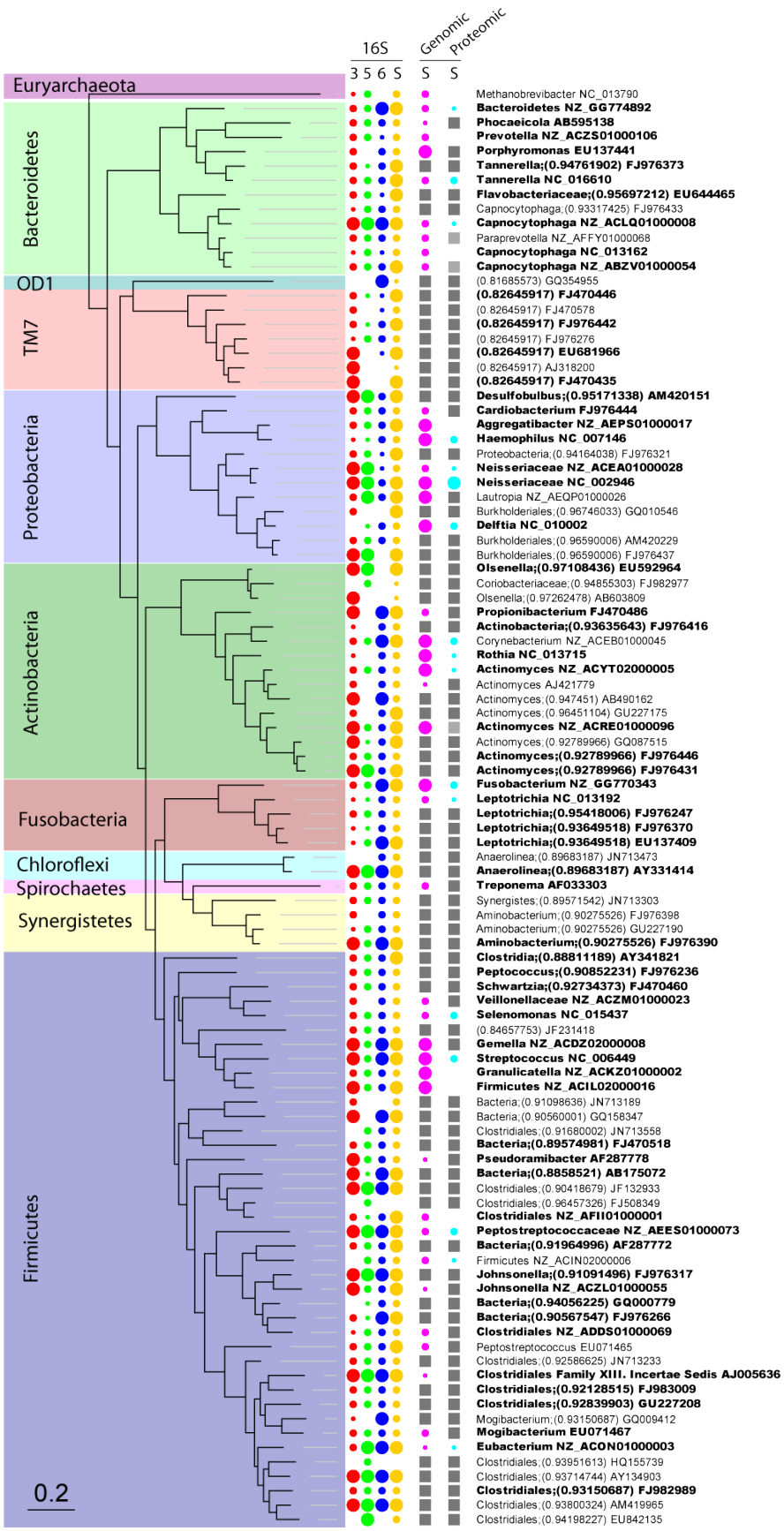

Supplementary Figure 2 | Phylogenetic tree of the 100 most abundant OTUs in ancient dental calculus samples, pooled from four individuals (from Fig. 1b, enhanced view). Evidence for the presence and abundance of each microbial OTU is represented by colored, size-scaled circles for each targeted 16S rRNA variable region (3, 5, 6), shotgun (S) 16S rRNA sequences, and for other shotgun (S) genomic and proteomic sequences assigned to that OTU. OTUs for which no reference genome exists or which were not included in search databases are marked with a gray square. Labels on the tree show the lowest consensual rank at which taxonomy was consensual for all sequences in the OTU, as well as a representative genome accession. In OTUs where taxonomy was inferred due to lack of sequences with reliable taxonomy, the clustering threshold at which point sequences with reliable taxonomy were merged and used for inference is shown in parentheses. Bold labels indicate that at least one of the sequences in the OTU is included in the HOMD.

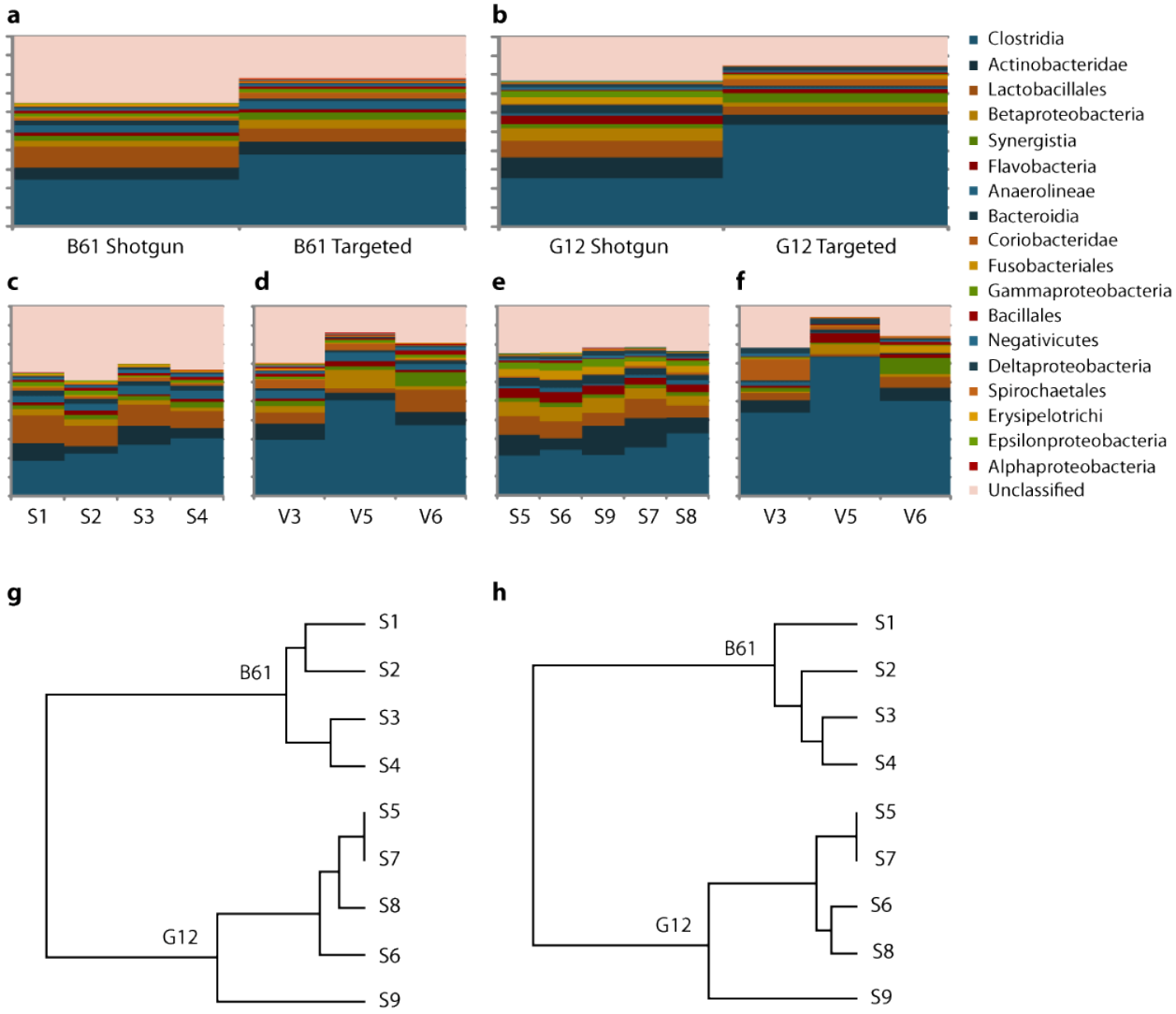

Supplementary Figure 3 | Analysis of biases introduced during decontamination, extraction, primer selection, and sequencing. Comparison of 16S rRNA OTU frequency distributions at the level of Class as a function of sequencing method for (**a**) B61 and (**b**) G12. Frequency distributions broken down by (**c, e**) shotgun library and (**d, f**) targeted 16S rRNA variable region for (**c, d**) B61 and (**e, f**) G12. Taxonomic frequency differences are observed between shotgun and targeted (amplicon) approaches. Greater variability is observed associated with 16S rRNA variable region and primer selection than with decontamination or extraction method. For clarity, only Classes present at ≥0.1% are shown. UPGMA phenograms were generated from (**g**) non-normalized and (**h**) normalized taxonomic data generated for B61 and G12 shotgun DNA libraries. Although a clear difference is observed between individuals, no consistent pattern is observed with respect to decontamination method or extraction method. One exception is the "contamination" library S9, which consistently clusters apart from the other G12 samples, suggesting that the surface layer of calculus contains a biased subset of bacterial taxa compared to calculus as a whole.

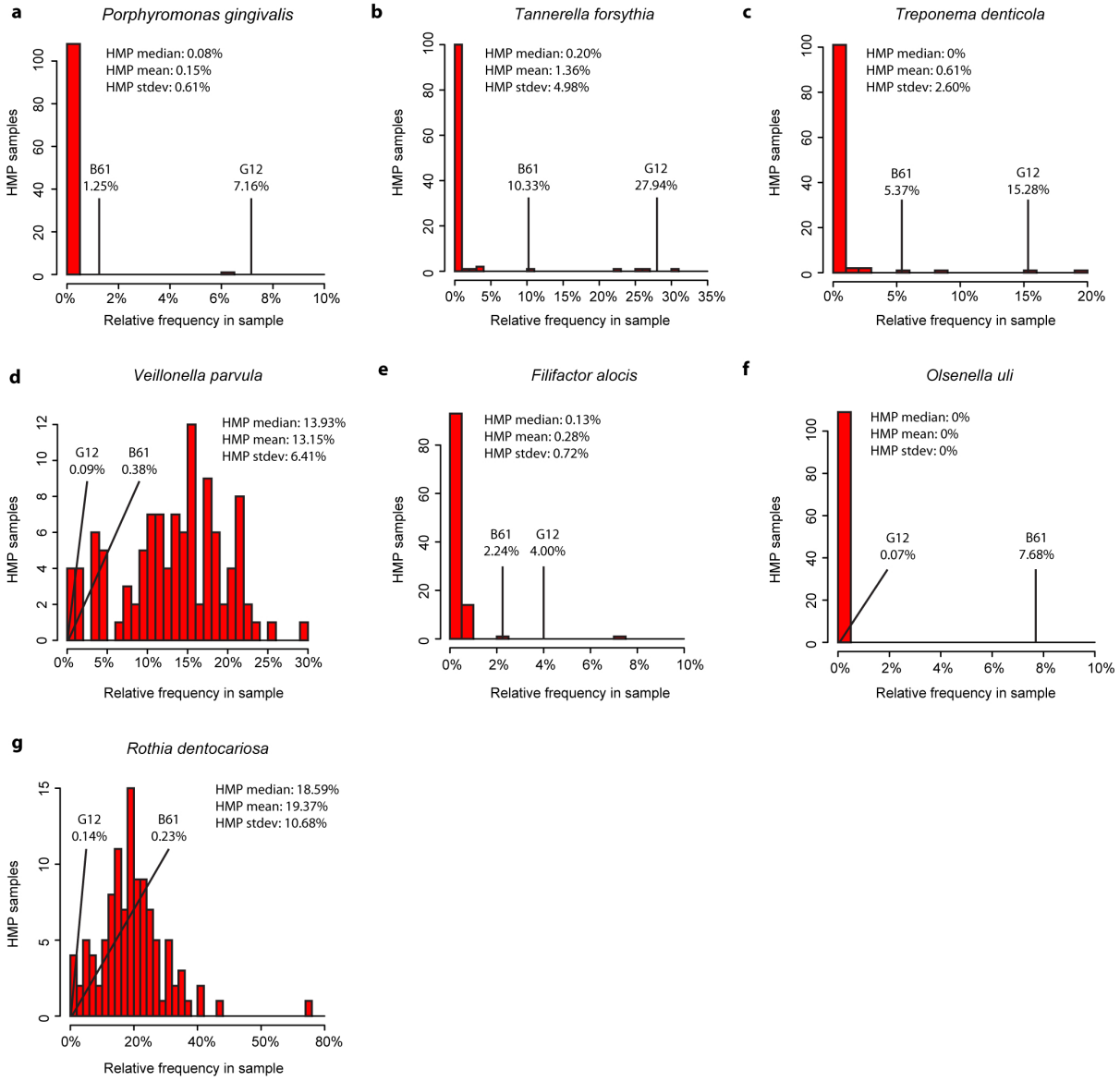

Supplementary Figure 4 | Taxa with strongly discordant relative frequencies in G12 and B61 ancient dental calculus compared to HMP healthy cohort dental plaque. Histograms depict the frequency distribution of selected PATRIC pathogens (**a-d**) and PATRIC non-pathogens (**e-g**) identified in shotgun metagenomic data from supragingival dental plaque of the HMP healthy cohort (red, n=109) compared to the frequency of the same taxa in G12 and B61 ancient dental calculus; bin sizes: 0.5% (a, e, f), 1% (b, c, d), and 2% (g). The relative frequency of the periodontal pathogens *P. gingivalis*, *T. forsythia*, and *T. denticola*, as well as the recently identified putative periodontal pathogen *F. alocis*, is higher in G12 and B61 dental calculus than in >95% of HMP healthy dental plaque samples; this observation is consistent osteological and proteomic evidence of periodontal disease in G12 and B61. The relative frequency of *O. uli*, a recently identified putative endodontic pathogen, is higher in B61 dental calculus compared to G12 and 100% of the HMP healthy cohort samples. The relative frequencies of *V. parvula*, an opportunistic pathogen that causes rare infections, and *R. dentocariosa*, an oral commensal, are lower in G12 and B61 dental calculus than in 97% the HMP healthy cohort.

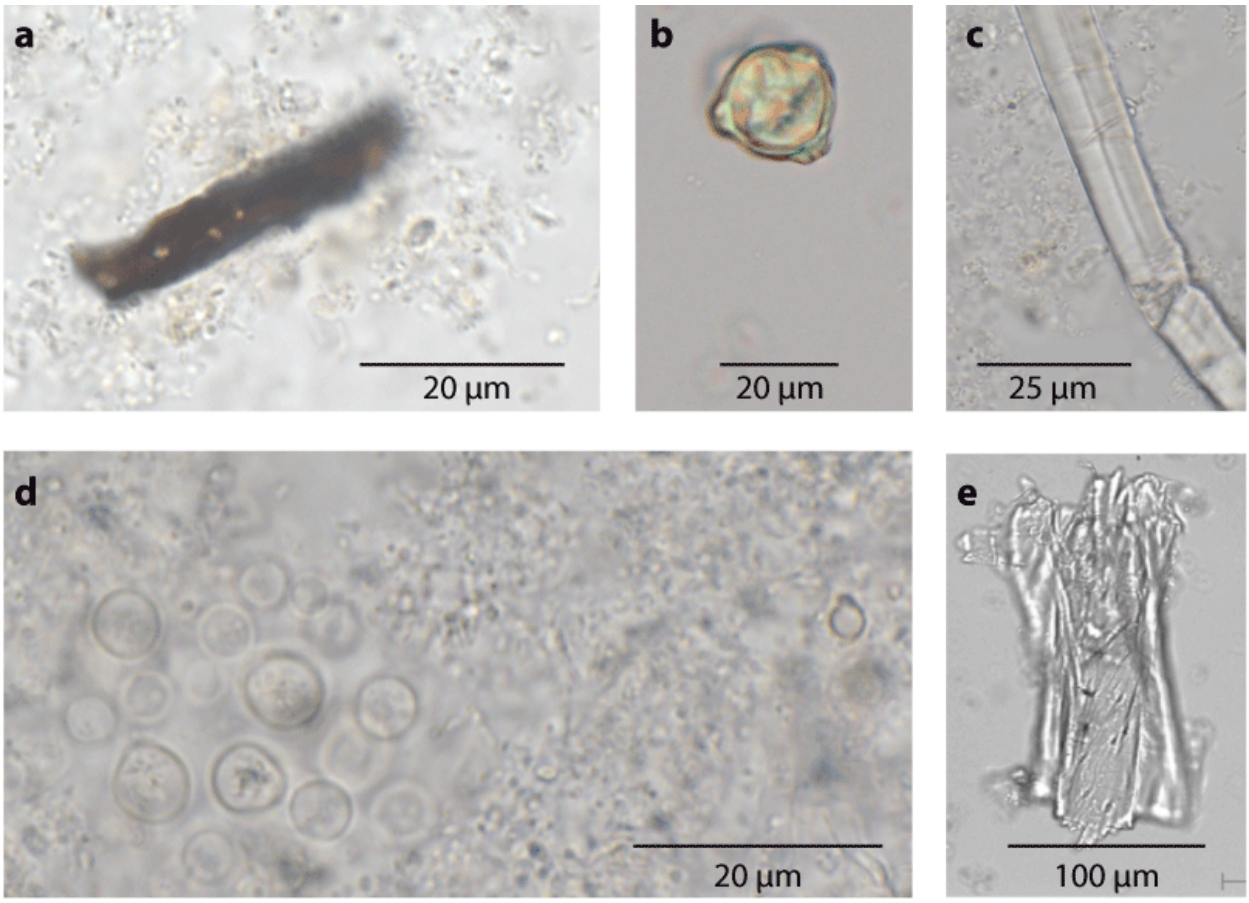

Supplementary Figure 5 | Additional microfossils within ancient dental calculus. a, Microcharcoal debris emerging from G12 dental calculus matrix during decalcification. **b**, Birch (*Betula* sp.) pollen grain from B61, with attached calculus matrix visible through it. **c**, Bast fiber, likely from flax, from B17. **d**, Yeast cells embedded within the dental calculus of B78. **e**, Large, unidentified organic remains recovered from B61.

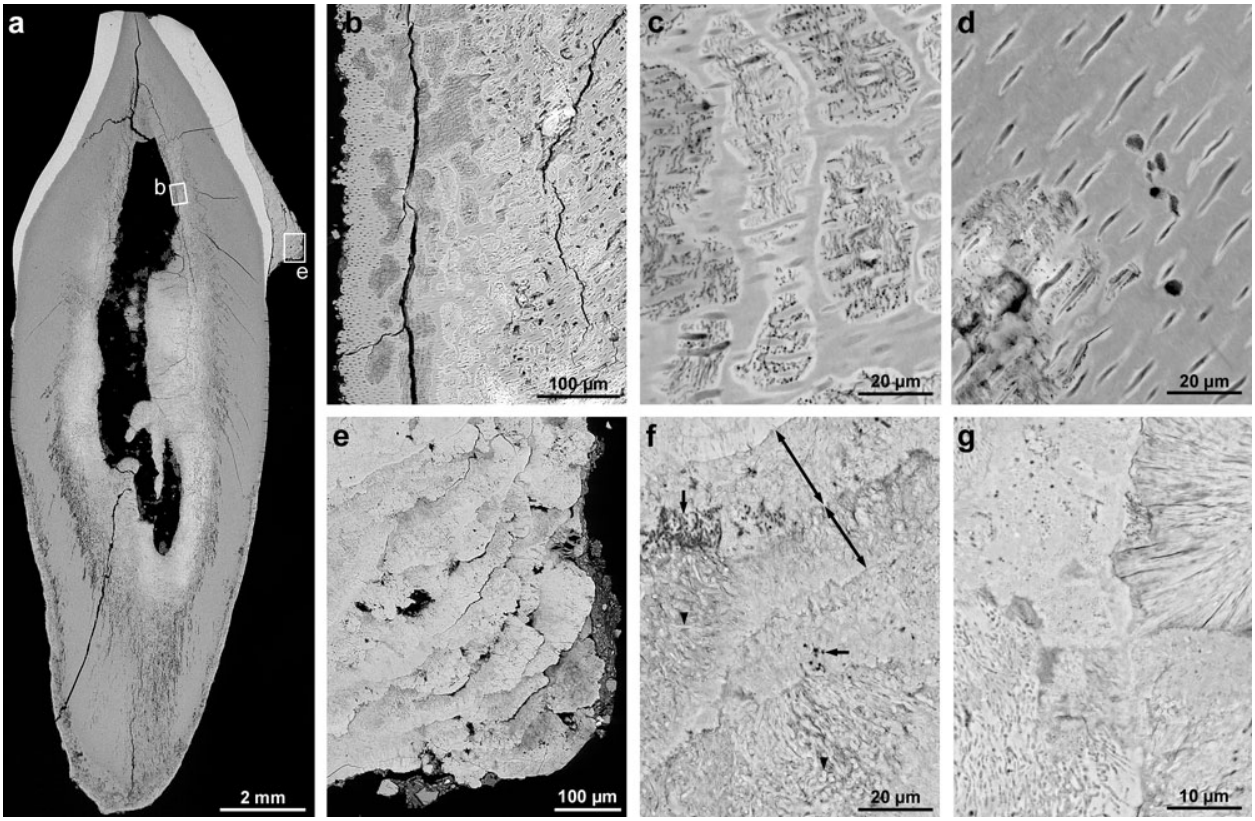

Supplementary Figure 6 | SEM images of a sectioned archaeological tooth with *in situ* calculus deposits. (a) Labio-lingual section of a mandibular incisor (individual B78) with dental calculus on the labial crown surface. Rectangles labeled (b) and (e) mark locations of respective details. (b) Detail of the dentine at the border of the pulp cavity showing areas of altered mineral density (left) and pitting (right) caused by acid-producing environmental microbes that invaded the pulp cavity post-mortem. (c) Detail of zones of hypomineralized (dark gray) and hypermineralized (white) dentine. (d) Detail of bacteria infiltrating the dentine tubules (arrows). (e-f) Details of the dental calculus which exhibits a layered structure suggesting outward-downward incremental growth (double arrows in f). The calculus matrix contains numerous lacunae of microorganisms (arrows in f), some of which are mineralized (arrow-heads in f). (g) Detail of microorganisms within dental calculus showing large crystal structures and high bacterial cell density.

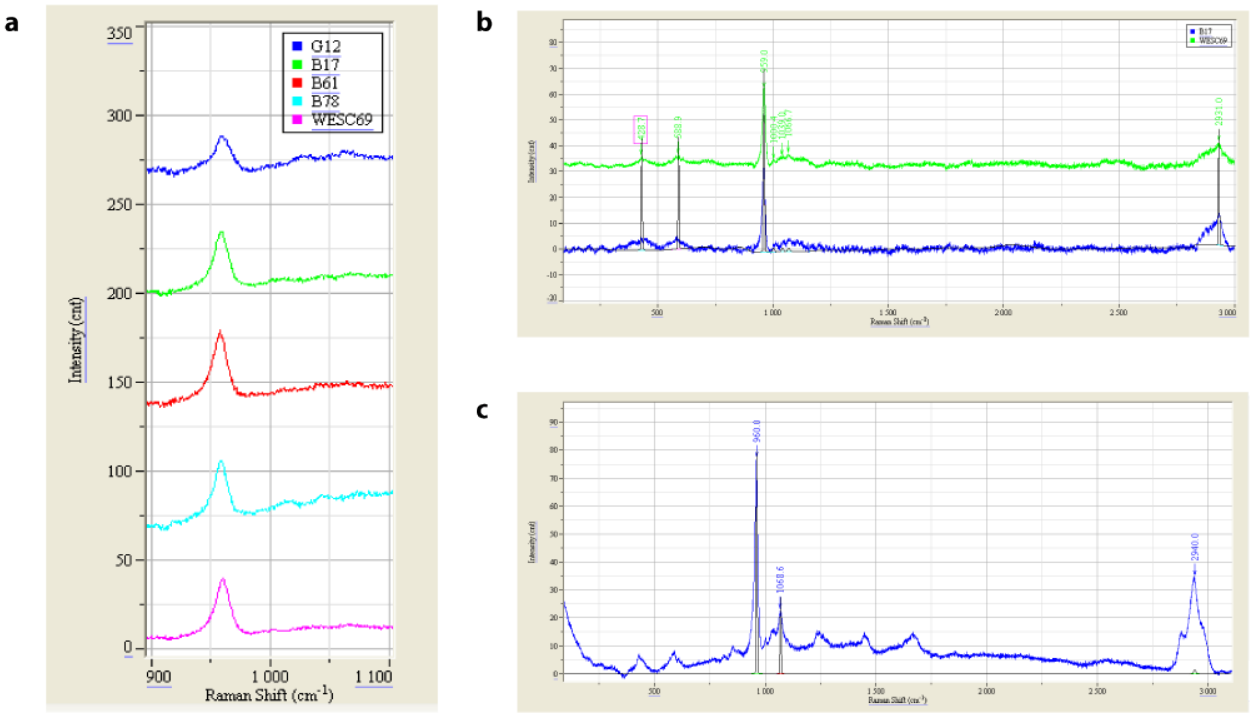

Supplementary Figure 7 | Raman spectra of ancient and modern dental samples. **a**, Raman spectra of ancient (G12, B17, B61, and B78) and modern (P3) calculus samples showing the main phosphate band at ~960 cm^{-1} (not baseline corrected). **b**, Full Raman spectrum of the ancient sample B17 compared to the modern sample P3 (baseline corrected). The main calculus peaks are highlighted. **c**, Raman spectrum of the ancient dentine sample B61 (not baseline corrected). The main peaks are highlighted.

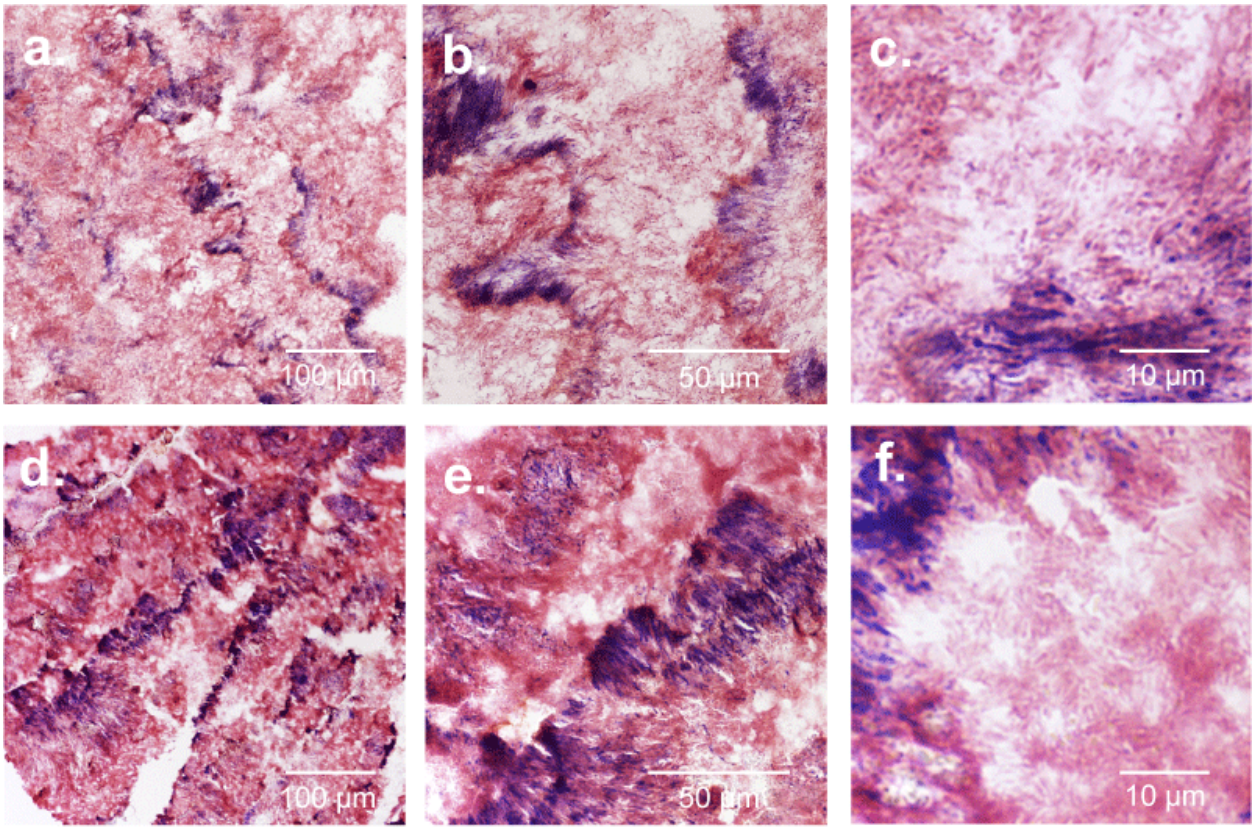

Supplementary Figure 8 | Histological sections of modern and ancient decalcified human dental calculus, Gram stain. **a-c**, modern patient P3. **d-f**, individual B78 of the medieval Dalheim cemetery. **a, d**, At 200x linear features formed by rows of Gram-positive bacteria are visible that demarcate laminations parallel to the tooth surface characteristic of periodic calculus growth. **b, e**, At 630x, the Gram-positive cells comprising the linear features can be recognized as individual filamentous bacteria oriented perpendicular to the tooth surface. **c, f**, At 1000x a high density of Gram-positive spherical and rod-shaped cells can be distinguished throughout the dental calculus matrix.

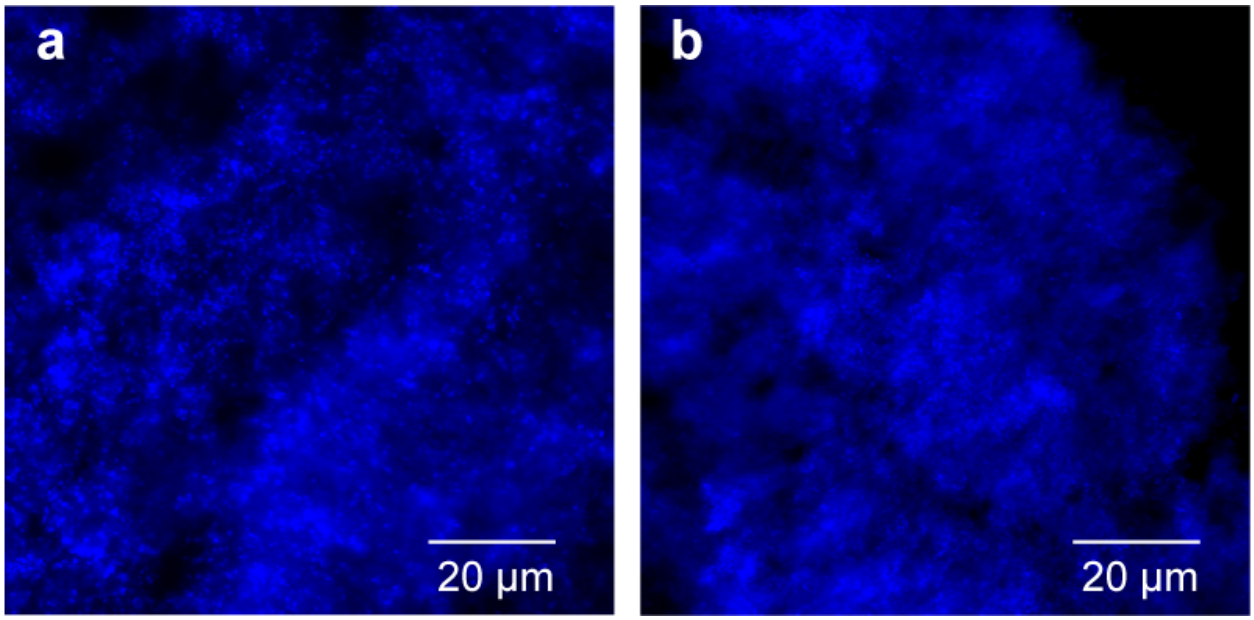

Supplementary Figure 9 | Details of histological sections of modern and ancient decalcified human dental calculus at 630x magnification, Hoechst stain. **a**, modern patient P3. **b**, individual B78 of the medieval Dalheim cemetery.

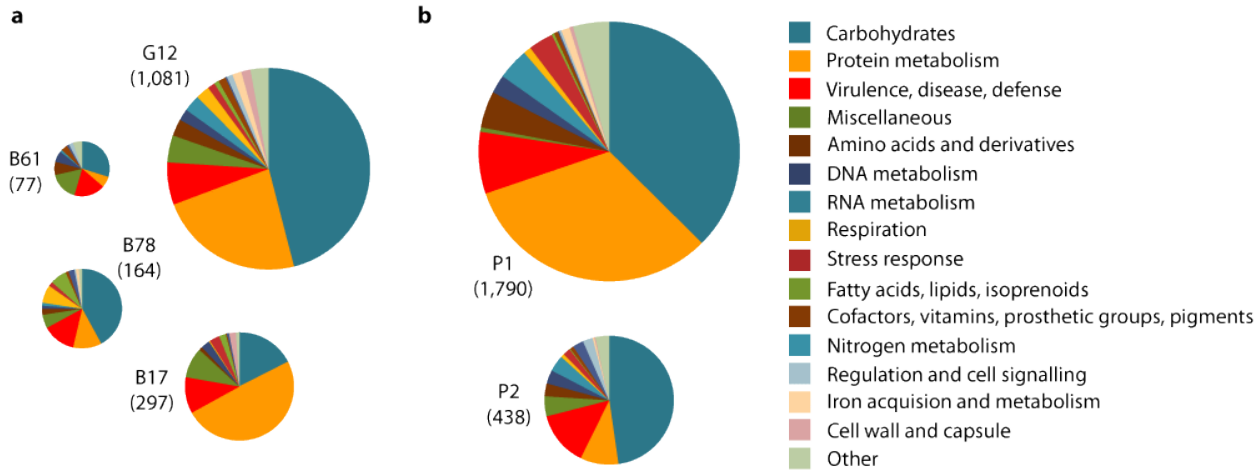

Supplementary Figure 10 | Protein functional profiles of (**a**) ancient and (**b**) modern dental calculus. Pie chart size is scaled by the number of assigned SEED functional classifications (provided in parentheses).

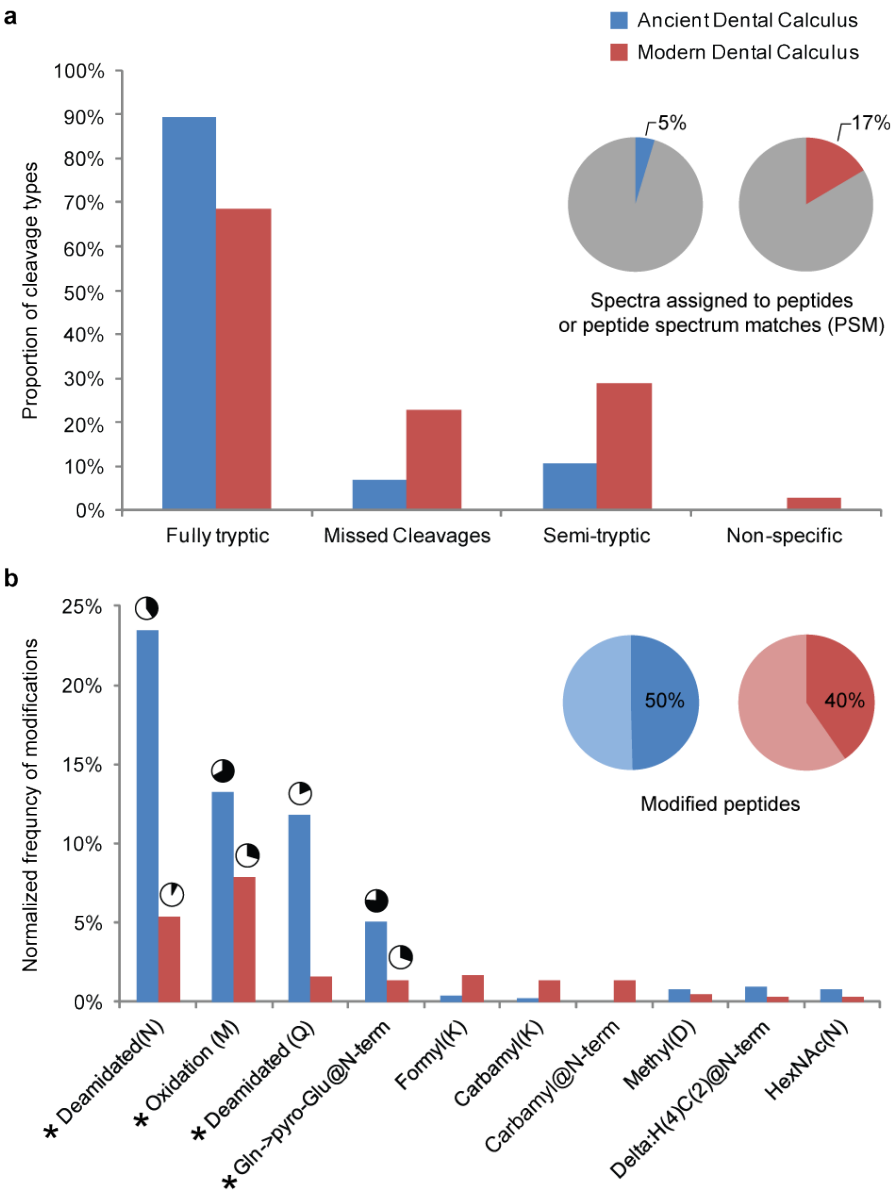

Supplementary Figure 11 | Modifications and damage observed in assigned peptides from ancient and modern human dental calculus samples using ProteinPilot v.4. **a**, Proportion of assigned peptides on total number of MS spectra and proportion of assigned cleavage types on total number of identified peptides. **b**, Proportion of modified peptides and normalized frequency of top ten ranked modifications. For each modification, the proportion of modified sites (black) of possible is indicated by a pie chart if >3%. Modifications selected for Mascot search are marked with an asterisk (*).

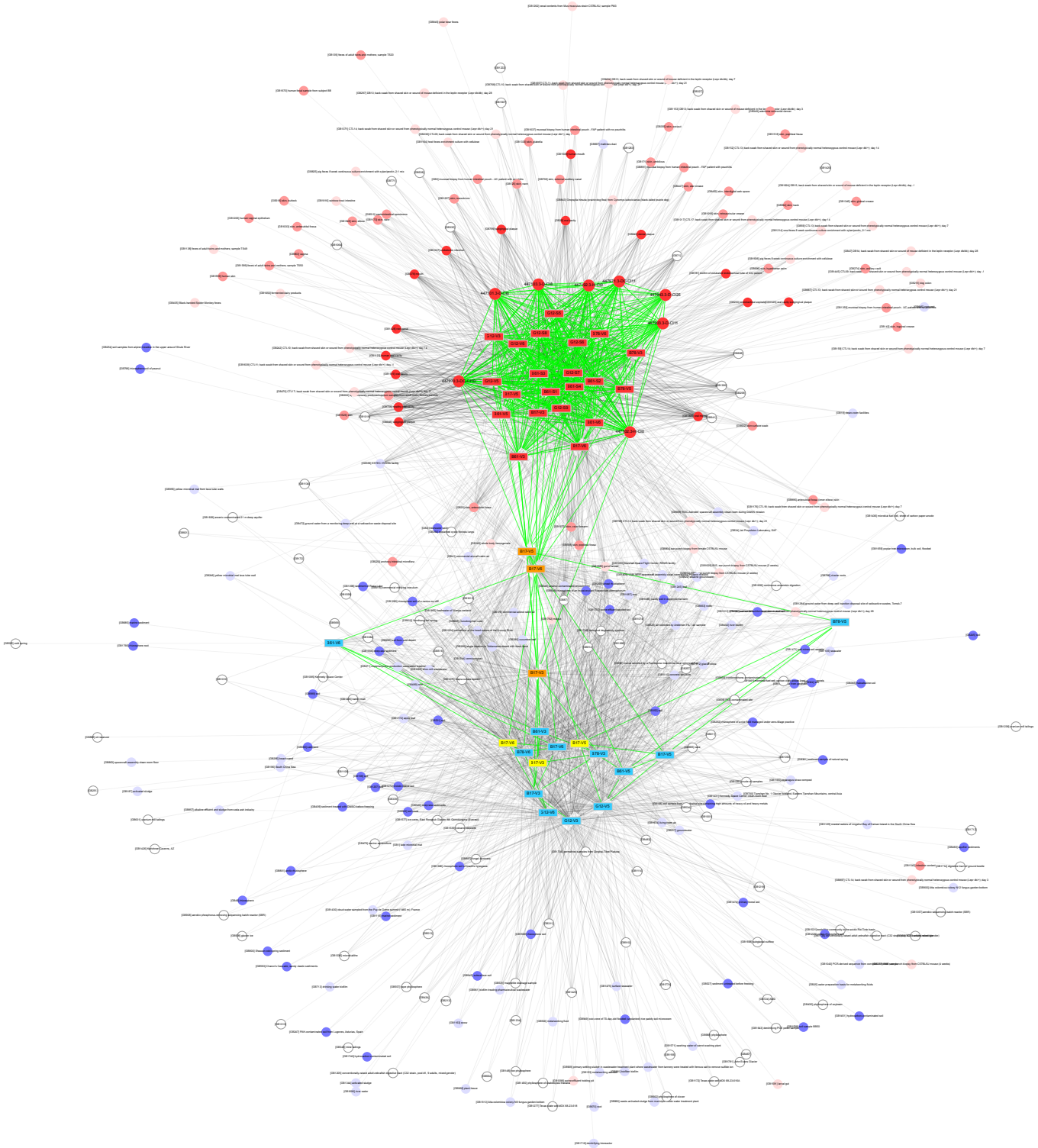

Supplementary Figure 12 | Enhanced view of Figure 5j with sample annotations and descriptors of recruited metagenomes.

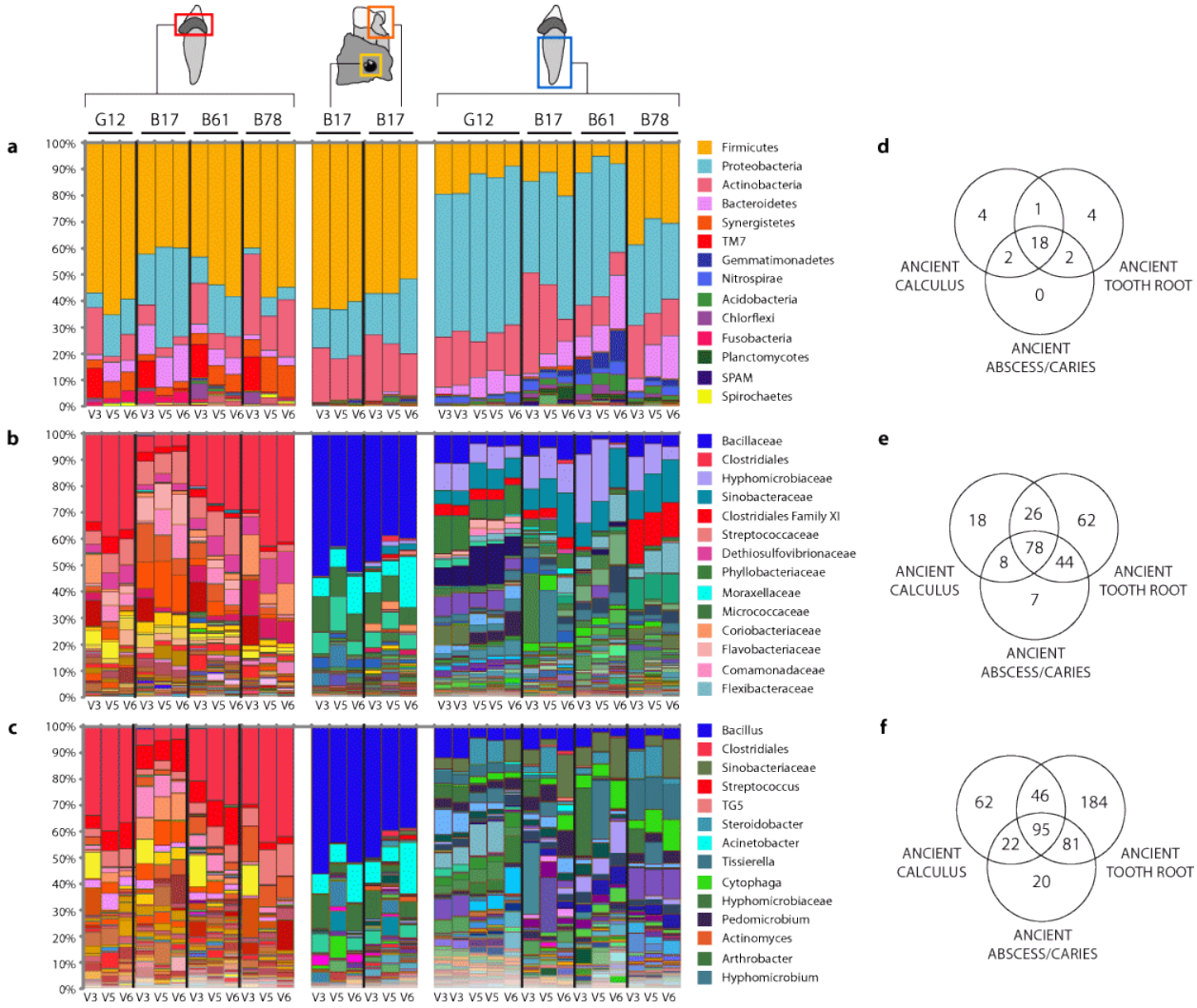

Supplementary Figure 13 | Comparison of microbial taxa identified in ancient dental calculus, abscessed bone, carious dentine, and tooth roots from deep sequenced 16S rRNA amplicons. Vertical columns represent ancient metagenomic samples by type, individual, and 16S rRNA gene variable region; columns indicate relative abundances colored by microbial (**a**) phyla (L2), (**b**) families (L5), and (**c**) genera (L6) from binned OTUs. For clarity, only genera present at ≥0.1% are shown. Legends include the 14 most abundant taxa in the combined data set at each level. **d-f,** Shared taxa among the three sample types are summarized with corresponding Venn diagrams.

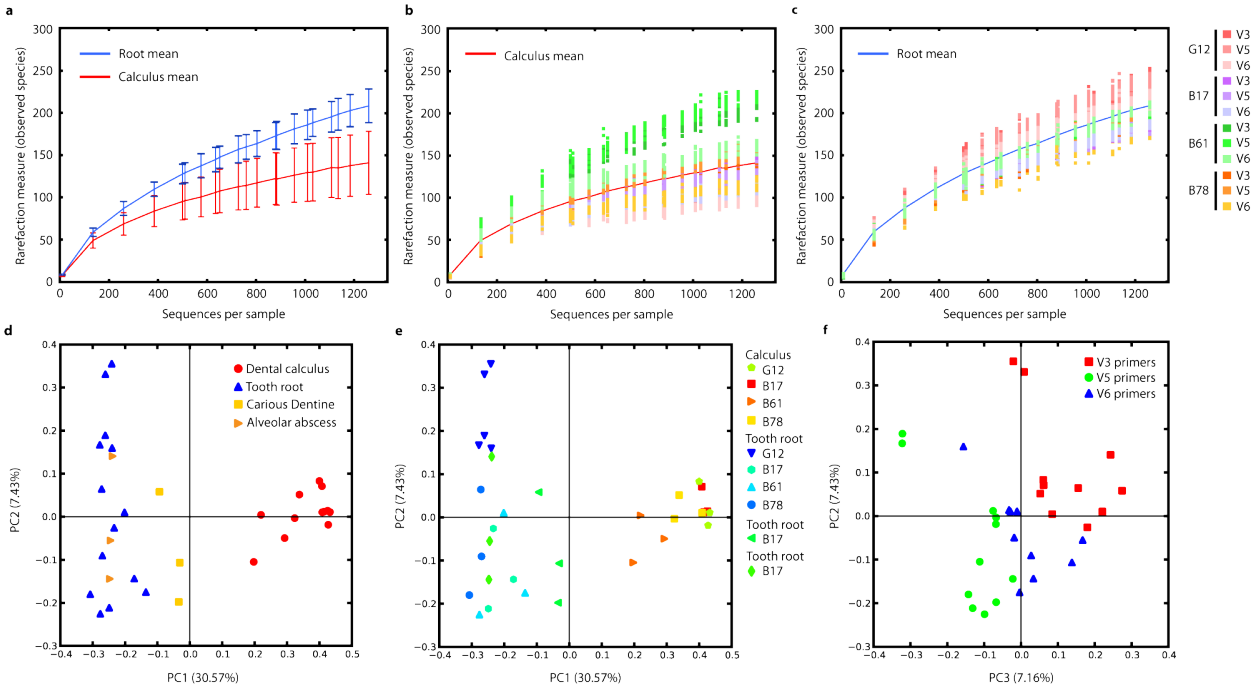

Supplementary Figure 14 | Alpha diversity rarefaction curves and beta diversity Principal Coordinates Analysis (PCoA) plots of ancient dental calculus and tooth root samples. (**a**) Mean rarefaction curves for dental calculus (red) and tooth root samples (green); error bars signify standard error. Mean rarefaction curves overlaid with data points from (**b**) dental calculus and (**c**) tooth roots. Species level comparison of ancient samples by (**d**) sample type, (**e**) individual within sample types, and (**f**) primer pair.

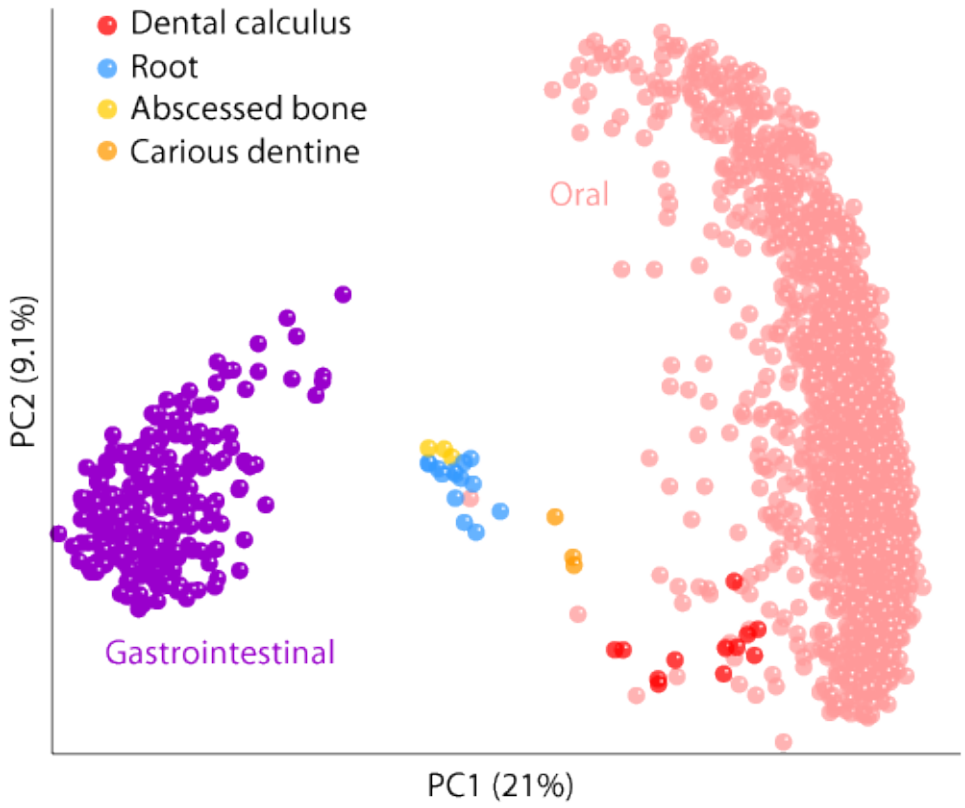

Supplementary Figure 15 | Principal Coordinates Analysis of Human Microbiome Project (HMP) oral and gastrointestinal samples compared to ancient dental samples (dental calculus, tooth root, carious dentine, abscessed bone) using unweighted UniFrac distances.

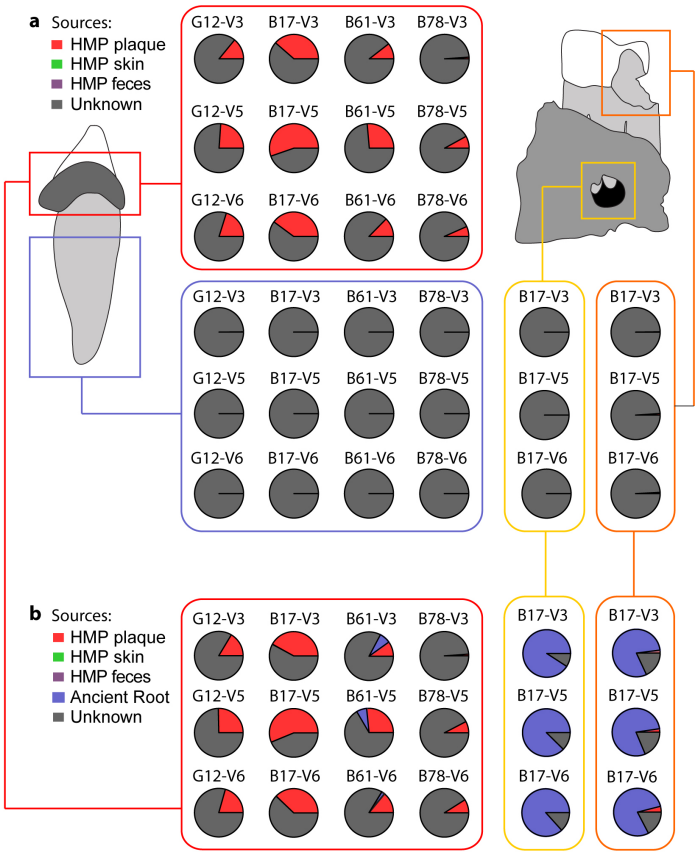

Supplementary Figure 16 | Source tracker proportion estimates for ancient sink samples. **a**, Source environment proportions for four ancient sink samples estimated using three HMP sources (Group 1 sources). **b**, Source environment proportions for three ancient sink samples estimated using the HMP and pooled ancient tooth root samples as sources (Group 2 sources).

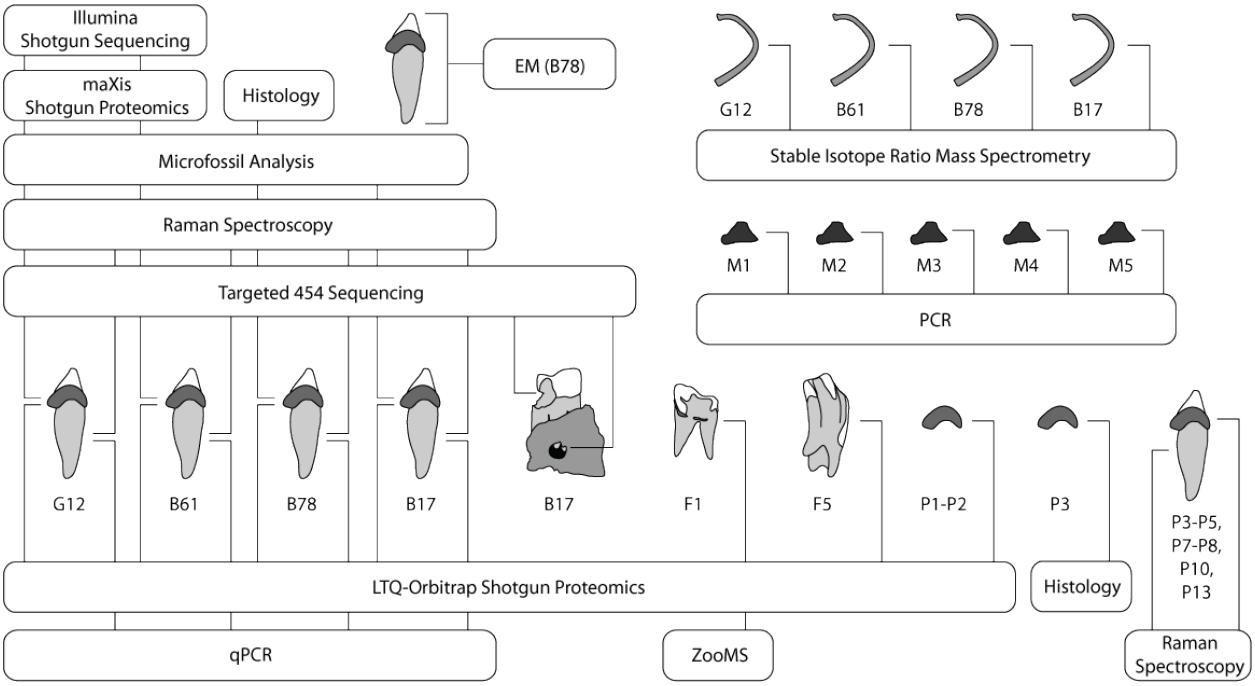

Supplementary Figure 17 | Graphical overview of the samples and analyses performed in this study. G12, B61, B78, and B17 are Dalheim human samples. F1 and F5 are Dalheim faunal samples. M1-M5 are Dalheim burial matrix samples. P1-P5, P7-P8, P10, and P13 are dental samples from modern patients.

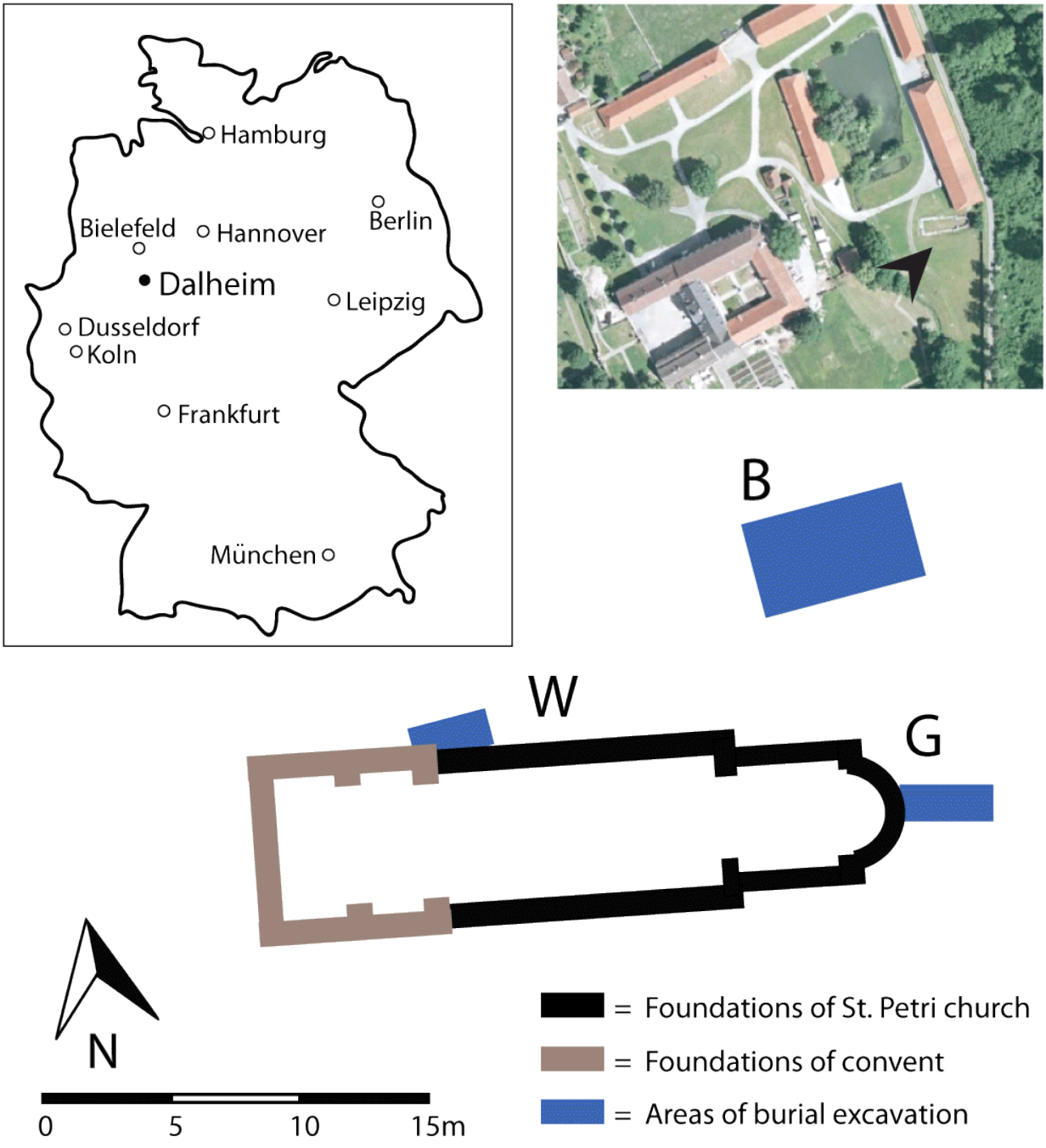

Supplementary Figure 18 | The Dalheim church and convent complex (9th-15th centuries CE). Aerial view of the Dalheim St. Petri church and convent complex (arrow) at the LWL-Landesmuseum für Klosterkultur (Google Earth, Image © 2013 GeoBasis-DE/BKG). During archaeological excavations, three principal areas (blue) were excavated around the church (B, G, and W). The majority of burials were excavated within B, an area now covered by a long outbuilding.

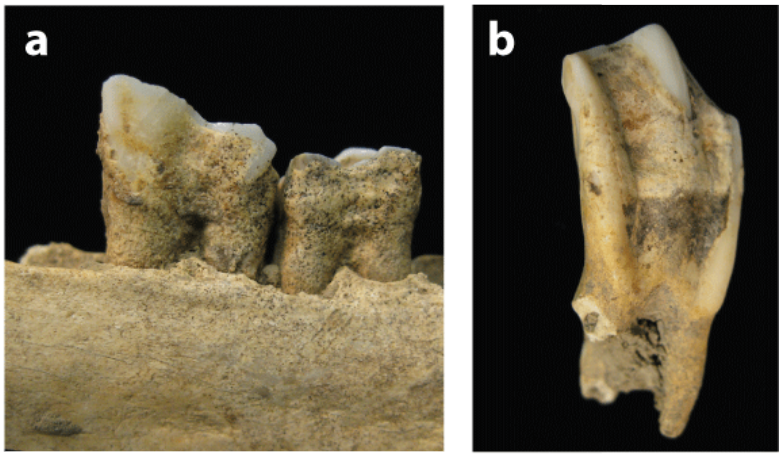

Supplementary Figure 19 | Dalheim faunal dental material from specimens (**a**) F1, *Ovis aries* and (**b**) F5, *Bos taurus*.

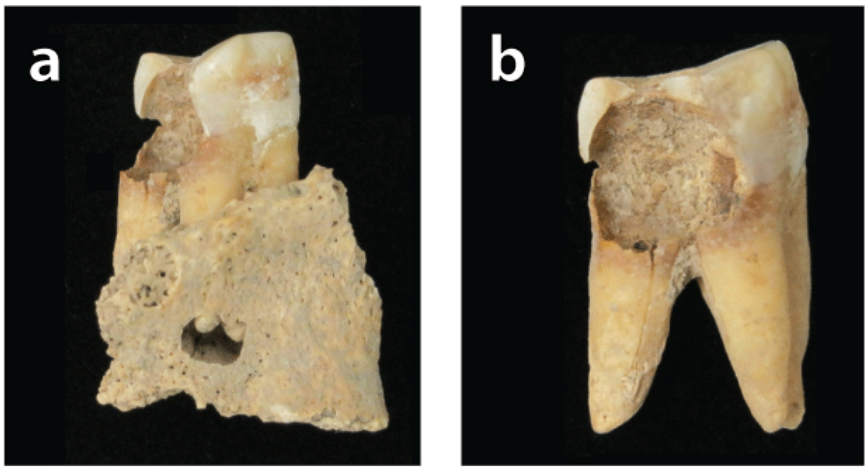

Supplementary Figure 20 | Carious molar and associated root abscess from the dentition of B17 with views of (**a**) the articulated molar and maxillary alveolar bone, (**b**) enlarged view of crown destruction and dentine discoloration. Note the abscess drainage fistula in the alveolar bone. The interior margins of the abscess were characterized by reactive bone formation.

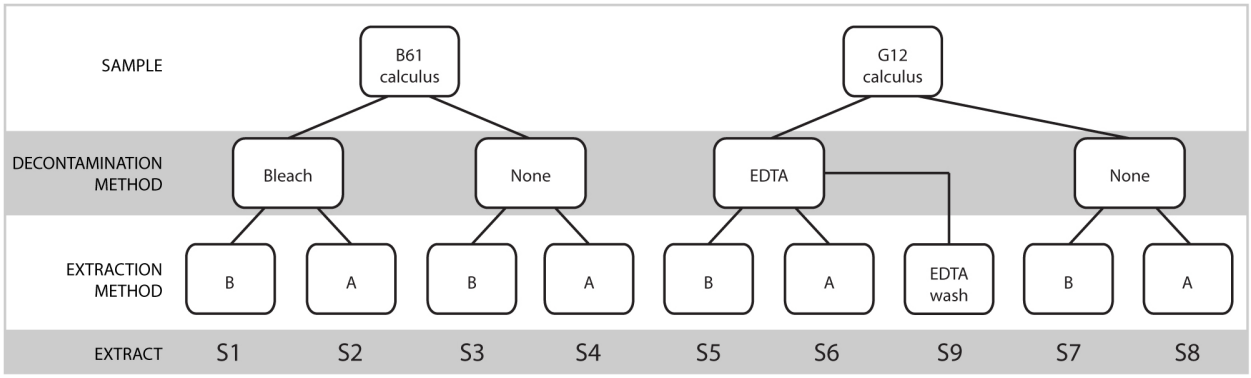

Supplementary Figure 21 | Experimental design for the comparison of decontamination and extraction methods for ancient dental calculus samples.

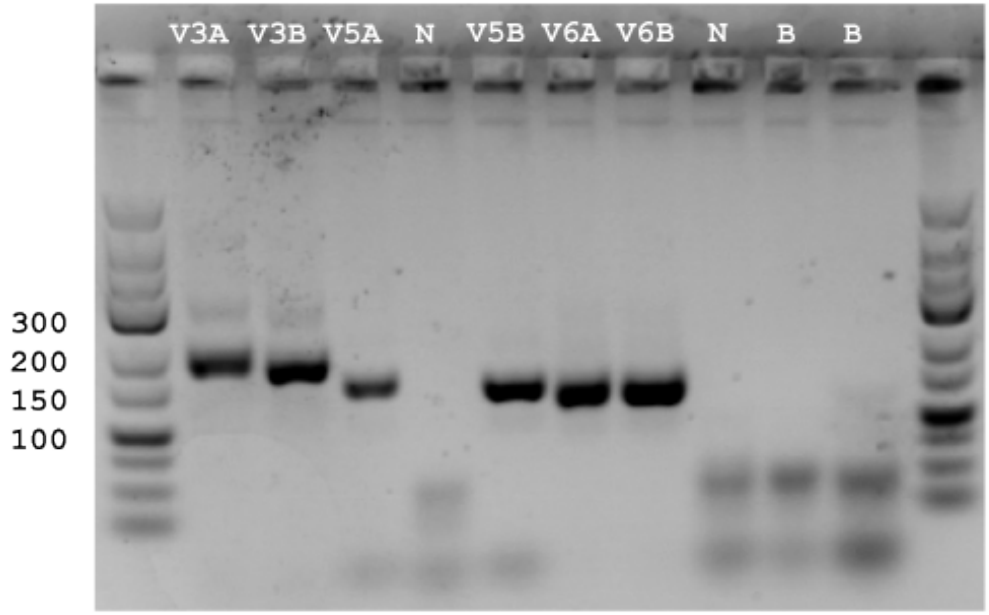

Supplementary Figure 22 | Gel of individual G12 dental calculus 16S rRNA primer amplifications with lanes marked for negative extraction blanks (N) non-template reagent blanks (B), and samples indicated by primer set (V3, V5, V6) and extract method (A, B) and. All three primer pairs were added to each negative extraction blank and non-template reagent blank.

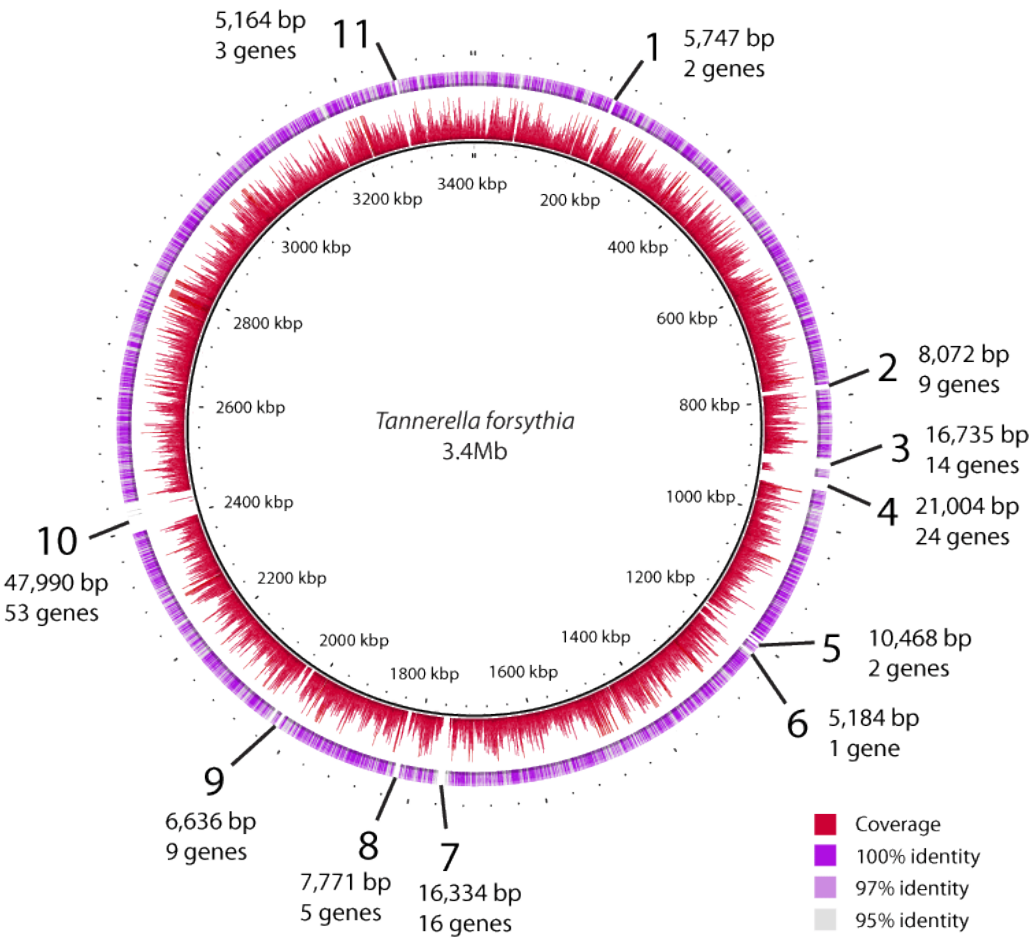

Supplementary Figure 23 | Major gaps in the *Tannerella forsythia* genome reconstruction from G12 ancient dental calculus.

II. Supplementary Tables

Supplementary Table 1 | Ten most abundant phyla observed in ancient dental calculus

Phylum	Mean	Standard deviation	1st quartile	Median	3rd quartile
Firmicutes	49.52%	10.57%	41.75%	47.74%	57.56%
Actinobacteria	12.03%	6.09%	7.14%	10.65%	15.05%
Proteobacteria	11.46%	8.85%	5.69%	9.17%	13.80%
Bacteroidetes	6.62%	3.60%	3.13%	5.95%	9.68%
TM7	4.60%	4.02%	0.07%	4.78%	7.16%
Synergistetes	3.27%	2.65%	1.92%	2.28%	3.15%
Chloroflexi	2.66%	1.54%	1.26%	2.35%	4.02%
Fusobacteria	2.08%	1.76%	0.55%	0.90%	3.28%
Spirochaetes	0.60%	0.27%	0.39%	0.55%	0.74%
Euryarchaeota	0.38%	0.61%	0.00%	0.17%	0.36%

Notes:
Data compiled from 16S rRNA gene DNA sequence data from B17, B61, B78 and G12 targeted (V3, V5, V6) and B61 and G12 shotgun (S1-S9) metagnomic analyses.

Supplementary Table 2 | Comparison of putative pathogens identified in ancient dental calculus and HMP healthy cohort dental plaque samples (provided as a separate .xlsx file)

Supplementary Table 3 | Specific virulence factors and mobile elements identified within ancient dental calculus metagenomic and metaproteomic data (provided as a separate .xlsx file)

Supplementary Table 4 | Putative antibiotic resistance genes identified from ancient dental calculus metagenomic data (provided as a separate .xlsx file)

Supplementary Table 5 | Radiocarbon dating of the Dalheim St. Petri church burials

Individual	AMS ^{14}C age (BP)	δ^{13}C (‰)	Calibrated age (CE)	Laboratory Reference
B64	885 ± 40	-20.5 ± 1.1	1127 ± 63	ETH-30728
B78	965 ± 40	-20.5 ± 1.1	1079 ± 51	ETH-30729
G3	870 ± 40	-21.9 ± 1.1	1138 ± 66	ETH-30730
G9	1025 ± 40	-18.3 ± 1.1	1002 ± 26	ETH-30731

Notes:
Radiocarbon dates calibrated with CalPal Online (http://www.calpal-online.de/), and are reported within 1σ (68% confidence).

Supplementary Table 6 | Dental paleopathology scoring codes

Tooth Presence/Absence	
MI	Tooth and alveolar bone missing
CA	Congenital absence
AL	Antemortem tooth loss
PL	Postmortem tooth loss (alveolar bone intact)
NE	Non-erupted
PE	Partially erupted
Abrasion	
0	No wear
1	Wear of cusps: tips worn but enamel mostly intact
2	Wear to dentine: dentine partially exposed but some enamel visible on cusp surface
3	Occlusal surface worn to dentine: no enamel visible on surface
4	Severe wear: pulp chamber exposed, wear to tooth root, cusp may be absent
Caries	
0	Sound: smooth surface
1	Enamel caries: white or stained opaque area or small cavity
2	Dentinal caries: cavity which clearly penetrated dentine
3	Dentinal caries to pulp: gross cavity to the dental pulp
4	Complete crown destruction: gross cavity with large scale destruction
Calculus	
0	No calculus
1	Minor: Small, thin calculus accumulation at DEJ (dental enamel junction)
2	Moderate: Wide band of calculus covering part of both crown and root; thick accumulation
3	Heavy: Complete obstruction of tooth crown and root with a thick layer of calculus
Periodontal Destruction	
0	Sound: attachment level ≤ 1.5mm from DEJ to alveolar margin
1	Probable gingivitis: alveolar porosity and attachment loss ≤ 1.5mm from DEJ to alveolar margin
2	Minor: bone loss up to one third of the root length or attachment loss up to 3mm
3	Moderate: bone loss greater than one third but less than one half of the root length or attachment loss 4-5mm
4	Severe: bone loss greater than one half of the root length or attachment loss ≥ 6mm

Supplementary Table 7 | Dental calculus samples from modern patient controls

Patient	Code	Smoker?	Caries	Periodontitis	Analysis
P1	CPMAIR	Yes	Active	Generalized mod/severe periodontitis	Proteomics, DC
P2	CPNATR	Yes	Active	Generalized moderate periodontitis	Proteomics, DC
P3	CPWE7C	Yes	Active	None	Microscopy, DC Raman, DC
P4	CP2ARV	No	No	Generalized severe periodontitis	Raman, TR
P5	CPT2A7	Yes	No	Generalized severe periodontitis	Raman, TR
P7	CP7A2A	Yes	Active	Generalized severe periodontitis	Raman, TR
P8	CPD4L9	No	Active	Generalized moderate periodontitis	Raman, TR
P10	CP6LUA	Yes	No	Generalized severe periodontitis	Raman, TR, DC
P13	CPX3XX	NA	NA	NA	Raman, DC

Notes:
DC, dental calculus; TR, tooth root; NA, not available

Supplementary Table 8 | Weight of dental calculus analyzed for microfossils

Sample	Weight (mg)
G12	17.0
B17	12.3
B61	25.8
B78	25.2
F5	4.4

Supplementary Table 9 | Summary of microfossil and micro-debris finds

Indiv.	Starches	Phytoliths	Pollen	Other organic finds
G12	None	None	None	Micro-charcoal; unidentified organic material
B17	Fabaceae (1)	None	Birch (1)	Bast fiber (1); animal connective tissue fibers (2); micro-charcoal; unidentified organic material
B61	Triticeae (12)	Monocot (1)	Birch (1)	Bast fiber (2); micro-charcoal; unidentified organic material
B78	Triticeae (15)	None	None	Yeast; micro-charcoal; unidentified organic material
F5	None	Monocot (2)	None	Micro-charcoal

Supplementary Table 10 | Raman results for ancient and modern dental samples.

	Main PO_4^{3-} peak position and mean peak area				Peak intensity ratios of C-H (~2940 cm^{-1}) I(CH) and the main phosphate peak I(P)		
CALCULUS	PO_4^{3-}	Mean Area	Area Range	N	I(CH)/I(P)	I(CH)/I(P) Range	N
Ancient							
G12	959	430	386 - 471	4	-	-	-
B17	958	592	463 - 690	10	0.47	0.44 – 0.52	3
B61	960	583	340 - 802	9	0.39	0.29 – 0.44	5
B78	959	509	274 - 629	10	0.36	0.28 – 0.39	4
Modern							
P3	960	523	723 - 320	12	0.42	0.27 – 0.57	8
P13	959	496	604 - 438	5	0.35	0.32 – 0.54	5
DENTINE	PO_4^{3-}	Mean Area	Area Range	N	I(CH)/I(P)	I(CH)/I(P) Range	N
Ancient							
G12	959	1258	1549 - 872	7	0.49	0.32 - 0.63	7
B17	959	983	1170 - 791	5	0.44	0.35 - 0.61	5
B61	959	934	1330 - 760	9	0.54	0.43 - 0.71	9
B78	959	1102	1532 - 792	5	0.48	0.35 - 0.73	5
Modern							
P4	957	920	1000 - 826	5	0.58	0.64 – 0.54	5
P5	957	825	874 - 785	5	0.52	0.89 – 0.54	5
P7	958	785	1056 - 540	5	0.83	0.94 – 0.58	5
P8	959	706	749 - 666	5	0.67	0.62 - 0.75	5
P10	958	800	1090 - 636	5	0.62	0.68 – 0.57	5

Notes:
Peak positions are measured in cm^{-1}.
N, number of measurements.

Supplementary Table 11 | Carbon and nitrogen stable isotope values for Dalheim human rib collagen samples

Individual	S-EVA[a]	% Collagen[b]	% C[c]	% N[d]	C:N[e]	$\delta^{13}C$ (‰)	$\delta^{15}N$ (‰)
G12	26215	6.3	42.0	15.6	3.1	-18.9	10.5
B17	26212	2.6	35.3	12.7	3.2	-19.6	9.3
B61	26213	5.2	39.7	14.9	3.1	-19.2	10.3
B78	26214	3.5	37.7	14.0	3.1	-19.5	11.1

Notes:

[a]Sample code at the Max Planck Institute for Evolutionary Anthropology, Leipzig, Germany.

[b]Determined by (mg of collagen*100)/(mg of bone). Samples with >2% collagen by weight are considered suitable for analysis [73].

[c] ≥35% C is considered sufficient preservation for analysis.[73].

[d] ≥10% N is considered sufficient preservation for analysis.[73]

[e]The C:N of human bone collagen during life is approximately 3.2. Archaeological bone samples with C:N values ranging 2.9-3.6 are considered sufficiently preserved for analysis.[73]

Supplementary Table 12 | Dalheim calculus DNA extraction data

Extract	Individual	Extraction Method	Sample (mg)	Yield (ng/uL)	Normalized Yield (ng/mg)	Inhibition dilution factor
S4	B61	A	46.6	11.6*	5.0	1:4
S3	B61	B	48.3	3.08*	1.3	nd
S11	B61	C	47.3	0.69**	0.4	1
S12	B61	D	54.1	0.79**	0.4	1
S13	B61	E	48.5	0.15***	0.2	1

Notes:

*Eluted into 20uL; **Eluted into 30uL; ***Eluted into 50uL; nd=not determined

Supplementary Table 13 | Dalheim calculus DNA extraction yields with and without decontamination

Extract	Indiv.	Extraction Method	Decontamination Method	Sample (mg)	Yield (ng/uL)	Normalized Yield (ng/mg)
S1	B61	B	Bleach	48.2	1.9	0.8
S2	B61	A	Bleach	48.3	13.9	5.8
S3	B61*	B	None	48.3	3.1	1.3
S4	B61*	A	None	46.6	11.6	5.0
S5	G12	B	EDTA	55.3	34.3	12.4
S6	G12	A	EDTA	59.6	94.7	31.8
S7	G12	B	None	48.7	29.7	12.2
S8	G12	A	None	49.1	110.0	44.8
S9	G12	***	**	114.9	8.8	1.5

Notes:

*As reported in Supplementary Table 12.

**EDTA wash from the G12 decalcification step.

***DNA from the EDTA wash solution was extracted without further digestion using a high salt-modified phenol/chloroform extraction, followed by purification on a Qiagen MinElute column and elution into 20uL EB buffer.

Supplementary Table 14 | Dental calculus DNA extraction yields across individuals

Extract	Individual	Extraction Method	Sample (mg)	Yield (ng/uL)	Normalized Yield (ng/mg)	Inhibition dilution factor
S4	B61*	A	46.6	11.6	5.0	1:4
S10	B61	A	53.3	13.4	5.0	nd
S15	B78	A	50.3	74.9	29.8	1:49
S8	G12*	A	49.1	110.0	44.8	1:49
S14	B17	A	54.9	1,200.0	437.2	1:49
S28	P2†	A	11.9	33.1	83.4	nd

Notes:

*As reported in Supplementary Table 13; † Modern dental calculus eluted into 30 μl; nd = Not determined

Supplementary Table 15 | Dental calculus DNA extraction yields from comparative UK individuals

Sample ID	Period	Sample (mg)	Yield (ng/μl)	Normalized Yield (ng/mg)
UK-1a	Medieval	37	214.3	289.6
UK-1b	Medieval	39	127.6	163.6
UK-2	Roman	21	35.6	84.8

Notes:

UK-1a and UK-1b are two independent extractions from the same individual.

Supplementary Table 16 | Dalheim dentine and bone DNA extraction data

Extract	Tissue	Individual	Sample (mg)	Yield (ng/μL)	Yield (ng/mg)	Inhibition dilution factor
Healthy						
S16	Root	G12	104.7	2.38	0.5	1
S17	Root	G12	104.3	2.27	0.4	nd
S18	Root	B17	103.6	1.28	0.3	1
S19	Root	B17	107.3	1.01	0.2	nd
S20	Root	B61	102.1	2.38	0.5	1
S21	Root	B61	98.0	0.62	0.1	nd
S22	Root	B78	101.8	0.88	0.2	1
S23	Root	B78	100.8	3.16	0.6	nd
Diseased						
S24	Root (carious)	B17	101.7	1.43	0.3	0.2
S25	Root (carious)	B17	100.4	0.54	0.1	nd
S26	Bone (abscess)	B17	102.7	1.52	0.3	0.2
S27	Bone (abscess)	B17	101.9	2.50	0.5	nd

Notes:
nd = not determined

Supplementary Table 17 | Dalheim burial matrix DNA extraction and amplification results

Extract	Sample (Burial)	Soil (mg)	Yield (ng/uL)	Yield (ng/mg)	Lambda dilution factor*	HVRI (A B C D)	16S (V3)
S28	M1 (B28)	220	0.030	0.027	1	- - - -	-
S29	M2 (B55)	220	0.027	0.025	1	- - - -	-
S30	M3 (B84)	219	0.030	0.027	1	- - - -	-
S31	M4 (B85)	203	0.052	0.051	1	- - - -	-
S32	M5 (W)	223	0.072	0.065	1	- - - -	-
S33	Coprolite**	218	0.470	0.431	1	+ - + +	+

Notes:

*Dilution required to successfully amplify a 500bp target from 1pg of lambda genomic DNA in a 20 μl PCR reaction volume after 35 PCR cycles.

**Unrelated coprolite sample (3^{rd}-5^{th} century BCE) from Dürrnberg, Germany was used as a positive extraction and amplification control.

Supplementary Table 18 | Primers targeting the human mitochondrial HVRI region and bacterial 16S rRNA gene

Primer	Target[a]	Sequence (5'-3')	bp[b]	Reference
mtA	Human mitochondrial HVRI (16035-16161)	TTCTCTGTTCTTTCATGGG GATGTGGATTGGGTTTTTA	161	[74]
mtB	Human mitochondrial HVRI (16131-16228)	CACCATGAATATTGTACGGT TTGCAGTTGATGTGTGATAG	140	[74]
mtC	Human mitochondrial HVRI (16225-16325)	AAGTACAGCAATCAACCCTC CTGTAATGTGCTATGTACGGTA	141	[74]
mtD	Human mitochondrial HVRI (16307-16406)	TACCCACCCTTAACAGTACA TATTGATTTCACGGAGGA	136	[74]
V3	16S rRNA V3 region (351-507)	ACTCCTACGGGAGGCAGCAGT GTATTACCGCGGCTGCTGGCAC	*	This study

Notes:

[a]Nucleotide positions of targeted region (exclusive of primers) are reported relative to the revised Cambridge Reference Sequence for HVRI and *Escherichia coli* JN049591 for rRNA 16S.

[b]Total amplicon length (inclusive of primers).

*The length of the V3 region is variable across taxa. This primer pair was designed to amplify an approximately 150-250bp target for a diverse range of bacterial taxa.

Supplementary Table 19 | DNA extraction yields and results of genetic sex typing of ancient dentine decontaminated with bleach

Indiv.	Weight (mg)	Yield (ng/uL)	Yield (ng/mg)	AMEL-X	AMEL-Y	Genetic Sex	Morphological Sex[†]
G12	100	1.0	0.20	X X X	- - -	Female	Probable Female
B17	98	1.1	0.22	- - -	- - -	I	Probable Female
B61	102	0.2	0.04	X X X	Y Y Y	Male	Male
B78	103	0.9	0.17	- X X	- - -	Female	Female

Notes:

- = no amplification; I = indeterminate

[†]Determined from analysis of cranial and pelvic osteological features.[75]

Supplementary Table 20 | Ancient dental calculus DNA extracts used for Illumina library preparation

Extract	Indiv.	Extraction Method	Decontam. Method	Total extract ng (in 19μl)	μl used for library build	Total ng used in library build
S1	B61	B	Bleach	37	19	37
S2	B61	A	Bleach	254	19	254
S3	B61	B	None	59	19	59
S4	B61	A	None	220	19	220
S5	G12	B	EDTA Wash	652	19	652
S6	G12	A	EDTA Wash	1799	6.5†	615
S7	G12	B	None	564	19	564
S8	G12	A	None	2090	6†	660
S9	G12	*	*	168	19	168

Notes:

* Wash solution for EDTA decontamination step.

† H_2O added to bring to a total volume of 19μl.

Supplementary Table 21 | Illumina read and quality filter statistics

Metagenome Library	Total Reads	Post-QC Reads	% Passing QC	SRA Accession
S1-Shot-B61-calc	13,800,231	13,228,381	95.9%	SRS473742
S2-Shot-B61-calc	13,806,019	13,260,566	96.0%	SRS473743
S3-Shot-B61-calc	9,266,804	8,869,866	95.7%	SRS473744
S4-Shot-B61-calc	11,674,935	11,275,013	96.6%	SRS473745
S5-Shot-G12-calc	9,279,308	8,978,974	96.8%	SRS473747
S6-Shot-G12-calc	9,365,468	8,999,409	96.1%	SRS473746
S7-Shot-G12-calc	10,542,600	10,187,301	96.6%	SRS473748
S8-Shot-G12-calc	10,406,819	10,087,890	96.9%	SRS473749
S9-Shot-G12-calc	9,146,166	8,790,145	96.1%	SRS473750
Total	97,288,350	93,677,545	96.3%	

Supplementary Table 22 | Universal bacterial 16S rRNA gene primers

Primer pair	Target[a]	Sequence
V3	16S rRNA V3 region (351-507)	F 5'-ACTCCTACGGGAGGCAGCAGT-3' R 5'-GTATTACCGCGGCTGCTGGCAC-3'
V5	16S rRNA V5 region (800-900)	F 5'-CAGGATTAGATACCCTGGTAGTCC-3' R 5'-CCCGTCAATTCCTTTGAGTT-3'
V6	16S rRNA V6 region (958-1044)	F 5'-GGTGGAGCATGTGGTTTAATTCGA-3' R 5'-GAGCTGACGACAGCCATGCA-3'

Notes:

[a]Nucleotide positions of targeted region (exclusive of primers) are reported relative to the *Escherichia coli* JN049591 16S rRNA gene.

Supplementary Table 23 | Oral bacterial species included in design of 16S rRNA universal primers

Phylum	Species included in primer design
Bacteria	
Actinobacteria	*Actinomyces naeslundii; Rothia dentocariosa; Atopobium parvalum*
Bacteriodetes	*Prevotella denticola; Prevotella tannerae; Porphyromonas endodontalis; Capnocytophaga gingivalis; Capnocytophaga ochracea*
Firmicutes	*Streptococcus salivarius; Streptococcus mitis; Streptococcus oralis; Streptococcus mutans; Lactobacillus pontis; Gemella morbillorum; Mycoplasma salivarium; Eubacterium saphenum; Filifactor alocis; Catonella morbid; Veillonella parvula; Selenomonas sputigena*
Fusobacteria	*Fusobacterium naviforme; Fusobacterium animalis; Leptotrichia buccalis*
Proteobacteria	*Neisseria mucosa; Rhodocyclus purpureus; Enterobacter hormaechei; Escherichia coli; Haemophilus parainfluenzae; Bartonella henselae; Campylobacter gracilis; Shewanella putrefaciens; Shewanella oneidensis*
Spirochetes	*Treponema medium; Treponema denticola; Treponema maltophilum; Treponema socranskii*
Synergistetes	*Desulfothiovibrio peptidovorans*
TM7	Oral clone I025 AF125206
Archaea	
Euryarchaeota	*Methanobrevibacter oralis*

Supplementary Table 24 | 454 library amplification and sequencing results

			Amplifications[b]			Total Reads Post-QC		
Extract(s)	Individual	DNA (ng)[a]	V3	V5	V6	V3	V5	V6
Calculus								
S8	G12 (1:49 dilution)	4.4-5.5	5	6	6	6155	5362	8928
S14	B17 (1:49 dilution)	12.0	5	3	3	8077	4491	6644
S10	B61 (1:4 dilution)	5.4	3	3	3	7469	5957	6179
S15	B78 (1:49 dilution)	6.0	3	3	3	5260	4212	4036
Root (pooled)								
S16, S17	G12[c]	2.6-3.6	3	3	3	6653 5866	5788 5272	4718
S18, S19	B17	2.0	3	3	3	5224	4955	3867
S20, S21	B61	2.4	3	4	3	7033	5516	4354
S22, S23	B78	3.2	3	3	5	5088	4695	5726
Pathological Tissue (pooled)								
S24, S25	B17 carious root	0.7-2.0	5	5	5	5524	3987	2945
S26, S27	B17 alveolar abscess	2.5	3	3	3	5122	4007	1697

Notes:

[a]Amount of extract DNA added to each PCR reaction.

[b]Number of amplifications required to yield ≥300ng pooled DNA post-PCR cleanup required for 454 sequencing.

[c]G12 root libraries for the V3 and V5 regions were sequenced again in a subsequent run as duplicates.

Supplementary Table 25 | RDP pyrosequencing pipeline OTU assignment statistics

Sample	Region	Post-QC reads	Passing additional filters	Assigned to OTUs	Different OTUs	SRA accession
Calculus						
G12	V3	6155	4936	3321	156	SRS480530
G12	V5	5362	4994	3799	170	SRS480529
G12	V6	8928	7740	5409	142	SRS473751
B17	V3	8077	6523	4573	223	SRS473753
B17	V5	4491	4124	3533	193	SRS473754
B17	V6	6644	5682	4355	152	SRS473756
B61	V3	7469	6045	4022	351	SRS473752
B61	V5	5957	5442	3918	367	SRS480531
B61	V6	6179	5236	3540	235	SRS480532
B78	V3	5280	4275	3058	186	SRS473755
B78	V5	4212	3876	2712	218	SRS473757
B78	V6	4036	3429	2332	147	SRS473758
Abscessed alveolar bone						
B17	V3	5122	4249	3575	243	SRS473769
B17	V5	4007	3655	3361	305	SRS473771
B17	V6	1697	1458	1265	156	SRS473770
Carious dentine						
B17	V3	5524	4630	3814	327	SRS473766
B17	V5	3987	3692	3317	356	SRS473767
B17	V6	2945	2538	2178	242	SRS473768
Tooth Root						
G12	V3	6653	5524	4214	417	SRS480533
G12	V3	5866	4818	3611	402	SRS480534
G12	V5	5788	5332	4562	451	SRS480535
G12	V5	5272	4829	4215	427	SRS480536
G12	V6	4718	4017	2840	313	SRS480537
B17	V3	5224	4392	3028	285	SRS473759
B17	V5	4955	4589	3550	289	SRS473760
B17	V6	3867	3260	1455	198	SRS473761
B61	V3	7033	5875	3390	350	SRS480538
B61	V5	5516	5209	4442	368	SRS480539
B61	V6	4354	3744	1608	236	SRS473762
B78	V3	5088	4256	3059	308	SRS473763
B78	V5	4695	4292	3654	369	SRS473765
B78	V6	5726	5031	3279	306	SRS473764

Supplementary Table 26 | Contig assembly statistics

	B61 (S1-S4)	G12 (S5-S8)
Reads		
Shortest read (bp)	25	25
Longest read (bp)	96	96
Median read length (bp)	87	96
Mean read length (bp)	79	86
Total reads	46,633,826	38,253,574
Contigs		
Shortest contig	100	100
Longest contig	10,705	15,811
Median contig length	146	150
Mean contig length	197	209
Total contigs	1,099,672	905,601

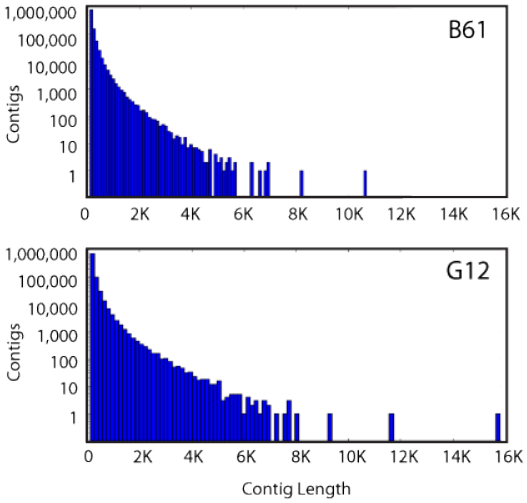

Supplementary Table 27 | Samples and extractions analyzed using shotgun proteomics

		Sample	Tissue	Extract ID	Extract Lab	Seq. Lab	Source	PRIDE Accession
Ancient	Human	G12	Calculus	Z1[a]	CGG	CPR	Q-Exactive Orbitrap	34625
		G12	Calculus	Z2[b]	CGG	CPR	Q-Exactive Orbitrap	34607
		G12	Calculus	Y48	YORK	PABL	maXis LC-MS/MS	34616
		B17	Calculus	Z27	ZEM	FGCZ	LTQ-Orbitrap Velos	34619
		B61	Calculus	Z46[c]	ZEM	FGCZ	LTQ-Orbitrap Velos	34627
		B61	Calculus	Z46[c]	ZEM	PABL	maXis LC-MS/MS	34515
		B61	Calculus	Y46	YORK	PABL	maXis LC-MS/MS	34628
		B78	Calculus	Z28	ZEM	FGCZ	LTQ-Orbitrap Velos	34614
		G12	Root	Z23	ZEM	FGCZ	LTQ-Orbitrap Velos	34624
		B17	Root	Z24	ZEM	FGCZ	LTQ-Orbitrap Velos	34605
		B61	Root	Z25	ZEM	FGCZ	LTQ-Orbitrap Velos	34609
		B78	Root	Z26	ZEM	FGCZ	LTQ-Orbitrap Velos	34626
		B17	Carious dentine	Z29	ZEM	FGCZ	LTQ-Orbitrap Velos	34618
		B17	Bone abscess	Z30	ZEM	FGCZ	LTQ-Orbitrap Velos	34606
	Fauna	F1	Cementum/ calculus[d]	Z31	ZEM	FGCZ	LTQ-Orbitrap Velos	34617
		F5	Cementum/ calculus[d]	Z33	ZEM	FGCZ	LTQ-Orbitrap Velos	34608
Modern	Human	P1	Calculus	Z5[a]	CGG	FGCZ	LTQ-Orbitrap Velos	34611
		P1	Calculus	Z6[b]	CGG	FGCZ	LTQ-Orbitrap Velos	34623
		P2	Calculus	Z7[a]	CGG	FGCZ	LTQ-Orbitrap Velos	34612
		P2	Calculus	Z8[b]	CGG	FGCZ	LTQ-Orbitrap Velos	34620
Negative	Control	N	Negative control	Z34	ZEM	FGCZ	LTQ-Orbitrap Velos	34613
		N	Negative control	Z47	ZEM	FGCZ	LTQ-Orbitrap Velos	34621
		N	Negative control	K82	CGG	CPR	Q-Exactive Orbitrap	34622
		N	Negative control	Z47	ZEM/ YORK	PABL	maXis LC-MS/MS	34610

Notes:

[a]Extraction from first supernatant fraction (EDTA-dialyzed fraction).

[b]Extraction from second supernatant (protein pellet) fraction.

[c]This extract was sequenced in two laboratories.

[d]This sample contains both dental calculus and crown cementum.

Supplementary Table 28 | Spectrum assignment and quality statistics for ancient and modern human dental calculus samples using ProteinPilot v.4

	Ancient Dental Calculus[a]	Modern Dental Calculus[b]
Basic statistics		
Total spectra	16,304	20,928
Peptide assignment conf. threshold (%)[c]	95.5	95.9
Assigned peptides	754	3,447
Proportion of assigned peptides (%)	5	17
Over- and under-cleavage		
Fully tryptic assigned peptides (%)	89	69
Assigned peptides with full cleavage (%)	93	77
Modifications		
Unmodified assigned peptides (%)	50	60

Notes:

[a]Includes pooled spectra from B17 (Z27), B61 (Z46), and B78 (Z28).

[b]Includes pooled spectra from P1 (Z5, Z6) and P2 (Z7, Z8).

[c]Confidence level determined by distinct peptide level 5% local FDR.

Supplementary Table 29 | Contaminants identified in non-template extraction negative controls

Accession	Unique Peptides	Assigned Spectra	Protein Coverage	Gene	Description	Taxon
P00761	69	321	90.5%	TRYP	Trypsin	*Sus scrofa*
P04264	31	80	44.1%	KRT1	Keratin, type II cytoskeletal 1	*Homo sapiens*
P13645	27	77	52.4%	KRT10	Keratin, type I cytoskeltal 10	*Homo sapiens*
P35908	22	32	46.3%	KRT2	Keratin, type II cytoskeletal 2 epidermal	*Homo sapiens*
P02452	16	21	13.9%	COL1A1	Collagen alpha-1(I) chain	*Homo sapiens*
P35527	13	35	26.8%	KRT9	Keratin, type I cytoskeletal 9	*Homo sapiens*
P08123	13	16	13.9%	COL1A2	Collagen alpha-2(I) chain	*Homo sapiens*
P13647	9	10	25.4%	KRT5	Keratin, type II cytoskeletal 5	*Homo sapiens*
-	9	58	-	TRYPA5	Promega trypsin artifact	-
P02533	7	9	19.9%	KRT14	Keratin, type I cytoskeletal 14	*Homo sapiens*
P02769	6	7	7.6%	ALB	Serum albumin	*Bos taurus*
Q8N1N4	2	2	5.6%	KRT78	Keratin, type II cytoskeletal 78	*Homo sapiens*
P13646	2	2	13.8%	KRT13	Keratin, type I cytoskeletal 13	*Homo sapiens*
Q63PZ6	2	2	5.8%	TUF	Elongation factor Tu	*Proteobacteria*

Notes:
Data are from MudPIT results for negative controls Z34 (FGCZ), Z47 (FGCZ, PABL), and K82 (CPH). Mascot searched against the UniProtKB/Swiss-Prot, Human Oral Microbiome, and Soil databases. Only results with a minimum peptide probability of 95%, a minimum of 2 peptides, and a minimum protein probability 99% were accepted for identification. Accessions are from UniProtKB/Swiss-Prot.

III. Supplementary Note

The following note provides further detail on the study design and methods. The study can be broken down into four main categories: 1) microscopy and spectroscopy, 2) stable isotope ratio mass spectrometry, 3) metagenomic analysis, and 4) metaproteomic analysis. Within each category, multiple analytical techniques were employed. Supplementary Figure 17 presents an overview of the samples and analytical techniques employed in this study.

1. Archaeological Context

1.1 Site Location

In 1989/1990, the Westphalian Museum of Archaeology excavated the architectural ruins of a medieval parish church located in the town of Dalheim near Lichtenau, Germany (Am Kloster 9, 33165 Lichtenau, Germany).[76] On the basis of archaeological evidence, a wooden church was probably first constructed at the site during the Carolingian period (c. 800 CE), and later replaced with a small stone structure in the 9th century. This church was later razed and replaced with St. Petri, a new stone church built in the early 12th century. In the late 12th or early 13th century, an Augustinian convent (Kloster Dalheim) was added to the western end of the St. Petri. Outbreaks of plague in 1348/1350 and 1383 greatly reduced the population of the region, and a fire destroyed the convent and church during a late 14th century battle.[76] After a short period of abandonment, the complex was repaired and converted into an Augustinian monastery c. 1429, and there is reference to the production of manuscripts in the monastery's scriptorium.[76] Fire again damaged the building in 1436[76], and by 1470 the monastery was relocated to new buildings, including a larger church, dormitory, refectory, kitchen, brewery, bakery, and workshops, constructed to the west of St. Petri. The former St. Petri church fell into disuse and the eastern portion of the church was rebuilt in the 18th century as a small, one-room chapel, the St. Bartholomew Chapel.[76]

During excavation of the former Dalheim church and convent more than 100 burials were encountered (Supplementary Figure 18), and skeletal remains (MNI=151) of both sexes ranging in age from neonates to elderly adults were recovered.[75] All individuals were likely buried in simple shrouds, as no evidence of coffin use was observed.[76] The majority of individuals were excavated from a cemetery in area B (n=126), while a smaller number (n=25) were excavated from area G immediately to the east of the church. Disarticulated skeletal remains lacking primary context were recovered from area W on the northern side of the church, where a water mill was later constructed. In addition to human remains, isolated faunal bones and teeth were also recovered during excavation. In 2005, the Dalheim skeletal assemblage was donated to the University of Zürich's Institute of Anatomy, where it is now curated.

1.2 Radiocarbon Dating

To better date the Dalheim skeletal assemblage, bone samples from four skeletons from areas B and G were submitted for AMS radiocarbon dating at the ETH Laboratory of Ion Beam Physics (Supplementary Table 5). The calibrated radiocarbon dates establish the cemetery's period of use

as ca. 950-1200 CE and indicate that the Dalheim burials are primarily associated with St. Petri's function as a parish church with some possible carryover to the period of the church's function as a convent.[75]

2. Paleopathology Assessment of Human Remains

Examination of the Dalheim skeletal assemblage revealed that relatively complete adult dentitions were preserved for 46 individuals. The dentitions of these individuals were then photographed and assessed for paleopathology indicators by Dr. Roger Seiler, DDS. For each dentition, each tooth was scored for 1) presence/absence, 2) abrasion, 3) caries, 4) calculus, and 5) periodontal destruction (Supplementary Table 6).

3. Selection of Ancient Human Specimens

After paleopathology assessment, the Dalheim human assemblage was screened for the following criteria:

1. >50% of adult dentition present
2. Caries active (at least one score of 1-4)
3. Moderate or heavy calculus with a total weight >100mg
4. Moderate or severe periodontal destruction for >25% teeth scored

Multiple individuals met these criteria and four individuals were randomly selected for further study: G12, B17, B61, and B78 (Supplementary Figure 1).

3.1 Osteological and Paleopathological Description of Selected Ancient Individuals

Age, sex, and skeletal paleopathology were obtained from previous reports.[75] For individuals G12, B61, and B78, sex was successfully confirmed using a genetic sex typing assay (see section 6.1.6). Dental pathologies follow the observations made in this study.

<u>G12</u>
Individual G12 is an adult female of middle age (35-50 years). Slight spondylosis deformans was observed on the cervical vertebrae (C6 and C7), but no further skeletal pathologies were reported. The dentition of G12 was complete with the exception of the antemortem loss of both lower M3s and the postmortem loss of the upper right M3. Postmortem breakage of the maxilla led to the destruction of the alveolar bone from the upper right I1 to P3. Tooth abrasion was generally mild (scores 0-2), although the upper central incisors and the occlusal surfaces of the upper and lower M1s were heavily worn (score 3). The dentition was generally sound with only three teeth exhibiting enamel opacities and discolorations indicative of possible early stage caries formation. Periodontal destruction was mild to moderate, with attachment loss of 2-5mm observed for all measured teeth (scores 2 and 3). Dense dental calculus deposits were observed adhering primarily to the enamel crown and extending onto the root slightly beyond the DEJ along the former gingival margin of the dentition. These deposits were particularly heavy at the anterior of the dentition along both the lingual and buccal surfaces of the incisors and canines. Although the calculus deposits were primarily supragingival, the lower-most portions of the

shelf-like deposits likely extended into the periodontal pocket and thus include subgingival calculus.

B17

Individual B17 is a middle-aged adult of indeterminate sex (40-55 years). No significant skeletal pathologies were reported. The skull of B17 was severely damaged postmortem. The maxilla was heavily fractured but could be reconstructed with the exception of the alveolar bone supporting the upper right I1 and I2 and the upper left M3. The upper right I1 was lost postmortem, but the maxillary dentition was otherwise complete. The mandible was entirely missing, but several mandibular teeth were recovered, including all of the lower incisors, the lower right P4 and the lower left P3 and P4. Overall dental health was poor. Periodontal destruction, as characterized by maxillary attachment loss, was moderate to severe with one third to more than one half of each tooth root exposed (attachment loss of >4mm). Large dental abscesses with drainage fistulas were observed in the alveolar bone supporting the upper right P3 and the upper left M2. The interior abscess margins were characterized by the presence of reactive bone growth with a smooth, woven appearance. The crown of the upper left M2 was approximately 50% destroyed by a large caries penetrating to the pulp cavity. The exposed dentine was dark in color and the discoloration continued down the root canal to the base of the root and the site of an alveolar abscess. Additional dentinal caries were observed in the upper right M2, the upper left M3, and the lower incisors. Enamel opacities were observed throughout the dentition. Tooth abrasion was moderate with dentine exposure for nearly all teeth, and heavy abrasion (score 3-4) was observed on the anterior upper and lower teeth. Thick, crown-obstructing deposits of dental calculus were present on the right and left maxillary molars and upper left P4. These diffuse and amorphous deposits extended far below the DEJ and as far as the root bifurcations on two molars. The remaining maxillary and mandibular teeth exhibited only a thin band of dental calculus along the former gingival margin.

B61

Individual B61 is an adult male of middle age (40-50 years). Spondylosis deformans of the thoracic (T4) and lumbar (L1-L4) vertebrae was observed, as well as spina bifida of the L5 and sacrum. No further significant skeletal pathologies were reported. The maxillary dentition of B61 was complete with the exception of the antemortem loss of the upper right and left M2 and M3, and the postmortem loss of the upper right I2 and upper left C1. Only the bottom tips of the roots of the upper central incisors were present, suggesting antemortem tooth loss through facial trauma. The mandibular dentition was complete with the exception of the antemortem loss of the lower right M2 and the lower right and left M1s. Dental abrasion was moderate for most teeth (score 2), but greater for the lower left M2 and upper left M1 where the entire occlusal surface was worn to dentine (score 3). Four dentinal caries were observed on the mandibular premolars and molars, and enamel opacities were observed on the upper molars and upper left premolars. Periodontal destruction was moderate to severe with attachment loss of 4-5mm (one third to one half of the root) scored across the mandibular teeth and attachment loss of 4 to >6mm (one third to more than one half of the root) scored for the maxillary teeth. Thick, shelf-like and crown-obstructing deposits of diffuse calculus were present on the buccal aspect of the lower incisors and canines and on the lingual aspect of the lower left P3. Although primarily supragingival, portions of the calculus extended below the DEJ and onto the root surfaces. Calculus deposits

formed thin bands following the former gingival margin on the lingual aspect of the lower incisors and canines and on the remaining teeth.

B78

Individual B78 is an adult female of middle age (45-60 years). No significant skeletal pathologies were reported. The maxillary dentition of B78 was complete except for the antemortem loss of the left and right M2 and the postmortem loss of the right I1 and left P3. The mandibular dentition was complete except for the antemortem loss of the right and left M2 and M3 and the postmortem loss of the right P3 and C1. Dental abrasion was generally mild with minor wear of enamel cusps and some dentine exposure. Abrasion of the upper right P3 was heavy with the entire occlusal surface worn to dentine (score 3). Minor enamel opacities were observed for multiple maxillary teeth and the lower left M3. Dentinal caries were observed in the upper right M1 and M3. Postmortem damage to the maxilla made it difficult to reconstruct the alveolar margin, and thus maxillary attachment loss could not be scored. Periodontal destruction in the mandibular dentition was mild to moderate (up to one half of the root exposed) with attachment loss of 2-5mm for all teeth except the M3s, where the attachment loss was <1.5 mm. Moderate dental calculus deposits were present in the same pattern as observed for individual B61, namely shelf-like deposits on the buccal aspect of the lower incisors and canines and the lingual aspect of the lower left P3. Although primarily supragingival, portions of the calculus extended below the DEJ and onto the root surfaces. As with B61, only minor bands of dental calculus were observed along the former gingival margin of the lingual aspect of the lower incisors and canines and on the remaining teeth.

3.2 Comparative Material and Environmental Controls

As comparative material and in order to control for environmental contaminants, additional samples were collected from the Dalheim cemetery and from modern clinical patients.

Ribs

One rib from each of the four Dalheim individuals (G12, B17, B61, and B78) was collected to provide comparative bone stable isotope data for paleodietary interpretation.

Faunal Material

Isolated faunal bones and teeth were observed comingled with human remains in the storage containers of several burials and from the W area of the site. The faunal remains are consistent with secondary context waste that was unintentionally incorporated into grave fill during burial. Identified faunal taxa include cow (*Bos taurus*), pig (*Sus scrofa*), and sheep/goat (Caprinae).

Burial Matrix

Burial matrix (soil) was found adhering to the bones of several individuals in the Dalheim skeletal assemblage. Several grams of burial matrix (M1-M5) were collected from four individuals excavated from the B area of the cemetery (B28, B55, B84, and B85) and from one human femur recovered from area W.

Modern Comparative Material

Modern dental calculus samples were donated under informed consent by patients visiting a dentistry practice for routine dental work in Zürich, Switzerland. Dental calculus samples from fifteen adult patients (P1-P15) between 44 and 82 years of age were selected as modern controls (Supplementary Table 7). All sample and patient information was irreversibly anonymized with a six-digit code. Protocols relating to the collection and analysis of the clinical dental samples were approved by the Zürich Ethics Commission (Ref. Nr. KEK_ZH-Nr. 2012-0119).

3.3 Sample Collection

Archaeological Human Dental Calculus

Dental calculus was collected from human and faunal teeth using a bleach-sterilized dental scalar. All collection was performed within the Centre for Evolutionary Medicine (ZEM) Ancient DNA Laboratory and protective clothing, masks, and gloves were worn at all times. Total dental calculus collection was performed for individuals G12 and B61, yielding 569 mg and 593 mg, respectively. For individual B17, the upper left M2 was set aside, and all calculus was removed from the remaining dentition, yielding a total of 392 mg. For individual B78, the lower left I2 and P3 were set aside for histological analysis, and all calculus was removed from the remaining dentition, yielding a total of 119 mg.

Calculus collected from each individual was combined into a single tube, mixed, and coarsely ground with a bleach-sterilized micropestle. Although it has been demonstrated that supragingival and subgingival calculus have distinct etiologies and differing clinical significance,[77] no attempt was made to separate these two calculus types as it was not possible to distinguish between supragingival and subgingival calculus in our archaeological specimens. In the absence of soft tissue it is difficult to reconstruct with exact precision the location of the former gingival margin, and archaeological subgingival calculus is not darkened or discolored, as it may appear in living patients. For this reason, it was decided to combine all calculus together for analysis without making further distinctions between supragingival and subgingival calculus.

Archaeological Faunal Calculus and Cementum

Dental calculus was collected from two faunal specimens, one sheep (F1) and one cow (F5), recovered from archaeological sediments in areas W and B, respectively (Supplementary Figure 19). Dental calculus in animals with hypsodont teeth can be difficult to identify by visual inspection alone as these animals also produce cementum on their crowns that can mimic the appearance of dental calculus in archaeological samples. For the faunal specimens in this study, all mineralized material adhering to the tooth crowns was collected and presumed to contain a mixture of calculus and cementum.

Modern Clinical Patient Dental Calculus

Dental calculus samples from seven volunteers were collected during routine dental cleaning performed by a dental hygienist in a Swiss dental practice. Dental calculus was removed from the teeth using a sterile steel dental scalar and either placed directly into a sterile tube or wiped onto a sterile dental bib. The bib was folded, sealed in a sterile tube, and stored frozen until analysis. Seven teeth (one with adhering dental calculus) were obtained from volunteers following tooth extraction in the same dental practice in preparation for dental implants. The

entire tooth (with dental calculus in place) was sealed in a sterile tube and stored frozen until analysis.

Archaeological human carious dentine and alveolar bone abscess
The upper left M2 of individual B17 is characterized by a massive caries that has penetrated to the pulp cavity and destroyed approximately 50% of the crown. The exposed dentine and pulp chamber is darkened and this discoloration continues down the root canal where the root enters a large abscess in the alveolar bone below (Supplementary Figure 20). Carious dentine was collected by coarsely grinding the tooth root with a bleach-sterilized agate mortar and pestle and collecting discolored dentine into a single tube. Diseased bone from the dental abscess was collected by trimming away excess healthy alveolar bone around the abscess and grinding the diseased/reactive alveolar bone with a bleach-sterilized agate mortar and pestle.

Archaeological human teeth
Tooth roots (dentine and cementum) are often a site of postmortem microbial attack by environmental bacteria and fungi.[51] Microorganisms invade the tooth via the apical foramen at the base of the tooth root and travel up the root canal and into the pulp cavity. From the pulp cavity, acid-producing bacteria then invade the dentine, often traveling along the dentine tubules. At the same time, microbial attack can also proceed from the outside of the tooth inwards, often beginning with the breakdown and infiltration of cementum. Because tooth roots are generally sterile during life and rapidly invaded by environmental bacteria postmortem, tooth roots were collected from each of the individuals under study (G12, B17, B61, B78) as a control for environmental contamination. Two healthy, non-carious, single-rooted teeth (canine or premolar) were collected from each individual. The crown was removed with a diamond-bit saw and the tooth root was crushed to a coarse powder with a bleach-sterilized agate mortar and pestle. A third healthy tooth root was collected from each individual and set aside for genetic sex testing.

Archaeological human ribs
Ribs from G12, B17, B61, and B78 were cut to yield a fragment of approximately 2-3cm in length. This fragment was set aside for bone collagen carbon and nitrogen light stable isotope analysis.

Burial Matrix
Burial matrix (soil) originating from the Dalheim cemetery was collected as an environmental control. Burial matrix was found to be adhering to several unwashed skeletons in the Dalheim skeletal assemblage. Burial matrix was removed from the long bones of individuals B28, B55, B84, B85, and an unnumbered individual from the W area of the site using a sterile steel spatula. The five burial matrix samples were numbered sequentially (M1-M5) and set aside for genetic analysis of microbial diversity in the burial environment.

4. Microscopy and Spectroscopy

4.1 EM

4.1.1 Sample preparation

Electron microscopy analysis was carried out at the Centre of Dental Medicine (Zentrum für Zahnmedizin, ZZM) in the Institute of Oral Biology at the University of Zürich, Switzerland. A mandibular incisor from individual B78 was hydrated in Ruffer solution (1% Na-carbonate in 30% ethanol) and then fixed for 1 day at room temperature in a solution of 4% paraformaldehyde and 0.2% glutaraldehyde in 0.1 M phosphate buffer (pH 7.2). After an overnight rinse in 0.185 M Na-cacodylate buffer (pH 7.2), the specimen was dehydrated in ethanol, cleared in xylol, and embedded in methyl methacrylate (MMA). Using a diamond band saw (EXAKT, Norderstedt, Germany) polymerized blocks were divided along the long axis of the tooth. One half was glued on SEM aluminium stubs, polished with silicon carbide paper and diamond paste, and coated with a 10-15 nm thick layer of carbon.

4.1.2 EDS and SEM

The prepared tooth section was examined in a Tescan VEGA (Tescan, Brno, Czech Republic) scanning electron microscope (SEM) using backscattered electron (BSE) imaging at 20 kV and a working distance of 23 mm. At the same SEM settings, energy-dispersive X-ray spectroscopy (EDS) with a Si(Li) detector (Oxford Instruments, Abingdon, UK) served for analyzing the composition of the dental calculus. Using the INCA energy software (Oxford), elemental maps were derived from 300 frames of 512x384 px recorded with a counting time of 40s/frame. Dentine and dental calculus were compared at low and high magnification, revealing stark differences between the two tissues (Supplementary Figure 6).

Taphonomic degradation is highest in the lower portion of the root in proximity to the root canal and apical foramen, which serves as the primary postmortem entry point for environmental microbes into the pulp cavity. This finding contrasts with the common practice of sampling the tooth root tip to obtain host DNA from archaeological specimens. While DNA content in this region may be high, our results suggest that a disproportionate amount of this DNA is likely to be post-depositional microbial, rather than host, in origin.

4.2 Histology

4.2.1 Preparation of Histological Sections

Histological sections of modern (P3) and ancient (B78) dental calculus were prepared and analyzed in the Institute of Anatomy and the Center for Microscopy and Image Analysis at the University of Zürich, Switzerland. For orientation, the dental calculus surface was marked with permanent black ink and the entire tooth (with *in situ* calculus) was then rehydrated in Tyrode rehydration solution for 48H at +4°C and fixed in 4% paraformaldehyde for 48h at +4°C. The tooth was briefly rinsed in running water and decalcified in Immunocal (Decal Chemical, Congers, NY) at RT for ≈48h, until the dental calculus had separated from the tooth surface and was susceptible to probing with a needle. The dental calculus was then immersed in a solution of 10% sucrose in PBS for 1 hour, followed by 20% sucrose for 1 hour, followed by 30% sucrose overnight at +4°C. To prepare for cryosectioning, the dental calculus was embedded in Tissue-Tek O.C.T. Compound (Sakura Finetek Europe B.V., Zoeterwoude, Netherlands), wrapped in an aluminium foil capsule, and slowly frozen to -70˚C in 50 ml 2-methylbutane (MB) on dry ice. The embedded dental calculus was mounted on a cryostat (Hyrax C 60, Zeiss) and cut in 5µm

thick sections at -25°C. The sections were mounted on SuperFrost Plus slides (Menzel-Glaeser, Braunschweig, Germany).

4.2.2 Gram Staining

Cryosections were rehydrated in deionized water and stained according to manufacturer protocols (Gram Stain Kit, HT90, Sigma-Aldrich, USA) with modifications: Crystal Violet Solution -1 min, Iodine Solution -5 min, differentiate in alcohol/acetone 1:1, stain in Safranin Solution 0.3% in 20% ethyl alcohol – 5 sec. Sections were rinsed twice in absolute alcohol, cleared in xylene, and mounted with Eukitt mounting medium (Sigma-Aldrich, St. Louis, MI, USA). Samples were analysed using an Axio Imager M2 (Zeiss, Germany) with a CX-9000 camera (MBF Bioscience, USA) and Stereo Investigator software (MBF Bioscience, USA). Comparison of modern and ancient dental calculus histological sections reveals a high degree of similarity in cell density, presence of voids, discrete features (e.g., linear arrangements of gram positive bacteria separating zones of gram negative bacteria), and overall structural organization at multiple magnifications (Supplementary Figure 8).

4.2.3 Hoechst staining

Following rehydration, cryosections were washed twice with phosphate-buffered saline (PBS) and stained with Hoechst 33342 fluorescent dye (Life Technologies, USA) at a concentration of 1.5 μg/ml at RT overnight in darkness. After three washes with PBS samples were mounted with fluorescence mounting medium (Dako, USA) and visualized using a Leica DMI6000 B microscope with a Leica DPC350 FX camera and LAS AF 2.3.0 software (Leica, Heidelberg, Germany). Both modern and ancient dental calculus histological sections exhibit high DNA density (Supplementary Figure 9). DNA fluorescence appears to be resolvable to discrete areas approximately 0.5-1 μm in diameter, suggestive of *in situ* DNA presence within cells.

4.3 Microfossil Microscopy

4.3.1 Sample Preparation

Microfossil analysis was performed at the Laboratory of Starch Analysis at the School of Archaeology and Ancient History at the University of Leicester. Dental calculus from each ancient human individual (G12, B17, B61, and B78) and one ancient cattle specimen (F5) was investigated using optical microscopy for the presence of preserved dietary microfossils and other micro-debris. Samples were first weighed before analysis (Supplementary Table 8) and then transferred to sterile 15mL centrifuge tubes.

Contamination precautions
As with all microfossil analysis, it is essential to take precautions to prevent and monitor potential sources of contamination. The three main sources of contamination in ancient dental calculus research are:

1. Microscopic food contamination on the hands of the analyst.

2. Modern contamination of airborne pollutants or settled dust moved during collection, preparation, and analysis of the material.
3. Burial and modern soil attached to the dental calculus in micro-cracks not visible to the naked eye.

The following procedures were taken to avoid analyst contamination: sterile masks and gloves were worn at all times.

The following procedures were taken to avoid modern contamination by airborne pollutants or dust: Before transport to the University of Leicester, the dentition of each individual was removed from its storage container, photographed, and transferred to a sterile plastic bag and sealed. Sterile gloves and masks were worn at all times. The bag was then transported to the University of Zürich's Ancient DNA Laboratory where dental calculus samples were collected and packaged for transport under sterile conditions. Once at the University of Leicester, samples of settled dust were regularly collected in the area where the procedures of extraction and mounting were to take place. This allowed the identification of one contaminant, a single *Lycopodium* sp. spore, that was later found in a slide prepared for B61. As several spores of *Lycopodium* sp. were recovered in all dust samples collected from the laboratory that day, this was excluded from analysis. We believe that these spores entered the laboratory from a nearby palynology facility where this spore is used to normalize pollen counts on slides. No other remains present in the dust samples were recovered in any of the ancient dental calculus slides.

The following precautions were taken to avoid soil contamination: The 15mL tubes containing dental calculus were filled with ultrapure water and vortexed at high speed to liberate any loosely-attached debris or soil contaminants present on the surface of the dental calculus. The calculus fragments from B61 and B78 were large enough to be handled with needle-nosed forceps. For these samples, the calculus was removed, washed with ultrapure water, and transferred to a new 15mL tube. This sequence was repeated three times. Dental calculus samples from G12 and B17 were too small to be handled with forceps. Instead, the water and suspended particles in the tube were carefully siphoned out using a sterile pipettor, while not disturbing the settled dental calculus fragments at the bottom of the tube. This procedure was repeated five times, until the water appeared clear. Finally, the calculus samples of B61 and B78 were bathed in 0.04M HCl for five minutes and sonicated for 30s to encourage the removal of the outermost calculus layer along with any residual contaminants. Calculus samples of B17 and G12 were bathed in 0.04M HCl for one minute and then washed three times with ultrapure water.

Extraction and Mounting
Following decontamination procedures, the calculus samples were transferred to tubes containing 0.05M HCl and allowed to decalcify under agitation for one week at 4˚C. Microfossils and micro-debris released by the decalcifying dental calculus were then carefully collected by inserting a sterile pipettor into the bottom of the tube and transferring the insoluble particles to a sterile microscope slide. To the remaining undecalcified calculus fragments, we replenished the tube with 0.05M HCl, sonicated the tube for one minute, and then allowed it to further decalcify under agitation at 4˚C for five days. The above procedure was repeated until the dental calculus was completely dissolved, up to four times (B61). At each interval, the liberated microfossils and micro-debris were mounted onto a sterile microscope slide so that the

decalcification process could be monitored in sequence. This method of extraction was developed because it allows for a *pseudo-in situ* visualization of micro-debris. Using this method, it was possible to observe microfossils still partially embedded within dental calculus matrix (Supplementary Figure 5a), thereby validating the ancient origin of the microfossil. Using this method, it was also observed that certain kinds of debris entered the dental calculus in discrete quantities or lumps.

The microfossils and micro-debris removed from the decalcification tube were mounted onto glass slides to which a drop of a 50:50 mixture of glycerol and water had been added. This is necessary for microfossil description and identification, as it allows the rotation of three-dimensional objects such as phytoliths, pollen, and starch granules. A sterile cover slip was added to the slide, and a drop of clear nail polish was placed at each corner of the slide to keep it in place. This procedure leaves the side of the slide unsealed, allowing staining or rehydration if necessary. Following analysis, the slide was sealed on all sides with nail polish before archiving.

Reference collections
In addition to published resources, a good reference collection is essential for accurate microfossil analysis. For this analysis, a custom-built dietary reference collection was consulted that includes pollen grains, starch granules, and phytoliths for most common known major plant crops, weeds, and wild taxa used for food, economic, and medicinal purposes in Northwest Europe, with a particular emphasis on the medieval period. In addition to unprocessed material, the collection also includes chewed, cooked, and otherwise prepared starchy material. An additional reference collection at the University of Leicester Archaeological Services (ULAS) containing textiles (e.g, cotton, flax, hemp, ramie, wool and silk), pottery fragments, and a variety of environmental and occupational pollutants (e.g., wood dust, charcoal, and ash) was also consulted during identification.

4.3.2 Identification of Microfossils and Micro-debris

Slides were analyzed using a Zeiss compound microscope at magnifications of 200x, 400x, and 630x (oil immersion), as well as under polarized light. A diverse range of microfossils and micro-debris was observed, with individual finds ranging in size from sub-micron particles to structures with dimensions in excess of 200μm. All finds were described, recorded, and photographed. After analysis, the slides were archived at 4˚C. Material described as *in situ* consists of micro-debris that were recovered still partially embedded within the calculus matrix or showing other clear evidence of dissolving calculus adhering to it. Micro-finds up to 50 μm in diameter could be rotated, implying that the glycerol:water layer was at least this thick. As multiple layers of debris can overlap within this space, various techniques were employed to isolate the finds for better viewing. A fine acupuncture needle was used to impart light pressure on the cover slip of the slide in order to make the micro-debris move and turn. Normally if the remains were indeed *in situ*, the dental calculus would hold the debris in place or restrict their movement. Overlapping micro-finds were also investigated by adjusting the optical zoom. When the inspected debris was located just above (rather than inside) the fleck of calculus, gentle pressure on the cover slip resulted in the micro-debris and calculus flecks separating, often moving in different directions. Supplementary Table 9 provides a summary of the finds. Detailed descriptions are provided in the text below.

Starch granules
Starch granules were identified at low quantity in three of the four human dental calculus samples (B17, B61, and B78). Starch granules were described and identified according to their overall shape, measurements, surface features, characteristics of the hilum and extinction cross[78], and by comparison with modern reference material. All starch granules were simple in form and yielded a visible extinction cross under polarized light. According to their shape/size, they were divided into four main types:

1. Small round to sub-oval granules, 2-6μm diameter: found in B61 (n=10) and B78 (n=13).
2. Large round to oval granules, 15-25μm diameter: found in B61 (n=1) and B78 (n=1).
3. Large reniform granule, c. 30μm in length: found in B17 (n=1).
4. Large damaged starches: found in B61 (n=1) and B78 (n=1).

Types 1 and 2 were identified in B61 and B78. Their size and shape were consistent with the bimodal distribution encountered in members of the plant tribe Triticeae, which includes the important European cereal crops wheat (*Triticum* spp.) and barley (*Hordeum vulgare* L.). In both samples, the small Type 1 granules displayed a central hilum and presented a more or less bright, centered extinction cross. The large Type 2 granules differed slightly in size and shape. The granule in B61 was round to oval in shape, lenticular in side view, and measured 22μm x 19μm. It displayed lamellae close to the central hilum and small dimples/craters on the surface. The granule in B78 (Figure 4g) was more oval in shape, smaller in size, and lamellae were only visible on the outer part of the granule. Both granules are consistent with starch of the tribe Triticeae, but they may have originated from different species.

A type 3 starch granule, reniform in shape, was observed embedded in the dental calculus matrix of B17 (Figure 4h). The granule was damaged, with a collapsed hilum and a faint extinction cross. Nevertheless, the shape, size (29μm x 22μm), and presence close lamellae in the outer layer of the granule allow an assignment of the granule to the plant family Fabaceae. Fabaceae contains several edible species of legumes commonly consumed during the medieval period in Europe, including lentil (*Lens culinaris* Medikus), broad bean (*Vicia faba* L.), and green pea (*Pisum sativum* L.).

Finally, two type 4 starches were observed in B61 and B78. These large damaged starch granules exhibited cracks and surface distortions but clear lamellae, possessed a clear central hilum but an indistinct extinction cross, and appeared swollen. Based on size and visible features, they may belong to members of Triticeae, although the damage precludes secure identification.

Phytoliths
Only three phytoliths were recovered during the analysis, one from B61 (Figure 4f) and two from the cattle (F5) calculus sample. The identification of phytoliths and their description was carried out using standard literature[79] and our reference collection. The phytolith recovered from B61 consisted of a smooth long cell phytolith (20.4 x 5.4 μm), while the phytoliths from the F5 sample were sinuate and smooth/sinuate long cell phytoliths (12.6 x 3.2 μm and 24.5 x 9.3 μm). The recovered phytoliths are non-diagnostic and are found in the leaves and stems of many monocot plants.

Pollen
Two grains of birch (*Betula* sp.) pollen were observed in B17 and B61 (Supplementary Figure 5b). The pollen grains were identified by their round shape in polar view and their three protruding pores with a thin exine forming a vestibulum underneath each pore.[80] Silver birch (*B. pendula* Roth) and white birch (*B. pubescens* Ehrh.) are the two main European species, and they are pioneer species that grow well on pastures and disturbed ground. Birch trees produce a large quantity of airborne pollen and their presence within human dental calculus suggests that the individuals were exposed to live birch trees during their flowering period of March to May/June.

Other organic finds
In addition to starch granules, phytoliths, and pollen grains, a number of other organic finds were encountered in the dental calculus samples, including animal and plant fibers, yeast cells, and non-diagnostic organic debris.

Plant and animal fibers:
Two types of fibers were observed within the dental calculus samples: bast fibers, most likely from flax (*Linum usitatissimum* L.), and corium fibers, most likely from leather. One damaged and two intact bast fibers were recovered from individuals B17 and B61 (Supplementary Figure 5c). They were identified by comparison with modern and archaeological reference collection fibers using morphological criteria such as dislocations (sometimes referred to as "x features"), the lumen (the fiber's small, central channel), and the aspect of the fibers under polarized light. All bast fibers exhibited a degree of mineralization, as may be expected given their isolation from dental calculus. Although it was not possible to determine the species of origin on the basis of white light and polarized light compound microscopy alone,[81] nettle could be excluded, leaving flax and hemp as the most probable sources. One of the fibers, together with dislocations, exhibited a narrow lumen highly suggestive of flax (Supplementary Figure 5c). Flax is used in the production of linen, a textile in widespread use during the medieval period to produce household cloth and clothing, as well as religious textiles.

Two long fibers of animal origin were recovered from individual B17 (Figure 4e). The fibers, measuring >100μm in length and 5-6μm in diameter, were found to be consistent with leather corium (dermis collagen) fibers in our reference collection, which included both scrapings from tanned leather and fibers obtained from mouth swabs after brief mastication of leather pieces. A study of medieval leatherwork in the medieval city of York found that human tooth marks were present in tanned leather cutoffs, suggesting the mouth was used as a "third hand" during leather production.[82] Because collagen swells when hydrated, the reference collection fibers were also soaked in 0.05M HCl and mounted using 50:50 glycerol:water in order to allow comparison of the modern and ancient fibers under the same conditions. The identification of corium fibers within dental calculus of individual B17 suggests that this individual may have participated in hide or leatherworking.

Yeast:
A large number (>45) of yeast cells, each measuring 2-7μm in diameter, were observed in the dental calculus of individual B78 (Supplementary Figure 5d). Although similar in size to plant starch granules, the yeast cells did not exhibit an extinction cross under polarized light and they lacked other starch features, such as a hilum and lamellae. Moreover, some of the cells exhibited

a darkened circular to oval area on their surface, similar in appearance to a small hole, and resembling a budding scar. Some of the larger cells seemed to have smaller cells attached to them, as is found in budding yeast; however, budding could not be confirmed. Many species of non-budding yeast, especially of the genus *Candida*, are normal inhabitants of the human oral cavity,[52] and wild yeasts (including budding yeasts) have long been used for brewing and as a raising agent for bread in Europe. Unfortunately, it is not possible at present to determine if the yeasts found in the dental calculus of B78 are of dietary origin.

Fine particulate carbon (micro-charcoal):
Micro-charcoal was recovered from G12 (Supplementary Figure 5a), B61, B78, F5, and in greatest quantity from B17. Most micro-charcoal was approximately 10 μm in diameter, but smaller fragments (2-6 μm) were also common, and a few large particles >35 μm in diameter were observed in B61. Possible pathways of incorporation into dental calculus include exposure to domestic, industrial, and wild fires, as well as consumption of smoked or charred foods or medicinals.

Non-diagnostic organic debris:
Non-diagnostic organic debris were recovered in all dental calculus samples, although they were particularly abundant in B61 (Supplementary Figure 5e).

4.4 Raman Spectroscopy

Raman spectrographic analysis was performed in the Department of Physics at the University of York, UK. Micro-Raman analysis was performed on calculus and dentine samples obtained from ancient human individuals (G12, B17, B61, and B78), as well as on modern human calculus (P3 and P13) and modern dentine (P4, P5, P7, P8 and P10) samples, which were used as controls. Five burial matrix soil samples (M1-M5) were also analyzed by Raman spectroscopy to characterize possible contaminants in ancient dental samples.

4.4.1 Methods

Solid specimens were placed onto clean glass microscope slides. For dental calculus, the concave, dental-side of the calculus was oriented face-up, thereby minimizing the risk of contamination from external factors such as the burial matrix. For the dentine, small sections were prepared by gently smoothing down the sample using diamond paper to achieve a flat surface, as this is beneficial for Raman analysis. The modern calculus and dentine samples were briefly irradiated (2.45 GHz, 60s) before analysis to reduce biohazard risk during handling.

Micro-Raman measurements were performed using a HORIBA XploRA instrument x100 magnification and 532nm laser wavelength on the solid calculus and dentine specimens from G12, B17, B61, and B78, as well as on the modern calculus (P3 and P13) and modern dentine (P4, P5, P7, P8 and P10) controls. For the calculus measurements, 1.8mW power at the sample was used; for dentine, which is a harder material, 3.5mW power at the sample was tolerated. The Raman spectra were obtained using 40 1-second acquisitions over which each spectrum was averaged. Careful checking of the calculus and dentine specimens both optically and also

spectrally using dynamic Raman acquisition at 1-second intervals revealed that there was no laser damage at the sample.

Previous Raman studies on calculus[83] used long exposure times of 90s and higher to remove the organic component of the calculus and hence background fluorescence in the Raman results. With careful adjustment of the laser filter, exposure time, and in using the Raman in confocal mode, it was possible to obtain signatures from representative Raman bands in both the calculus and dentine (Supplementary Figure 7). For some of the calculus specimens, the organic C-H stretch Raman band (at ~2940 cm-1) was also obtained and included in this analysis. The retention of the organic component of the calculus is an important indicator of the non-destructive potential of Raman to investigate the calculus material, this being of paramount importance for archaeological samples.

4.4.2 Data analysis

The Raman spectra were baseline corrected and then integrated peak area fitting was performed using HORIBA's peak searching and fitting algorithms with Lorenztian peak choice. To reduce uncertainties from the baseline correction procedure, each spectrum was baseline corrected a minimum of 5 times with the peak searching and fitting determined for each baseline fit. The same Raman settings were maintained, as well as the HORIBA ICS correction was used to standardize each spectrum so that direct comparisons could be made for each respective material sample (calculus and dentine).

4.4.3 Results

Previous Raman studies on enamel and bone have used the peak intensity ratio of the C-H organic peak at ~2940cm-1 to the main (ν1) phosphate (PO43-) band ~960cm-1 (I(CH)/I(P)) to characterize diagenesis.[84,85] Diagenesis in these materials is determined by the loss of organic component, hence it is expected that a drop in the I(CH)/I(P) ratio occurs as a function of increasing time. Other markers that have been used to characterize diagenesis are the integrated peak area ratio between the carbonate (CH32-) band at ~1070cm-1 and the main phosphate band (A(C)/A(P)), which is indicative of demineralization processes.[85] Despite being an obvious marker, the A(C)/A(P) ratio is not 'clean' due to the convolution of the carbonate peak with the phosphate band centered at ~1076cm-1.[86] More recently, studies on fossilized fish teeth have turned to investigating markers in the main phosphate peak only, such as the full width half maximum, which is expected to be reduced due to increased sample crystallinity, and a shift in the peak position to higher wavenumbers.[87]

The main peaks in the Raman spectra of the calculus and dentine were identified in both the ancient and modern samples (Supplementary Figure 7) by comparing each spectrum against published literature.[83,88] Cementum was excluded as a possible sampled material through rigorous examination of the ratio of the main phosphate and C-H stretch ~2940 cm-1 Raman bands, in knowing that cementum was lower in inorganic compared to organic content relative to dentine.[89] Raman analysis of the calculus and comparison with Raman studies on synthetic hydroxyapatite phases[83] confirmed that both octocalcium phosphate (OCP) and hydroxyapatite

(HAP) are present in the ancient dental calculus samples. OCP and HAP are the main inorganic components of mature supragingival and subgingival dental calculus in living subjects.[8]

Raman studies on the Dalheim soil matrix (M1-M5) indicated that the main soil components were calcium carbonate and quartz. Neither of these soil components was found on the calculus samples, therefore confirming that the dental-side of the calculus had not been contaminated.

The I(CH)/I(P) marker was investigated for both the calculus and the dentine specimens (Supplementary Table 10). The decrease in the I(CH)/I(P) maker seen in ancient dentine compared to modern dentine indicates that this material has undergone diagenesis. A larger range of values for this marker in both the ancient and modern dentine is also indicative of inhomogeneity in the material possibly related to diagenetic change. By comparison, the I(CH)/I(P) ratios for the ancient and modern calculus are very similar and are characterized by a narrower range in values, suggesting that ancient calculus is relatively stable against diagenesis.

Given that the organic C-H band is difficult to obtain by Raman analysis on dental calculus and therefore may not be prevalent, the effects of diagenesis on the main phosphate band on its own were also investigated. Results in Supplementary Table 10 show that the integrated peak area of the main phosphate band is larger in the ancient dentine samples than in the modern samples, while for the calculus samples there were no detected changes to the main phosphate peak. Further studies are underway to determine if the main phosphate band alone could serve as a definitive marker for diagenesis.

5. Isotope Ratio Mass Spectrometry

Isotopic analysis was performed in the labs of the Department of Human Evolution and the Research Group on Plant Foods in Hominin Dietary Ecology at the Max Planck Institute for Evolutionary Anthropology, Leipzig, Germany. A rib fragment from each ancient human individual (G12, B17, B61, B78) was sampled for carbon and nitrogen stable isotopic analysis. Prior to analysis, visible contaminants were removed by abrasion with aluminium oxide powder. Collagen extraction proceeded following Richards and Hedges,[57] with the addition of an ultrafiltration step. To summarize, whole bone pieces weighing ca. 300 mg from each of the fragments were demineralized in 0.5M HCl solution at 5˚C for about a week, and then rinsed three times with deionized water until the pH became neutral. This was followed by gelatinization over 48 hours at 70˚C, and later by filtering with a 5μm EZEE© filter and ultrafiltering with >30 kDa Amicon© ultrafilters. The purified solution was finally frozen and lyophilized before being weighed into tin capsules and loaded into the mass spectrometers. The carbon and nitrogen isotope ratios of the collagen were measured in duplicate using a Delta XP continuous-flow isotope-ratio mass spectrometer after being combusted in an elemental analyzer Flash EA 2112 interfaced with it (Thermo-Finnighan, Bremen, Germany). Stable carbon isotope ratios are expressed relative to VPDB (Vienna PeeDee Belemnite) and stable nitrogen isotope ratios are measured relative to AIR (atmospheric N_2), using delta notation (δ) in parts per thousand (‰). Repeated analysis of internal and international standards determined an analytical error always less than 0.2‰ (1σ) for both $\delta^{13}C$ and $\delta^{15}N$. The results of the carbon and nitrogen stable isotope analysis are presented in Supplementary Table 11.

The four Dalheim individuals yielded similar carbon and nitrogen stable isotope values suggesting that they consumed diets of similar composition. The $\delta^{13}C$ values, ranging from -19.5‰ to -18.9‰, show that dietary protein was obtained mainly from terrestrial C_3 resources, a finding that is consistent with a reliance on domesticated C_3 grains of the tribe Triticeae (such as wheat, barley, and rye), and distinct from diets with marine protein input. The $\delta^{15}N$ values range from 9.3‰ to 11.1‰, mainly situating the humans at a high trophic level with respect to European average foodwebs, but within the range of isotopic values measured for populations from the late Mesolithic to medieval periods in present-day Germany.[47-50]

6. Genetic Analysis

Genetic analysis was performed at the Centre for Evolutionary Medicine at the University of Zürich, Switzerland, the Center for GeoGenetics at the University of Copenhagen, Denmark, and Omya A.G., Switzerland. Genetic analysis was performed on the following archaeological source materials from the Dalheim mortuary assemblage: 1) dental calculus 2) dentine, 3) bone, and 4) burial matrix (soil).

6.1 DNA Extraction

All archaeological DNA extractions were performed in a dedicated ancient DNA laboratory facility at the University of Zurich's Centre for Evolutionary Medicine. The Ancient DNA Laboratory, comprised of four self-contained rooms serviced by an independent, HEPA air filtration system, is dedicated solely to ancient DNA research and follows established contamination control workflows, including physical separation from all laboratories in which PCR is performed, unidirectional work flows to avoid cross-contamination, regular sterilization of all work surfaces with bleach solution, and the use of full body Tyvek suits, masks, gloves by all researchers. All chemicals are purchased molecular biology grade and reagents used for amplification are additionally decontaminated in-house using a combination of UV irradiation and reagent pretreatment with heat labile double-stranded DNAse (ArcticZymes, Norway) to purify dNTPs, primers, and enzymes. Within the Ancient DNA Laboratory, a dedicated sample preparation area contains an additional HEPA-filtered vacuum system, and all sensitive aspects of extraction and library preparation were performed in HEPA-filtered laminar flow hoods located in a separate dedicated extraction and PCR set-up room within the laboratory. Additionally, all rooms in the Ancient DNA Laboratory are equipped with a built-in UV irradiation system for daily laboratory decontamination. Non-template extraction controls and reagent blanks are processed in parallel with all samples and are continuously monitored for contamination.

6.1.1 Calculus: Comparison of Extraction Methods

DNA extraction and purification from ancient dental calculus is complicated by the mineralized nature of the calculus matrix and the diverse range of possible bacterial, soil, and plant inhibitory compounds that may be present, including proteins, polysaccharides, polyphenols, terpenoids, humic acids, and metals, among others. Because there are currently no established DNA extraction methods for modern or ancient dental calculus, five different extraction methods were tested and compared using calculus samples from individual B61. These protocols were

developed for their ability to break down or remove a wide range of PCR-inhibitory compounds from complex biological samples. Before extraction, dental calculus samples were gently crushed to a course powder in a 2mL Eppendorf tube.

Extraction Method A: Basic Archaeological Mineralized Tissue Extraction Method
Approx 50mg calculus was digested overnight at 55˚C in 1mL of a buffer of 0.45M EDTA and 10% proteinase K, followed by 24 hours digestion at room temperature on a rotating nutator. After pelleting of the cellular debris, the supernatant was extracted twice with a mixture of phenol, chloroform, and isoamyl alcohol (25:24:1), and a third time with chloroform only. The DNA was isolated on a Qiagen MinElute column and eluted into 20uL EB buffer.

Extraction Method B: Archaeological Soft Tissue Extraction Method
Approx 50mg calculus was digested overnight at 55˚C in 750uL of a digestion buffer comprised of 10mM Tris-HCl, 10mM NaCl, 2% w/v SDS, 5mM CaCl2, 2.5mM EDTA, 40mM DTT, and 10% proteinase K. 250uL 0.5M EDTA was then added and the digestion continued for 48 hours at room temperature on a rotating nutator. After pelleting of the cellular debris, the supernatant was extracted twice with a mixture of phenol, chloroform, and isoamyl alcohol (25:24:1), and a third time with chloroform only. The DNA was isolated on a Qiagen MinElute column and eluted into 20uL EB buffer.

Extraction Method C: Modified Salivary Stone Extraction Method
Approx 50mg calculus was digested overnight at 37˚C in 1mL of a digestion buffer comprised of 0.425M EDTA, 1% SDS, 1% CTAB, 10% proteinase K, and 20mg lysozyme, followed by 24 hours digestion at room temperature on a rotating nutator. After pelleting of the cellular debris, the supernatant was extracted twice with a mixture of phenol, chloroform, and isoamyl alcohol (25:24:1), and a third time with chloroform only. The DNA was isolated on a Qiagen MinElute column and eluted into 30uL EB buffer.

Extraction Method D: Modified Aromatic Plant Extraction Method
Approx 50mg calculus was digested overnight at 37˚C in 1mL of a digestion buffer comprised of 0.375M EDTA, 1% SDS, 2% CTAB, 10% proteinase K, 20mg lysozyme, and 2% PVP (Mr 750k), followed by 24 hours digestion at room temperature on a rotating nutator. After pelleting of the cellular debris, the supernatant was extracted twice with a mixture of phenol, chloroform, and isoamyl alcohol (25:24:1), and a third time with chloroform only. The DNA was isolated on a Qiagen MinElute column and eluted into 30uL EB buffer.

Extraction Method E: Modified Qiagen DNeasy Mericon Food Kit
Approx 50mg calculus was digested overnight at 55˚C in 1mL of a buffer of 0.45M EDTA and 10% proteinase K, followed by 24 hours digestion at room temperature on a rotating nutator. After pelleting of the cellular debris, the supernatant was concentrated to 500uL using a 30kDA Amicon filtration unit. The concentrate was then extracted following the DNeasy kit protocol and eluted into 50uL EB buffer.

After extraction, DNA yield was quantified using a Qubit fluorometer high sensitivity assay and extract purity was assessed using a lambda inhibition test in which PCR reactions containing lambda phage primers (Applied Biosystems, USA) and 1pg lambda genomic DNA were then

spiked with 1uL of the following calculus extract titration: undiluted extract, ½, 1/5, 1/10, 1/100. The sequence of the lambda forward primer was: λPC01, 5'-GATGAGTTCGTGTCCGTACAACTGG-3'. The sequence of the lambda reverse primer was: λPC02, 5'-GGTTATCGAAATCAGCCACAGCGCC-3'. Each 20µl PCR reaction was set us as follows: 0.2µl Phusion Hot Start II polymerase, 4µl 5X Phusion HF buffer, 2µl of 2mM dNTPs, 1µl of 2.5mg/mL BSA, 1µl of 10mM lambda forward primer, 1µl of 10mM lambda reverse primer, 1pg lambda genomic DNA, and 8.8µl H_2O, plus 1µl of titrated calculus extract. Cycling conditions were performed as follows: enzyme activation at 98˚C 30s, followed by 45 cycles of denaturation at 98˚C for 15s, annealing at 65˚C for 20s, and elongation at 72˚C for 20s, and ending with 72˚C for 5 min. Extract concentrations that failed to allow robust lambda amplification of a 500bp target were scored as inhibited, and a minimum required dilution factor for successful amplification was determined for each extract.

The highest DNA yields were measured from Extraction Method A (Supplementary Table 12), while Extraction Methods B, C, D, and E resulted in much lower DNA yields. Extraction Method A required dilution factor of 1:4, while Extraction Methods C, D, and E required no dilution. Extraction Method B was not evaluated. Although extraction Methods C, D, and E yielded the highest quality extracts and removed inhibitory compounds to non-detectable levels, these extraction methods also removed a substantial amount of DNA, resulting in DNA yields only 3-8% that of Extraction Method A. Even after dilution to a non-inhibitory concentration, Extract A contained more DNA per microliter than undiluted Extracts C, D, and E. As a result of these findings, extraction methods C, D, and E were no longer pursued.

6.1.2 Calculus: Comparison of Decontamination Methods

As a mineralized matrix, dental calculus may be amenable to the removal of contaminating surface DNA using sodium hypochlorite (NaOCl) or an EDTA wash, as is performed on archaeological bones and teeth. To determine to what degree decontamination methods affect calculus DNA extraction yield, calculus samples from B61 and G12 were divided into two groups, and one group was pretreated with a decontamination agent before extraction while the other was left untreated. Calculus from B61 was soaked in 1mL of a 1% NaOCl solution for 1 minute and then washed to pH neutrality with UV-irradiated biomolecular grade water. Calculus from G12 was soaked in 1mL of 0.5M EDTA for 1 hour to solubilize loosely bound DNA and then the EDTA wash solution was removed. The treated and untreated calculus samples were then extracted in parallel using Extraction Methods A and B (Supplementary Figure 21), and the resulting DNA yields were compared (Supplementary Table 13).

Decontamination method was found to have little consistent influence on total DNA yield, demonstrating that a pretreatment of calculus samples with NaOCl or EDTA does not result in significant DNA loss compared to untreated samples. This is true despite the fact that measurable amounts of DNA are removed, as evidenced by the DNA recovered from the EDTA wash solution. Thus, DNA extracts from the same individual using the same extraction method result in similar DNA yields regardless of decontamination method. Within individuals, extraction method strongly affects DNA yield, with Extraction Method A consistently yielding 2-8 fold higher DNA yields than Extraction Method B. Further consideration of the effects of decontamination on taxonomic composition of the DNA extracts are discussed below. DNA

yield differed greatly between B61 and G12, with the highest extract yield for B61 (5ng/mg) measuring only half as much as the lowest extract yield from G12 (12.2ng/mg). The effects of decontamination treatment and extraction method on microbial community composition are discussed in sections 6.4.1 and 6.4.2.

6.1.3 Calculus: Comparison Across Individuals

Dental calculus DNA yield was next evaluated across multiple individuals. Using Extraction Method A, DNA was obtained and analyzed from approximately 50mg of untreated calculus from individuals B17, G12, B78, and B61 (Supplementary Table 14). DNA yield ranged from 5 to more than 400ng/mg, and extracts required 5-50-fold dilutions to overcome inhibition in a lambda test. In general, extracts with higher DNA concentrations required greater dilution for successful PCR amplification.

In general, the DNA content of dental calculus is very high and contains 10-1,000 times more DNA than bone or dentine from the same individual (Figure 5i; see below). This finding is not unexpected given the bacterial etiology of dental calculus from dental plaque, a biofilm with an estimated bacterial density of approximately 10^9 cells/mg of wet weight.[90] For comparison, DNA was also extracted from modern dental calculus sample P2, and found to yield similar amounts of DNA (Supplementary Table 14). To further demonstrate that high DNA yields are a general pattern for ancient dental calculus and not unique to this skeletal assemblage, we extracted DNA from two additional dental calculus samples from unrelated medieval and Roman sites in the UK for comparison (Supplementary Table 15). DNA from these samples were extracted using Extraction Method A, except that DNA purification was performed using a silica-based method.[91] DNA concentration was measured using a NanoDrop spectrophotometer (Thermo Scientific). Ancient dental calculus DNA extraction yields from the UK samples were very high (164-290 ng/mg), falling within the range of DNA yields from the Dalheim samples. Thus, we demonstrate that very high DNA yields, on par with average DNA yields reported for fresh liver, brain, and kidney using Qiagen commercial kits (e.g., http://www.qiagen.com/Products/Catalog/Sample-Technologies/DNA-Sample-Technologies/Genomic-DNA/DNeasy-Blood-and-Tissue-Kit#productdetails), can be reliably retrieved from archaeological dental calculus up to at least 900 years old.

6.1.4 Dentine and Bone DNA Extraction

Dentine and bone from healthy and pathological loci were collected using a handheld Dremmel drill with a bleach-sterilized diamond circular blade attachment. The dentine and bone were wrapped in bleach sterilized aluminum foil, crushed with a hammer, and transferred to sterile 2mL tubes. The resulting coarse poweder was extracted for DNA in duplicate using a basic mineralized tissue extraction protocol for archaeological samples (Extraction Method A, see above). In brief, approximately 100mg was crushed to a coarse powder in a sterilized mortar and pestle and digested overnight at 55˚C in 1mL of a buffer of 0.45M EDTA and 10% proteinase K, followed by 24 hours digestion at room temperature on a rotating nutator. After pelleting of the cellular debris, the supernatant was extracted using a high salt-modified phenol/chloroform extraction, purification on a Qiagen MinElute column, and elution into 20uL EB buffer. After

extraction, DNA yield was quantified using a Qubit fluorometer high sensitivity assay and extract purity was assessed using a lambda inhibition test (Supplementary Table 16).

Extracted DNA yields from dentine and bone were generally consistent between duplicates, and all yields fell below 1ng/mg, as is typical for archaeological samples. Interestingly, no increase in DNA yield was observed for dentine and bone samples with pathological lesions. DNA extracts from the healthy dentine required no dilution successful PCR-amplification in a lambda inhibition test, but DNA extracts from carious dentine and an alveolar bone lesion required a slight dilution for successful lambda PCR-amplifcation.

6.1.5 Burial Matrix DNA Extraction

Burial matrix (soil) adhering to unwashed bones in the Dalheim skeletal assemblage was collected and analyzed for DNA content (Supplementary Table 17). Five soil samples of approximately 200mg each were digested and extracted for DNA using a Qiagen Stool Kit, which we had previously found to be effective for extracting DNA from ancient environmental samples (unpublished data). Measured DNA yields from the 200µL eluted extracts were very low (<0.1ng DNA/mg soil). A coprolite excavated from an unrelated 3rd-5th century AD salt mine (Dürnberg, Germany) was processed in parallel as a positive control and yielded >8x more DNA. Inhibition testing with a lambda assay indicated no PCR-inhibition in the burial matrix or coprolite extracts.

To determine if human or bacterial DNA is present in the burial matrix, DNA extracts were PCR-amplified with four primer pairs covering the human mitochondrial HVRI and a universal bacterial primer pair targeting the 16S rRNA V3 region (Supplementary Table 17). The 20µl PCR reaction was set up as follows: 0.2µl Phusion Hot Start II polymerase, 4µl 5X Phusion HF buffer, 2µl of 2mM dNTPs, 1µl of 2.5mg/mL BSA, 1µl of 10 µM forward primer, 1µl of reverse primer, and 9.8µl H_2O, plus 1µl of burial matrix extract. Cycling conditions were performed as follows: enzyme activation at 98˚C for 30s, followed by 45 cycles of denaturation at 98˚C for 15s, annealing at 65˚C for 20s, and elongation at 72˚C for 20s, and ending with 72˚C for 5 min.

No amplification was observed for any Dalheim burial matrix extracts (Supplementary Table 18). By contrast, the coprolite sample processed in parallel yielded human mtDNA amplification products for 3 of 4 HVRI targets and the bacterial 16S rRNA target, indicating that the method is effective for extracting human and bacterial DNA. The poor DNA preservation in the Dalheim burial matrix suggests that post-excavation storage conditions were detrimental to DNA preservation in non-mineralized contexts and that ambient modern human and bacterial DNA contamination in the storage boxes fell below detectable levels.

6.1.6 Genetic Sex Typing

To confirm the sex of the individuals under study, genetic sex typing was performed on a decontaminated dentine sample from each individual. Three negative extraction controls were processed in parallel. One healthy tooth from each individual was decontaminated by submersion in 2% NaOCl solution for 1 min. The NaOCl was then removed by serial washing with H_2O to

pH neutrality. The tooth was then crushed to a coarse powder in a sterilized mortar and pestle and approximately 100mg extracted for DNA using Extraction Method A. DNA extract yield was quantified using a Qubit fluorometer high sensitivity assay. Genetic sex was assessed using a real-time PCR Taqman duplex assay to detect X and Y chromosome-specific sequences of the amelogenin gene.[92] In brief, the primer sequences were: forward, 5'-CCCTGGGCTCTGTAAAGAATAGTG-3', reverse, 5'-ATCAGAGCTTAAACTGGGAAGCTG -3'. The MGB probe sequences were FAM-TATCCCAGATGTTTCTC and VIC-CATCCCAAATAAAGTG. Real-time PCR set up was as follows: 10µl LightCycler 480 Probes Master Mix, 0.5µl 40x Custom Genotyping Assay (each primer 36µM, each probe 8µM, Applied Biosystems), 8.5µl H_2O, and 1µl sample extract. Real-time PCR was performed on a Roche LightCycler 480 with the following cycling conditions: enzyme activation at 98˚C for 30s, followed by 55 cycles of denaturation at 98˚C for 30s. Each extract and negative extraction control was analyzed in triplicate with three additional non-template reagent blanks. No amplification was observed in the negative extraction controls or non-template reagent blanks. Sample DNA extract yields and the results of the real-time genotyping assay are presented in Supplementary Table 19.

6.2 Illumina Whole Metagenome Shotgun Sequencing of Ancient Dental Calculus

Illumina libraries were prepared and sequenced at the University of Copenhagen's Center for Geogenetics. Two individuals were selected for dental calculus whole metagenome shotgun Illumina sequencing: B61 and G12.

6.2.1 DNA Polymerase Selection

Although Phusion is the standard DNA polymerase used in constructing Illumina high-throughput sequencing libraries,[93] Taq-based polymerases are more often used for ancient DNA studies. The main difference between these two enzymes is that Taq polymerases will amplify DNA sequences that contain damage (cytosine deaminations, abasic sites, etc.), while Phusion polymerase stalls at these sites and generally fails to amplify damaged DNA. As a result of these differences, ancient DNA authentication tools that rely on damage analysis, such as mapDamage[94] can only be applied to libraries constructed with Taq polymerases. However Phusion polymerase offers other advantages that are particularly suited to ancient microbiome studies.

Taq polymerases are best suited to ancient DNA studies focusing on the reconstruction of a single genome. In these studies, sequencing depth of coverage across the genome is typically high (>30), and therefore DNA damage can be identified and removed by sequence alignment. In these studies, accepting a certain amount of damage to be sequenced by using Taq polymerases during library construction does not interfere with determining the consensus genome sequence, and it provides the added benefit of allowing damage statistics to be calculated to assist in authenticating the results. However, this approach is poorly suited to metagenomic analysis of ancient microbiomes.

Microbiomes typically contain thousands of taxa at frequencies that differ by orders of magnitude. Thus, the depth of coverage for all but the most abundant taxa is expected to be very

low, and thus sequence alignment cannot be used to distinguish damage from true sequence differences. Because sequencing errors resulting from DNA damage can result in taxon misidentification, the disadvantages of using Taq polymerases during microbiome library construction greatly outweigh the benefits. Phusion polymerase represents an important alternative, as it produces libraries with high fidelity (accuracy) and a low error rate (damage artifacts). A recent comparative analysis of DNA damage patterns in archaeological human hair using both Taq and Phusion polymerases found a 3.8-fold reduction of cytosine deamination in Phusion libraries compared to Taq libraries prepared from the same sample.[94] Importantly, this study also showed that approximately 90% of reads from Taq libraries contained no DNA damage, thus demonstrating that a large proportion of ancient biomolecules are available for Phusion amplification. Because of the advantages offered by Phusion polymerase, it was selected for use in this study.

6.2.2 Illumina Library Preparation

Illumina libraries were built for the nine DNA extracts reported in section 6.1.2 (Supplementary Table 20) for individuals B61 and G12. Target DNA quantity for each library preparation was 500-700ng. For those extracts with low DNA concentration, all of the available extract was used. A negative extraction control was processed alongside the experimental extracts and monitored for contamination. No contamination was observed.

In an ancient DNA clean room, DNA extracts were repaired using a NEBNext End Repair and dA-Tailing kit following manufacturer's instructions. Short Illumina Indexed PE Adaptors were added to the extracts as follows: 1µl of 15µM adaptor for libraries S2, S5, S6, S7, and S8 (high concentration extracts), and 1µl of 5µM adaptor for libraries S1, S3, and S9 (low concentration extracts). A unique, 6-nucleotide index was used for each library, and each index was distinguished by at least two differences from other indexes. Quick T4 Ligase (1µl) was added to each library and incubated at 25˚C for 10 min. After adaptor ligation, the libraries were purified on a MinElute spin column (Qiagen) and eluted into 20µl EB buffer. The libraries were then PCR-amplified in two rounds to increase concentration and complete adapter assembly. At the end of library construction, the total length of the indexed adaptors is 122bp. PCR inhibition was observed during the first amplification step, and the following PCR reactions were optimized by sample to yield the best amplification.

The first PCR reaction was set up as follows: 25µl Phusion HF Master Mix (Finnzymes), 2µl 10µM forward PE primer, 2µl 10µM reverse indexed PE primer, 13µl H_2O. For libraries S1, S3 and the negative extraction control, 8µl library was added to the reaction. For libraries S2, S4 and S9, 1µl library and 7µl H_2O were added. Library amplification for S2 and S4 was repeated with 1µl library, 1µl BSA (2.5mg/ml) and 6µl H_2O. For libraries S5-S8, 1µl of diluted 1:9 libraries and 7µl H_2O were added. PCR tubes were then sealed and transferred to a PCR facility. Cycling conditions were: 98˚C for 60s, 12 cycles of (98˚C for 20s, 60˚C for 30s, 72˚C for 30s), and a final extension of 72˚C for 5 min. PCR products (4µl) were visualized on a 2% agarose gel to confirm amplification and purified on a MinElute spin column (Qiagen) and eluted into 20µl EB buffer. Amplification products were observed for all nine archaeological calculus samples, but no amplification was observed in the negative extraction control.

A second PCR reaction was set up as follows: 12µl Phusion HF Master Mix (Finnzymes), 1µl 10µM forward PE primer, 1µl 10µM reverse indexed PE primer, 1µl H_2O, and 8µl library. Cycling conditions were: 98˚C for 120s, 8 cycles of (98˚C for 20s, 60˚C for 35s, 72˚C for 30s), and a final extension of 72˚C for 5 min. PCR products (4µl) were visualized on a 2% agarose gel to confirm amplification and purified on a MinElute spin column (Qiagen) and eluted into 20µl EB buffer. Library DNA concentration was measured with a Qubit DNA High-Sensitivity Assay Kit (Invitrogen) and the duplicate S2 and S4 libraries were pooled. Concentration and size distribution of the libraries was determined on a Bioanalyzer 2100 DNA 1000 chip (Agilent Technologies). Mean library length ranged from 193 bp (S9) to 325 bp (S8), which, after subtracting the adaptor length of 122bp, indicates a mean extract insert length of 71-203bp. This length is consistent with ancient DNA, which is known to be highly fragmented.

6.2.3 Illumina Sequencing and Data Pre-Processing

DNA concentration was further characterized using a qPCR SYBRGreen Assay, and the nine libraries were pooled at equimolar concentrations. Following cluster generation, libraries were sequenced on one lane of an Illumina HiSeq 2000 in a 100 bp, single-end run, followed by base-calling using standard Illumina software (RTA version 1.12.4.2). Correctly indexed reads (100% index identity) were then filtered and binned using Illumina's CASAVA software (version 1.8.0). Reads containing Ns were trimmed, as were bases with Phred quality scores <35. Adapter sequences were removed using the AdapterRemoval tool,[95] and reads <25bp were discarded. The remaining reads were verified using fastqc analysis (http://www.bioinformatics.babraham.ac.uk/projects/fastqc/). Statistics for read generation and quality control filtering are provided in Supplementary Table 21. The FASTQ formatted files are available in the NCBI Short Read Archive (SRA) under the BioProject accession PRJNA216965 and on the MG-RAST server under Project 365 "Ancient Oral Metagenome," (http://metagenomics.anl.gov/linkin.cgi?project=365).

6.3 454 Amplicon Sequencing of 16S rRNA V3, V5, and V6 Regions

Targeted amplification assay design and 454 library preparation was performed at the Centre for Evolutionary Medicine, Institute of Anatomy, University of Zürich, Switzerland. All PCR reactions were set up in the ancient DNA laboratory. 454 libraries were sequenced at Omya AG, Switzerland.

6.3.1 Primer Design

Ancient DNA is characterized by a high degree of fragmentation, and primers designed to amplify the entire 16S rRNA gene of modern bacteria cannot be used for analysis of ancient specimens. Because ancient DNA fragments are typically very short (rarely exceeding a PCR amplifiable length of ca. 250 bp in truly ancient material), even primers targeting relatively short regions, such as the 515F/806R primers[96] targeting the 16S rRNA V4 region (~282-304 bp), are unsuitable for most ancient DNA studies. Instead, specially designed very short target (<250 bp) primer pairs targeting specific variable regions must be used. Because no 16S primer set is truly universal, three different primer pairs were designed to span the 16S rRNA V3, V5, and V6 regions, respectively (Supplementary Table 22).

Primer pairs for the V3 and V6 regions were obtained from published literature[97] and modified to avoid non-conserved sites and to shorten the amplicon length to under 250 bp. In both cases, the amplicon length was shortened by converting a probe into a primer. The V3 primers have been shown to yield good coverage of Actinobacteria, Bacteriodes, Firmicutes, and Proteobacteria, poor coverage of Spirochetes and Chlamydiae, and moderate coverage of other phyla. The V6 primers ("p891F" and "p1033R") have been shown to yield good coverage of Spirochetes and Chlamydiae, moderate coverage of Proteobacteria, Firmicutes, Bacteriodes, and other phyla, and poor coverage of Actinobacteria. We designed one additional primer pair targeting the V5 region by aligning a selection of 16S rRNA sequences from diverse oral and other human-associated microbial species belonging to nine different bacterial phyla (Supplementary Table 23). For all three primer pairs, the expected amplicon sizes across a diverse range of taxa is <250 bp: V3 (~200 bp), V5 (~145 bp), and V6 (~130 bp).

In silico primer testing
Each of the V3, V5, and V6 primers was tested *in silico* against 41,513 16S rRNA sequences spanning 72 Bacteria phyla and 7 Archaea phyla in the Greengenes database (v.6Oct2010) using the software tool Primer Prospector.[96] Between the three primer sets, bacterial coverage for 70 phyla is good; there are only two bacterial phyla (em3 and wm1006) that are poorly covered by all three primer pairs (<50% of phylum members predicted to be amplifiable). Neither of these phyla has been detected in human microbiomes. Overall coverage of Archaea is poor, except for the phyla Crenarchaeota and Euryarchaeota, which are both amplifiable *in silico* by the V5 primer pair; Euryarchaeota is the only phylum of Archaea that has been previously detected in the oral cavity. Of the twelve bacterial phyla that are known to inhabit the oral cavity, seven show good *in silico* coverage by all three primer sets: Actinobacteria, Bacteroidetes, Firmicutes, Fusobacteria, Gn02, Proteobacteria, and Synergistetes. Of the remainder, Spirochaetes are well covered by V5 and V6, Chlamydiae are well covered by V3 and V6, and Chloroflexi, SR1, and TM7 are well covered by V3 and V5.

Primer testing by amplification and cloning
The V3, V5, and V6 primer pairs were then tested on diluted (1:49) extracts from individual G12 (extracts S7 and S8, see Supplementary Table 13). Each 20µl PCR reaction was set up as follows: 0.2µl Phusion Hot Start II polymerase, 4µl 5X Phusion HF buffer, 2µl of 2mM dNTPs, 1µl of 2.5mg/mL BSA, 1µl of 10 µM forward primer, 1µl of reverse primer, and 9.8µl H_2O, plus 1µl of diluted calculus extract. Cycling conditions were performed as follows: enzyme activation at 98˚C for 30s, followed by 45 cycles of denaturation at 98˚C for 15s, annealing at 65˚C for 20s, and elongation at 72˚C for 20s, and ending with 72˚C for 5 min. All three primer pairs were found to yield robust amplifications for both G12 extracts (Supplementary Figure 22).

As a test of our assumption that DNA fragment lengths in ancient dental calculus are very short (<250 bp), we also attempted to amplify longer targets using the same primers in different combinations: V5F/V6R (~290 bp), V3F/V5R (~590 bp) and V3F/V6R (~735 bp). No amplification was observed in these three reactions, confirming that the DNA in the ancient dental calculus extracts is fragmented to very short lengths typical of ancient DNA.

Cleaned V3, V5, and V6 PCR products were cloned into a pBluescript II SK+ plasmid vector and transformed into competent E. coli cells. After plating and overnight incubation, 120 colonies were picked and 25µl PCR reactions were set up as follows: 0.2µl Promega GoTaq polymerase, 5µl 5x buffer, 2.5µl 25mM $MgCl_2$, 0.5µl 10mM dNTPs, 1µl each of 10µM T3 and T7 primers, and 14.8µl H_2O. Cycling conditions were as follows: enzyme activation at 95˚C for 2min, followed by 25 cycles of denaturation at 95˚C for 30s, annealing at 50˚C for 30s, and extension at 72˚C for 30s, and ending with a final elongation step at 72˚C for 5min. The resulting PCR products were cleaned and sequenced (BigDye Terminator v. 3.0 kit) on an ABI Prism 310 Genetic Analyzer and analyzed using CLC Bio Main Workbench Software (v. 5.7.1). After trimming vector and primer sequences, the remaining sequences were analyzed using Ribosomal Database Project (RDP) online tools.[98] One hundred percent of the calculus clones were assigned to two domains (Archaea and Bacteria) and 68% to nine phyla with 80% confidence: Euryarchaeota, Actinobacteria, Bacteriodetes, Firmicutes, Fusobacteria, Proteobacteria, Spirochaetes, Synergistetes, and TM7.

As taxonomic coverage was broad (including both bacterial and archaeal sequences) and amplification was robust, 454 Amplicon Fusion Primers were then generated using the V3, V5, and V6 primer sequences. The Fusion Adaptor sequences were: forward, 5'-CGTATCGCCTCCCTCGCGCCATCAG-3'; and reverse, 5'-CTATGCGCCTTGCCAGCCCGCTCAGA-3'. A unique, 9-base MID was included in each reverse Fusion Primer sequence, and a total of 10 MIDs were designed so that multiple samples could be pooled in a single 454 run. These MIDs also served to prevent cross-contamination in the 454 sequencing facility as only sequences with a valid MID from our study were accepted for further analysis. In total, thirty-three 454 Amplicon Fusion Primers were designed, one forward primer and 10 MID-tagged reverse primers for each of the V3, V5 and V6 regions.

6.3.2 454 Library Preparation

454 libraries were prepared for the calculus, root, carious root, and alveolar bone abscess extracts reported in Supplementary Tables 14 and 16 using each HPLC-purified 454 Fusion primer set. Before library preparation, each HPLC-purified Fusion primer was tested for contamination, and no contamination was observed. Throughout library preparation, negative extraction controls and reagent blanks were included with each amplification and monitored for contamination. Duplicate extracts for the root and bone samples were pooled before amplification. As with the Illumina library preparation, Phusion enzyme was selected for library amplification (see section 6.2.1 for discussion). Each 25µl PCR reaction was set up as follows: 0.25µl Phusion Hot Start II polymerase, 5µl 5X Phusion HF buffer, 2.5µl of 2mM dNTPs, 1µl of 2.5mg/mL BSA, 1µl of 10 µM forward primer, and 1µl of reverse primer, plus a sample-dependent volume of extract and water. The amount of DNA added to each PCR reaction is reported in Supplementary Table 24. Cycling conditions were performed as follows: enzyme activation at 98˚C for 30s, followed by 30 cycles of denaturation at 98˚C for 15s, annealing at 52˚C for 20s, and extension at 72˚C for 20s, and ending with 72˚C for 5 min. The V3 region was amplified for an additional 5 cycles (total of 35 cycles) to compensate for the fact that the V3 454 Fusion primers were found to form primer dimers. Slowing the temperature ramp speed of the thermocycler to ≤2˚C/s was found to reduce primer dimer formation. No amplification was observed in the negative extraction controls or reagent blanks.

A minimum of three amplifications were performed for each sample, and the resulting PCR products were pooled and concentrated using a QiaQuick PCR Purification Kit (Qiagen). DNA concentration was measured with a Qubit DNA High-Sensitivity Assay Kit (Invitrogen), and additional PCR amplifications were performed, if necessary, until the total DNA yield for the pooled and cleaned PCR products was ≥300ng (Supplementary Table 24). A 30µl aliquot with a concentration of 10ng/µl was submitted to Omya A.G. (Switzerland) for sequencing.

6.3.3 454 Sequencing of Amplicon Libraries

Amplicon libraries were titrated to equimolar concentrations and sequenced on a 454 GS Junior System using 454 Titanium Chemistry (Roche) by Omya AG. A second set of G12 root libraries for the V3 and V5 regions were sequenced again in a second run as quality control duplicates. Sequenced reads were quality filtered using the Roche GS RunProcessor amplicon pipeline with default settings, and reads without a valid MID were discarded. The average number of reads passing QC filters per region for each sample was 5,338, and the average number of total reads per sample was 15,969 (Supplementary Table 24). SFF formatted files are available in the NCBI Short Read Archive (SRA) under the project accession SRP029257 and FASTA files are available on the MG-RAST server under Project 365 "Ancient Oral Metagenome," (http://metagenomics.anl.gov/linkin.cgi?project=365).

6.4 Analysis of 16S rRNA Genetic Sequences

6.4.1 Community network analysis, taxonomic assignment, and phylogenetic tree construction

OTU reference dataset
A reference dataset containing full length 16S ribosomal RNA sequences was needed to make the comparison possible between the different 16S regions sequenced in the ancient tooth samples and other studies. Several curated 16S rRNA datasets are currently publicly available, including Greengenes and RDP, and these datasets exhibit a high degree of OTU overlap (89%). However, in order to ensure that all filtering and alignment methods were consistent for the reference set and the ancient dental calculus samples and to streamline Genbank data retrieval for network analysis, we constructed a new 16S rRNA reference dataset from the NCBI Genbank database. This dataset has high overlap with both Greengenes (90%) and RDP (92%). For this dataset, all publicly available 16S ribosomal gene sequences found in the NCBI Genbank database were downloaded, screened for chimeras, aligned, trimmed and clustered at a sequence identity cutoff of 98%. The alignment and filtering of 16S sequences was performed using the INFERNAL[59] aligner v1.0.2 (http://infernal.janelia.org/) using the bacteria and archaea 16S rRNA sequence consensus models from ssu-align (http://selab.janelia.org/software/ssu-align/). Chimeric sequences were removed using uchime[58] (http://drive5.com/usearch/). After alignment sequences were trimmed, and insertions were removed for the clustering step. Clustering was performed with a hierarchical clustering algorithm using sequence identity as the measure of distance and single linkage as the cluster metric. The final dataset contained 869,004 bacterial 16S sequences assigned to 79,120 OTUs, and 42,024 archaeal 16S sequences assigned to 6,264 OTUs.

Mapping of reads to reference OTUs
Sample reads were first aligned and filtered using the INFERNAL aligner with bacteria and archaea 16S rRNA sequence consensus models. Aligned reads with a bit score <40 or negative structure score were discarded. The remaining aligned reads were then mapped to the OTUs by finding the most identical sequences in the reference dataset. When all equally identical sequence matches belonged to the same OTU, the mapping was considered specific to the OTU, otherwise the mapping was considered unspecific and the read was discarded from further analysis.

Extraction, decontamination, and primer bias testing
Potential biases introduced by extraction, decontamination, primer selection, and sequencing method were next evaluated (Supplementary Figure 3). A comparison of 16S rRNA OTU frequency distributions at the level of Class as a function of sequencing method reveals consistent differences between shotgun and targeted approaches (Supplementary Figure 3a-b). These differences appear largely driven by higher variability in OTU frequency distributions as a function of primer selection (Supplementary Figure 3d, f), with lesser effect contributed by extraction or decontamination method (Supplementary Figure 3c, e).

The effects of extraction and decontamination bias were further investigated by searching all shotgun reads against the NCBI nr database using BLASTn, parsing the results at the species level using MEGAN, and using a Goodall matrix to generate UPGMA phenograms (Supplementary Figure 3g, h).[71] Individuals B61 and G12 show clear segregation regardless of data normalization, but there is no consistent clustering pattern with respect to decontamination or extraction method. For example, without data normalization, the shotgun data from B61 libraries cluster by decontamination method while the shotgun data from G12 libraries do not. Following data normalization, the shotgun data from G12 libraries show clustering by extraction method, but the shotgun data from B61 libraries do not. Thus decontamination and extraction methods appear to have little systematic effect on the taxonomic assignments of sequencing results.

The only exception is library S9, the "contamination" library prepared from G12 that consists of all DNA released during the first hour of extraction. In the phenograms, S9 clusters more closely with the shotgun data from other G12 libraries than with the shotgun data from the B61 libraries, but it is also clearly distinct from the other G12 samples. For this reason it was excluded from contig assembly with the remaining G12 libraries. However, subsequent network analysis of community similarity based on 16S rRNA sequences (see below) revealed that it is consistent with an oral microbiome and distinct from environmental contamination (Figure 5j, Supplementary Figure 12). Because growth of dental calculus is appositional, the separation of the S9 library from the other G12 libraries in the phenograms suggests that the bacterial DNA released from the outermost calculus layer during the first hour of extraction represents a taxonomically biased subset of the oral microbiome.

Network of sample community similarity
The microbial diversity of the ancient dental samples was characterized in terms of the OTUs generated from the reference dataset, through the mapping of the sequence reads. After the characterization of the ancient dental samples, the microbial composition similarity between a

pair of samples was calculated as the number of shared OTUs divided by the total number of different OTUs found in both samples.

For the rendering of the network, the neato program from the graphviz package (http://www.graphviz.org/) was used. A script was written to generate the dot file that served as input to neato. The microbial composition similarities were computed between all ancient dental samples, as well as between ancient dental samples and metagenomic samples in Genbank and MG-RAST (Project 128; http://metagenomics.anl.gov/linkin.cgi?project=128), but not between Genbank samples. Only Genbank samples with at least 20 OTUs were considered (1,818 out of 37,689 studies), and only samples found to be at least 20% similar to one of the ancient dental samples were shown (315 out of 1,818). Between ancient dental samples and Genbank samples, a link (gray line) was added when they were more similar than 20% in their microbial composition, while between ancient dental samples, a link (green line) was added when they were more than 25% similar. The lengths of the links were adjusted to reflect the similarity between samples, the closer the samples the higher their similarity.

For example, 18 studies were found to be highly similar (≥50%) in microbial composition to the ancient calculus samples. Of these, all but two were human oral samples (ranging in similarity from 52-80%), the exceptions being a sample of spontaneously produced sputum from a cystic fibrosis patient (62% similarity) and a collection of samples from the HMP (60% similarity) [3]. The majority of samples with lower OTU similarity (20-50%) to the ancient dental calculus samples are human- and animal-associated. By contrast, the bacterial communities found in the ancient tooth root samples are more diverse and show higher similarity to microbial communities found in soil and other environmental samples. Carious dentine and abscessed bone were found to have intermediate communities, likely reflecting a combination of endogenous oral bacteria and soil contamination.

The color code of the nodes representing Genbank studies (circles) in Figure 5j was assigned using regular expression matches. The dark red color (human oral-associated) was assigned to studies in which the isolation source or publication title matched the words: oral, mouth, tongue, gum, dental, endodontal, "root canal", endotrach*, or gingiv*. The red color (human-associated) was assigned if the fields matched the words: "human feces", "human fecal", "homo sapiens", human, skin, vagina, muco*, intestinal, intestine, sputum, cancer, or stool. The light red color (animal-associated) was assigned if the fields matched the words: pig, ileum, abdomen, body, swine, animal, feces, fecal, gut, dog, trout, mouse, mice, *Mus musculus*, dairy, or rumen. The blue color (soil-associated) was assigned when the fields matched the words: soil, rhizosphere, sediment, grass, mud, or coalbed. Finally, the light blue color (other environment-associated) was assigned when the fields matched the words: environment, atmosphere, snow, air, water, river, sea, lake, ocean, aquatic, forest, island, sand, microbial mat, biofilm, plant, leaf, compost, crop, root, feedbunk, garden, dust, room, facility, laboratory, floor, concrete, urban, metalworking, oil field, oil well, oil seep, sludge, waste, or bioreactor. Supplementary Figure 12 shows an enhanced view of the community similarity network with each of the recruited metagenomes labeled according to source. The computer source code used to generate this network has been deposited to GitHub (https://github.com/jfmrod/metagenome-sample-network-generator).

OTU taxonomy classification
OTUs which contained 16S rRNA genes belonging to reference genomes (NCBI RefSeq) or that were annotated as belonging to an organism in a culture collection, were assigned the consensus taxonomy of all such sequences in the OTU. In the case of OTUs that contained no reliable source of taxonomy, the taxonomy of the OTU was inferred by decreasing the clustering threshold until the point at which the OTU was merged with another in which sequences with reliable taxonomy existed. In the case of inferred taxonomy, the clustering threshold at which the OTU was merged with another having reliable taxonomy information was appended at the end of the taxonomy classification. From targeted 16S rRNA sequence reads, a total of 1,495 and 2,293 OTUs were identified in ancient dental calculus and tooth roots respectively. A total of 1,718 OTUs were identified from shotgun 16S rRNA data. Merging ancient dental calculus targeted and shotgun 16S rRNA OTU tables resulted in a total of 2,699 unique OTUs (Source Data Files for Figures 1 and 5). Abundant OTUs were largely shared between targeted and shotgun datasets, but rare OTUs were not. Summary statistics for the ten most abundant phyla are presented in Supplementary Table 1, and the full dataset is available in the Source Data File for Figure 1.

Phylogenetic tree construction
Targeted and shotgun 16S rRNA OTU tables were merged for ancient dental calculus. A full-length 16S sequence representative for each OTU was chosen from the sequences in the reference dataset. Sequences from Refseq genomes were preferred over Genbank sequences as representatives when available in an OTU. All representative sequences were then aligned to the bacterial 16S rRNA model using INFERNAL and their phylogenetic relationship was inferred with FastTree v2.1.3[62] using the generalized time-reversible model. A tree for the top 100 OTUs were generated (Figure 2b, Supplementary Figure 2), representing 86.6% of mapped 16S rRNA reads. Labels on the tree show the lowest rank at which taxonomy was consensual for all sequences with reliable taxonomy in the corresponding OTU. In OTUs where taxonomy was inferred due to lack of sequences in the OTU with reliable taxonomy, the clustering threshold at which point sequences with reliable taxonomy were merged and used for inference is shown in parentheses. The accession label for each of the representative 16S rRNA sequences is also included in the label of each OTU on the tree. Labels shown in bold indicate that at least one of the sequences in the OTU is included in the HOMD.

6.4.2 Alternative analysis of 16S rRNA data using RDP Pyrosequencing and QIIME pipelines for direct comparison to HMP data analysis, including contamination source-tracking.

OTU picking
454 sample reads were filtered for sequences containing 100% identity to both forward and reverse primers and for read lengths ≥70bp (exclusive of primers). Primer, adapter, and MID sequences were trimmed using the RDP Pyrosequencing Pipeline.[98] To reduce runtime, data were analyzed using closed-reference OTU picking against the Greengenes (v.4Feb2011) 16S rRNA database,[99] allowing comparison to HMP [3] data. OTUs were picked at the level of 97% sequence identity, and OTUs observed at a frequency of <0.0005% (value=1) were discarded. In total, 87% of post-QC reads passed additional quality filters and 65% of post-QC reads were assigned to OTUs (Supplementary Table 25). The OTU table was then rarefied to 1,265 sequences per sample (the lowest number of OTUs observed in the 454 data from this project). The BIOM file for this data is available as Supplementary Data 1.

Taxonomic summaries of the ancient samples at the phylum (L2), family (L5), and genus (L6) levels allow at least three distinguishable groups to be discerned: 1) dental calculus, 2) carious dentine/abscessed alveolar bone, and 3) tooth roots (Supplementary Figure 13). Duplicates for G12 root V3 and V5 regions show only minor OTU frequency changes. Comparison of V3, V5, and V6 primers for each sample reveals systematic primer bias. For example, at the phylum level in dental calculus, V3 primers detect more TM7 and Chloroflexi, while V5 and V6 primers detect more Spirochaetes. Differences in primer performance were expected given the primer design strategy, previously published data, and *in silico* testing (see section 6.3.1); however, despite this bias, OTU patterns for dental calculus, tooth roots, and carious dentine/abscessed alveolar bone remain distinguishable.

Alpha and beta diversity
Alpha and beta diversity were established using QIIME[100] default parameters. Ancient tooth root samples were found to have greater species richness than dental calculus (Supplementary Figure 14a-c), an observation consistent with higher alpha diversity expected in samples of environmental origin compared to an oral microbiome. Beta diversity was visualized using Principal Coordinates Analysis (PCoA; Supplementary Figure 14d-f). Ancient dental calculus is clearly different from tooth root, carious dentine, and abscessed alveolar bone at the species level (Supplementary Figure 14d), despite primer bias evident in principal coordinates 2 and 3 (Supplementary Figure 14f).

Comparison to HMP data
The OTU table was next merged with the HMP OTU table (http://www.hmpdacc.org/HMQCP/#data), which was generated and rarefied using the same settings. The BIOM file for this data is available as Supplementary Data 2. Beta diversity plots were generated on the merged OTU table for GI and Oral HMP OTUs. Nevertheless, ancient dental calculus samples were found to cluster with oral HMP samples, while ancient tooth root/abscessed alveolar bone and carious dentine formed separate clusters distinct from the HMP sample groups (Supplementary Figure 15).

Source tracking
Bayesian microbial source tracking was performed using SourceTracker[53] on the merged OTU file. Ancient experimental samples were modeled as sinks comprised of a mixture of the following source environment groups: Group 1, HMP plaque, HMP skin, HMP gut, and Unknown (Supplementary Figure 16a); and Group 2, HMP plaque, HMP skin, HMP gut, ancient tooth root, and Unknown (Supplementary Figure 16b). For each sample, the estimated proportion of each source was drawn after 1,000 "burn-in" iterations using Gibbs sampling. Gibbs sampling procedure was performed with 25 random restarts, drawing one proportion estimate per restart. To avoid underestimating the Unknown environment source proportions, $\alpha 2$ values of 0.00415 and 0.01 were used and found to produce similar results.

HMP plaque was identified as a major source environment contributing to all four ancient dental calculus samples (mean 22%), and only the B78 V3 region showed HMP plaque to be a minor source environment (1%). No HMP source environments were identified in ancient tooth root samples. Likewise, no HMP source environments were identified in abscessed alveolar bone, although carious dentine showed minor contribution from HMP plaque for the V5 (1%) and V6

(1%) regions. When the pooled ancient tooth root samples were added as a potential source environment, little change was observed in the source assignments of dental calculus samples with the exception of B61 (see below). By contrast, the tooth root source environment was estimated to account for 84% of the carious dentine and abscessed alveolar bone bacteria, demonstrating that these two tissues have undergone a substantial postmortem taphonomic shift in microbial communities. Interestingly, HMP skin was not indicated as a source environment for any ancient sample, suggesting that incidental contact with human skin through touching during excavation and subsequent curation did not contribute substantially to the bacterial communities detected in ancient samples.

The large proportion bacteria from unknown sources in the ancient dental calculus samples is not unexpected. The HMP source samples were analyzed from individuals living in metropolitan environments in the United States; oral microbiome diversity in non-metropolitan and non-globalized populations is poorly explored, but preliminary studies have indicated that there may be important oral microbiome differences in these populations[101] As the Dalheim cemetery represents a rural medieval population, differences with the HMP data are expected. Additionally, the HMP samples were collected from healthy human controls, whereas the ancient samples in this study were collected from individuals with osteological evidence of periodontitis and other dental pathologies. However, individual B17, who exhibited the highest degree of dental pathology (see section 3.1), was also found to have the highest proportion of dental calculus OTUs assigned to the HMP oral source environment.

Another issue to briefly address is primer bias. The Human Microbiome Project (HMP) data included in our SourceTracker analysis was generated using primers targeting ~570 bp of the 16S rRNA V3-V5 regions, and we include it because the HMP study represents the largest single source of human microbiome data published to date. However, because this 16S target region is so long, no ancient DNA study could ever use the same PCR primers (see discussion in section 6.3.1). Thus, the datasets presented in our SourceTracker analysis were generated using different primer sets. If a major factor, primer bias would result in over-assignment of dental calculus sequences to soil contamination (tooth root bacteria) because the same primers were used to generate these two data sets. Thus, this makes SourceTracker a conservative test for our study that errors on the side of over-assigning contamination. However, these are not the results we observe. Instead, we see that when dental calculus is presented with soil contamination as a potential source, it continues to strongly affiliate with HMP plaque, despite the fact that the dental calculus and HMP data sets were obtained with different primer pairs. Thus, the manner by which we designed our SourceTracker analysis allows us to confidently exclude primer bias as an important factor in our results.

Environmental contamination of calculus samples

Among the dental calculus samples, only B61 was found to exhibit consistent evidence of low-level environmental contamination. Of the ancient dental calculus samples, B61 had the highest species richness (Supplementary Figure 14b), similar to that of the root average (Supplementary Figure 14c), and although clustering with dental calculus on beta diversity PCA plots, the B61 calculus samples trend toward the tooth root samples (Supplementary Figure 14b). Finally, using source tracking, B61 calculus was the only calculus sample to indicate ancient tooth root bacteria as a source (2-7%).

One possible explanation for the low-level contamination observed in B61 calculus but not the other calculus samples relates to the much lower DNA extraction yield for B61 calculus (5 ng/mg) compared the other calculus samples (30-437 ng/mg). Ignoring mineralogical and anatomical differences between dental calculus and dentine, if we assume a constant contamination burden for all ancient dental tissues and use the average total DNA recovery from ancient tooth roots as a proxy for post-mortem environmental contamination (a generous estimate because this also includes host DNA), then an average of 0.35 ng of contaminant DNA can be estimated per mg of dental calculus. For high DNA-yielding dental calculus, such as that obtained from G12, B17, and B78, this represents a trivial fraction of the total DNA (≤1%), but for low DNA-yielding calculus, such as B61, contamination could account for 7% of the total DNA yield. Thus the relative DNA yield of dental calculus compared to paired tooth roots may be important factor to consider when selecting samples for further analysis.

Although minor DNA contamination is unlikely to strongly impact overall microbiome composition, it can result in inflated and unreliable alpha diversity estimates. We therefore strongly caution against the direct comparison of alpha diversity between modern and ancient dental calculus in cases where contamination is suspected or confirmed through Sourcetracker analysis.

6.5 Analysis of shotgun whole genome sequences

6.5.1 Dietary DNA sequence analysis

Post-QC reads ≥75 bp in length were searched against a complete collection of full mitochondrial and chloroplast genome sequences published to date (>6,000 organelle genomes) using BLASTn. Hits with <100% query coverage and/or <100% sequence identity were discarded. E-values for remaining reads were 2e-29 or better. Reads hitting either 16S or 23S rRNA genes were discarded, as sequence conservation in these genes was too high to allow genus/species-level taxonomic resolution. Reads were discarded if they pointed to more than one genus; specifically, any secondary hits outside the genus of the first hit had to show at least two diagnostic point mutations relative to the perfect hit (the one exception was for human sequences also matching *Pan*, i.e., chimp). A total of 20 reads matched these filter criteria. Of these, 17 reads matched human mitochondrial sequences and three reads matched putative dietary mitochondrial sequences: pig/boar (*Sus* sp.) 12S rRNA gene sequence, intergenic mitochondrial sequence shared by cruciferous vegetables in the genus *Brassica*, and a bread wheat (*Triticum aestivum*) intergenic sequence. These reads originated from 7 of the 9 libraries: human (S2, S4, S6, S7, S8, S9) and dietary (S5, S7).

6.5.2 De Novo Contig Assembly

Illumina fasta files were pooled by individual and reads were assembled into contigs with the software program Velvet v.1.02.3[64] using default settings, a k-mer length of 29, and a minimum contig length of 100. Contig assembly statistics and contig length histograms for B61 and G12 are provided in Supplementary Table 26.

6.5.3 Contig filtering and Genbank annotation

The assembled contigs for B61 and G12 were annotated using the Megablast search against nt and gss databases available from the NCBI website as of July 2012. The reported hits from the two database searches were merged and sorted on the basis of their bit score. Annotations that cleared the quality cutoffs were selected for constructing the high confidence taxon list. The cutoffs included an identity greater than 97% with an alignment length greater than 95 nucleotide base pairs and an expected value of $\leq 1e^{-14}$. The top two different species identified by each BLAST search were then compared; those belonging to different domains or annotated as "unclassified sequences" were further screened. Prophage sequences annotated as part of a bacterial genome were retained and re-classified as virus sequences. Contig sequences matching any accession of *Escherichia coli* phi X 174 (ΦX174) bacteriophage (n=10) were discarded because phi X 174 genomic DNA was used as an internal standard during Illumina sequencing. Contigs with equally good hits to "unclassified sequences" and known organisms were retained. Contigs with top hits only to "unclassified sequences" or "uncultured organism" were discarded. Contig sequences matching both Bacteria and Eukarya in top two hits were discarded. All contigs assigned to Eukarya were manually validated for sub-domain classification.

For B61 dental calculus, a total of 25,544 contigs (2% of total B61 contigs) passed these filters, with a mean contig length of 149 bp and a mean k-mer depth of 5.19. 99.7% of contigs were assigned bacterial taxonomy (n=25,477), 0.14% were assigned to Archaea (n=35), 0.08% are viruses (n=14), and 0.07% are human (n=18). For G12 dental calculus, a total of 36,040 contigs (4% of total G12 contigs) passed these filters, with a mean contig length of 183 bp and a mean k-mer depth of 6.05. 99% of contigs were assigned bacterial taxonomy (n=35,691). Of the remaining 1%, 88.3% are human (n=308), 6.9% are viruses (n=24), 2% are Archaea (n=7), 1.4% are plants (n=5), 0.9% are fungi (n=3), 0.3% are non-human animals (n=1), and 0.3% are other Eukarya (n=1).

6.5.4 *Identification of Pathogens*

Taxonomic classification of metagenomic datasets is an active area of research, and multiple BLAST-based and marker gene-based strategies are currently in use.[102-104] Because pathogen identification requires species-level taxonomic resolution and because not all oral pathogens can be detected using current marker gene-based approaches, we employed a conservative BLAST-based approach utilizing a series of conditional filters to reduce our full contig-assembled metagenomic dataset (2,005,273 contigs) to a set of highly unique sequences (53,924 contigs) that can be reasonably assigned to a single species, a reduction of 97.3%. Starting with the pool of 61,584 annotated contigs from section 6.5.3 (G12 and B61), we applied additional filters to reduce database bias and further exclude potentially ambiguous matches among closely related species. To do this, we examined second hits within the BLAST results. If the identity of the second hit was ≥90% (and the bit score was of comparable quality, i.e., not less than 10% of the top hit), the sequence was discarded as ambiguous. Thus, retained contigs have a top hit with >97% identity to a Genbank annotated species and either no second hit or a second hit with <90% identity to a different species. Accepted exceptions to these conditions are cases in which the second hit was to the same or a different accession of the same species. Next, the annotated contigs were filtered for taxa classified as pathogens in the Pathosystems Resource Integration Center (PATRIC; http://wwww.patricbrc.org/) database.[19] Only taxa with "Disease" field entries in PATRIC were considered pathogens in this study. Pathogen singletons (pathogens represented

by a single contig only) were excluded. A total of 40 putative pathogens were identified by this method (Table 1).

Comparison to Human Microbiome Project healthy cohort data
We next applied the same BLAST and conditional filter approach to shotgun metagenomic contigs reported for 109 supragingival dental plaque samples in the Human Oral Microbiome Project healthy cohort: SRS052876, SRS014894, SRS063999, SRS052604, SRS023358, SRS054430, SRS015574, SRS023938, SRS045313, SRS017025, SRS019387, SRS019225, SRS016331, SRS063603, SRS018157, SRS020340, SRS045197, SRS018337, SRS024289, SRS051941, SRS012285, SRS020862, SRS051244, SRS024649, SRS015803, SRS016200, SRS015378, SRS016575, SRS019333, SRS018665, SRS015158, SRS054653, SRS019906, SRS055450, SRS021477, SRS022725, SRS018394, SRS019591, SRS043755, SRS051378, SRS055378, SRS024144, SRS011343, SRS065310, SRS015989, SRS014476, SRS011098, SRS017814, SRS043018, SRS013723, SRS017304, SRS016746, SRS022536, SRS015278, SRS051930, SRS064493, SRS018778, SRS053917, SRS055401, SRS017445, SRS043772, SRS024381, SRS024561, SRS023841, SRS015044, SRS019077, SRS019128, SRS047100, SRS015470, SRS022083, SRS019980, SRS064329, SRS015650, SRS049268, SRS064219, SRS013836, SRS011126, SRS011152, SRS011255, SRS018975, SRS017088, SRS017139, SRS044366, SRS058808, SRS053630, SRS065099, SRS015215, SRS014690, SRS022602, SRS024087, SRS058053, SRS047265, SRS016541, SRS064449, SRS015899, SRS019028, SRS021960, SRS053584, SRS024447, SRS075410, SRS024021, SRS017511, SRS013949, SRS018573, SRS015440, SRS016043, SRS022149, SRS013252, SRS014578. Summary data for this analysis is provided in Supplementary Table 2. All pathogens identified in the ancient dental calculus samples were also represented in at least one individual in the HMP healthy cohort, but the mean relative frequency of some pathogens were substantially different between the two groups. Of additional note, we find that the frequency of human DNA in ancient dental calculus is comparable to that observed in dental plaque of living subjects: mean, 0.3%; median, 0.2%; range, 0-2.5%.

The number of contigs assigned to taxa for each individual in the HMP dental plaque data set averaged 5,907 (mean), while the number of contigs assigned to taxa for G12 (32,403) and B61 (21,521) dental calculus were >3-fold higher, reflecting the different sequencing strategies and goals of the two projects. To reduce bias in comparing the two datasets (e.g., low frequency taxon dropout), we restricted comparisons of the two datasets to only those taxa present at a mean frequency of >1% in either the ancient dental calculus dataset or the HMP dental plaque dataset.

Four pathogens were found to have a substantially different relative frequencies in ancient dental calculus compared to the HMP healthy cohort: *Porphyromonas gingivalis*, *Tannerella forsythia*, *Treponema denticola*, and *Veillonella parvula*. The relative frequencies of *P. gingivalis*, *T. forsythia*, and *T. denticola* were found to be substantially higher in G12 and B61 ancient dental calculus than in HMP dental plaque (Supplementary Figure 4a-c), an observation consistent with the periodontal disease status of these individuals. The relative frequency of *V. parvula* was found be substantially lower in G12 and B61 ancient dental calculus than in HMP dental plaque (Supplementary Figure 4d). *V. parvula* is a prevalent inhabitant of the oral cavity that causes rare opportunistic infections.

Three additional taxa were found to have strongly discordant relative frequencies in ancient dental calculus compared to the HMP healthy cohort: *Filifactor alocis*, *Olsenella uli*, and *Rothia dentocariosa*. The relative frequency of *F. alocis* was found to be substantially higher in G12 and B61 ancient dental calculus compared to HMP dental plaque (Supplementary Figure 4e). Although not listed as a pathogen in the PATRIC database, *F. alocis* has recently been shown to be associated with periodontal disease and endodontic infections.[105,106] The relative frequency of *O. uli* was found to be substantially higher in B61 ancient dental calculus compared to G12 ancient dental calculus or HMP dental plaque (Supplementary Figure 4f). Although not listed as a pathogen in the PATRIC database, *O. uli* has recently been shown to be associated with primary endodontic infections.[25] Finally, the relative frequency of *R. dentocariosa* was found to be substantially lower in G12 and B61 ancient dental calculus compared to HMP dental plaque (Supplementary Figure 4g). *R. dentocariosa* is a prevalent member of the oral cavity associated with both health and disease states; although not classified as a pathogen in the PATRIC database, it has been identified in a wide range of rare opportunistic infections.

Putative zoonoses, or their close relatives in the human oral cavity
Five putative pathogens are possible zoonoses: *Streptobacillus moniliformis, Streptococcus suis, Streptococcus equi*, *Streptococcus gallolyticus*, and *Histophilus somni*. *S. moniliformis* is a zoonotic pathogen that causes rat bite fever in humans. *S. suis*, *S. equi*, *S. gallolyticus*, and *H. somni* are common zoonoses in domesticated livestock. *S. suis* is a common porcine zoonosis that causes meningitis and septicemia in both pigs and humans; asymptomatic carriage rates of *S. suis* may be as high as 80% in domestic pigs worldwide, and healthy pigs have been shown to carry multiple serotypes throughout their genital, respiratory, and alimentary systems.[89] *S. suis* is easily transmitted to humans through direct contact with infected pigs or consumption of undercooked pork products. *S. equi* is the causative agent of strangles, a common equine disease,[90] but it is also known to opportunistically infect humans and a range of domesticated animals, including cattle, sheep, goats, pigs, dogs, and cats.[91] *S. gallolyticus* is a common opportunistic pathogen in humans that is closely related to *S. bovis* in cattle. It can infect a wide range of wild and domesticated animals, and in humans it is often associated with endocarditis and colon cancer.[92] *H. somni* (formerly *Haemophilus somnus*) is a common genital commensal in cattle and sheep that can cause opportunistic respiratory infections in ruminants, although it is not known to cause disease in humans.[93,94]

Given the identification of both porcine and ovine DNA sequences in human dental calculus (see section 6.5.1), as well as the presence of osteological porcine, ovine, bovine, and equine skeletal remains at the site, the presence of these zoonoses in ancient dental calculus is plausible, and may suggest close contact through animal husbandry or consumption of infected animal products. However, we have also identified sequences consistent with each of these putative zoonotic pathogens in HMP dental plaque from healthy human controls, suggesting that they are either human commensals or that human sub-clinical carriage of thesse zoonoses is more common than previously thought based on culturing and cloning studies. The putative zoonotic DNA sequences, while intriguing, remain inconclusive given the small number of sequences detected and the possibility that they instead belong to closely related taxa that have not yet been characterized in the human oral cavity.

6.5.5 Identification of virulence factors and mobile elements

To further characterize the pathogens detected in ancient human dental calculus, feature information for each contig was retrieved from the top hit BLAST results and manually screened for putative virulence-, drug resistance-, plasmid-, transposon-, and phage-associated genes with annotations in PubMed records. While not exhaustive, a preliminary list of well-supported virulence genes was compiled using this method (Supplementary Table 3).

6.5.6 Antibiotic resistance

Three strategies were employed for identifying putative antibiotic resistance genes in our metagenomic and metaproteomic datasets, combining both sequence-driven and keyword-driven search strategies.

Method 1: ARDB
All G12 assembled contigs were searched against the Antibiotic Resistance Database (ARDB)[65] using BLASTx. Positive hits in the ARDB output files were validated by reverse blasting the DNA sequences against the NCBI nr database. NCBI nr top hits with e-values >1e-14 were discarded. Sequences with matching gene feature information in both the ARDB and NCBI nr databases were filtered for further analysis. ARDB positive hits to the penicillin binding protein genes *pbp1a* (8), *pbp2b* (7), and *pbp2x* (9) and to the rRNA adenine dimethyltransferase gene *ksga* (1) were analyzed and discarded after they were not found to contain known antibiotic resistance mutations. A total of 15 DNA contigs showed homology to genes with putative antibiotic resistance function using Method 1.

Method 2: Translated Gene Function Keyword Search
All G12 assembled contigs were searched against the NCBI database using BLASTx. Hits of any frame homology with an e-value <1e-14 and a translated amino acid length >30 bases were filtered, and protein name and feature information was keyword searched for the following terms: antibiotic, resistance, drug, multidrug, bacteriocin, lantibiotic, *cin, *mycin, *cycline, macrolide, acriflavin, azaleucine, and beta-lactamase. The results were then manually reviewed and filtered to remove spurious hits unrelated to antibiotic resistance function. Positive hits were validated by reverse blasting the DNA sequences against the NCBI nr database. NCBI nr top hits with e-values >1e-14 were discarded. Sequences with matching gene feature information in both the ARDB and NCBI nr databases were filtered for further analysis. A total of 68 DNA contigs showed homology to genes with putative antibiotic resistance function using Method 2.

Method 3: Gene and Protein Annotation Keyword Search
Assembled and annotated DNA contigs from G12 and B61 and proteins from G12, B17, B61, and B78 that had been assigned to pathogens (see section 6.5.3) were manually screened for antibiotic resistance genes by reviewing the BLAST top hit gene name and function fields for DNA sequences and the Scaffold assigned protein name field for peptides. A total of 302 DNA contigs showed homology to genes with putative antibiotic resistance function. No proteins matched putative antibiotic resistance proteins.

Combined Search Results

DNA sequences with homology to a diverse range of putative antibiotic resistance genes were observed (Supplementary Table 4). These include multidrug efflux pump genes belonging to the Multi Antimicrobial Extrusion protein family (MATE), the ATP-Binding Cassette superfamily (ABC), the Major Facilitator Superfamily (MFS), and the Resistance-Nodulation-Cell Division superfamily (RND). The efflux genes observed in our dataset (e.g., *AcrAB*, *Bcr/CflA*, *MdrB*) encode proteins that can pump out a wide range of toxic compounds from bacterial cells. We also observed numerous metallo-beta-lactamase genes in the ancient dental calculus dataset; these enzymes can hydrolyse beta-lactam antibiotics including penicillins, cephalosporins, and carbapenems. Efflux pumps are abundant among Gram-negative bacteria and primarily function to eliminate self-produced secondary or toxic metabolites, but they can also export other antibiotic compounds to varying degrees. Metallo-beta-lactamases are likewise highly abundant and widespread among bacteria, serving multiple cellular functions in addition to beta-lactam hydrolysis. Thus, the observation of these genes is unsurprising and does not necessarily indicate functional antibiotic resistance, although mutations in these genes or their promoters can result in more active phenotypes of clinical significance.

Of greater interest are genes related to bacitracin, macrolide, aminoglycoside, glycopeptide, and tetracycline resistance, as these genes are more restricted among bacteria. Bacitracin is a mixture of related cyclic peptide antibiotics produced by growth antagonistic strains of *Bacillus subtilis and Bacilus licheniformis* that function as inhibitors of cell wall biosynthesis by sequestering C_{55}-PP, a carrier lipid essential for peptidoglycan cell wall biosynthesis.[107] The bacitracin resistance gene *uppP*, (formerly *bacA*) allows de novo synthesis of the carrier lipid, thus conveying bacitracin resistance. *Bacillus subtilis* is a resident of the human oral microbiome, and we observed 7,806 16S rRNA sequences corresponding to 6 OTUs matching the *Bacillus* genus in our ancient dental calculus data. *UppP* homologues have been reported for 116 bacterial species in the human oral microbiome,[69] and we observed 15 sequences with homology to the *uppP* genes of eight different taxa.

Macrolides, aminoglycoside, glycopeptides, and tetracyclines are natural antibiotic products produced by members of the genus *Streptomyces*. We observed 23 16S rRNA sequences corresponding to two *Streptomyces* genus OTUs in our ancient dental calculus, as well as at least 15 sequences with homology to macrolide export genes (e.g., *MacB*, *Fsr*), 11 sequences with homology to aminoglycoside degrading enzymes (e.g., adenyltransferase), 4 sequences with homology to glycopeptide resistance genes (e.g., glyoxalase/bleomycin resistance protein), and 44 sequences with homology to genes related to transcription regulation and mobilization of tetracycline resistance genes (e.g., *TetR* and *RteC*). *Streptomyces* species are uncommon in the oral cavity today, but they are found in the modern gut microbiome [108].

6.5.7 Ancient *Tannerella forsythia* Genome Reconstruction

Tannerella forsythia (formerly *Bacteroides forsythus* and *Tannerella forsythensis*) is an anaerobic, filament shaped, non-pigmented, non-motile gram-negative member of the phylum Bacteroidetes and a common inhabitant of supragingival and subgingival plaque.[32] Within the genus *Tanerella*, *T. forsythia* is the only abundant member in the oral cavity,[109] and it is

characterized by high homology among strains (75-100%). By contrast, it shows relatively low homology to the most closely related non-*Tannerella* oral taxon, *Bacteroides distasonis* (0-48%), and <30% homology to the most closely related abundant oral taxon, *Porphyromonas gingivalis,*[32] making it a good candidate for genome reconstruction from a metagenomic data set.

To create a reduced but inclusive contig pool for *Tannerella forsythia* genome reconstruction, all G12 contigs ≥100 bp were searched against the NCBI nt and gss databases using Megablast and filtered for contigs aligning to *T. forsythia* strain ATCC 43037 (INSDC accession CP003191.1) with an e-value ≤ 1e-6 within the top 100 hits. The filtered contigs were pooled and submitted to the BLAST Ring Image Generator (BRIG) tool for mapping.[66] Using BRIG, the contigs were aligned to the *T. forsythia* strain ATCC 43037 using the Megablast search option and a sequence identity cutoff of ≥95%. In cases where a contig aligned to the *T. forsythia* genome more than once, the alignment with the highest bit score was mapped. In cases where multiple alignments with identical top bit scores were observed, the contig was mapped to all top bit score loci, but the depth of coverage for each locus was divided by the number of loci. A genome recruitment plot was generated for the filtered G12 contigs against the *Tannerella forsythia* strain ATCC 43037 reference genome (3,405,453 bp).

A total of 10,991 contigs were recruited to the genome reconstruction, and mean nucleotide depth of coverage of the assembly is 5.715. The percentage of the genome mapped with at least one aligned read is 66.05% (2,249,205 bp); with at least two aligned reads is 65.57% (2,233,034 bp). Complete mapping is not expected given that there are likely strain differences between the ancient oral sample and the *T. forsythia* reference genome used for mapping. Genes were scored for presence/absence, and a closer analysis of the alignments revealed a non-random distribution of unmapped genes.

The *T. forsythia* strain ATCC 43037 reference genome contains a total of 3,087 genes (http://hpv-web.lanl.gov/microbe.php?class=oral), of which 54% have a known or predicted function (n=1680). In our genome reconstruction, 91% of *T. forsythia* genes (n=2799) were mapped by at least one contig. Of the genes that were not mapped (n=288), 67% are hypothetical or conserved hypothetical proteins of unknown function (n=194). Of the unmapped genes with a known or predicted function (n=94), 59% encode transfer factor mobilization proteins (transposases, integrases, excisionases, transfer proteins, and rte excision regulators; n=55) and 4% are related to antibiotic/lantibiotic function (tetracycline resistance and lantibiotic synthesis; n=5). The remaining unmapped genes consist of very short tRNA and rRNA 5S coding genes <110 bp in length (12%; n=11), and genes of miscellaneous function (26%; n=24; e.g., methyltransferases and outer membrane proteins).

The majority of unmapped genes were found to occur in groups, forming gaps in the reconstruction. 58% of all unmapped genes belong to gaps spanning at least 3 consecutive genes, and 41% of unmapped genes belong to gaps spanning 9 or more consecutive genes. Eleven regions around the genome are unmapped or poorly mapped (≥90% of nucleotides have a coverage of 0) for >5,000 bp, forming large gaps or gap clusters in the assembly (Supplementary Figure 23). These gap regions account for 50% of the unmapped genes (n=143), and seven of these eleven regions contain or are directly associated with transposases or other mobilization

genes (Gaps 1, 3, 4, 7, 8, 9, 10); of the remaining four gap regions, two contain only hypothetical or conserved hypothetical proteins of unknown function (Gaps 1, 11).

Like other members of the *Bacteroides* family,[110] *T. forsythia* carries conjugative transposon (CTn) sequences conveying antibiotic resistance genes and other virulence factors.[32] The *T. forsythia* ATCC 43037 reference strain contains one complete tetracycline resistance conjugative transposon resembling a CTnERL or CTn341, one partial tetracycline resistance CTn-like element, and multiple fragments of relic CTns. The largest gap region in the G12 *T. forsythia* genome reconstruction (Gap 10), which spans ~48,000 bp and 53 genes (interrupted by only two mapped contigs 220 bp and 178 bp in length), corresponds to the reference strain's entire CTnERL/341-like element. The gap begins with the gene encoding CTn integrase-recombinase protein (TF2220) followed by excision (TF2221-TF2230), tetracycline resistance (tetQ, TF2235), regulatory (TF2236-TF2240), and transfer regions (TF2243-TF2266), and ending with genes encoding 12 hypothetical proteins of unknown function (TF2270-TF2281). The third largest gap in the *T. forsythia* genome reconstruction (Gap 3) corresponds to a ~17,000 bp of a partial CTn-like element in the reference strain containing the tetracycline resistance repressor gene, *tetR*.

As only one full *T. forsythia* genome has been sequenced (strain ATCC 43037), the core-genome and pan-genome of the *T. forsythia* group has not yet been established. However, a gene-by-gene analysis of contig mapping in the ancient *T. forsythia* assembly suggests that many unmapped genes likely correspond to mobile elements of the pan genome, while mapped genes include both core genome and pan genome genes shared with the ATCC 43037 strain. These latter genes include, among others, multiple transposases and four genes associated with tetracycline resistance: TF0082 and TF1912 (*tetR*), TF0923 (*rteC*), TF1302 (conserved hypothetical protein, possible tetracycline resistance element). Because tetracycline resistance is coordinated by multiple genes, the significance of finding isolated tetracycline resistance-associated genes in an ancient oral bacterium is unclear. They may be components of a tetracycline resistance system that is present in another strain, they may be non-functional relics of a shared ancestral system, or they may serve alternative functions unrelated to antibiotic resistance. The latter is supported by the observation that despite the presence of tetracycline resistance and mobilization genes tetQ and rteC in the CTnERL-like conjugative transposon of the ATCC 43037 reference strain, no increased resistance to tetracycline was observed for this strain in culture.[32]

7. Protein Analysis

7.1 Protein Extraction and Purification

Protein extractions were performed in laboratories where no bacterial culturing takes place. Generation of tryptic peptides from tooth and dental calculus specimens was performed using a filter-aided sample preparation (FASP) protocol,[67] modified for mineralized and degraded samples. Total protein extraction was performed on a total of twelve samples: four ancient human calculus samples (indicated as: G12, B71, B61, and B78), four ancient human tooth root samples (indicated as: G12, B71, B61, and B78), two ancient fauna crown cementum/calculus samples (indicated as: F1 [sheep] and F5 [cattle]), and two modern dental calculus samples from clinical patients (indicated as: P1 and P2). All samples were extracted at the Centre for

Evolutionary Medicine (ZEM) at the University of Zürich with the exception of dental calculus from G12, P1, and P2, which were extracted at the Center for GeoGenetics (CGG) at the University of Copenhagen. Two samples (G12 and B61 calculus) were extracted a second time in an independent laboratory at the University of York (YORK) for comparison. Sample extracts were then sequenced at the Functional Genomics Center Zürich (FGCZ), the Novo Nordisk Foundation Center for Protein Research (CPR), and the University of York's Proteomics and Analytical Biochemistry Laboratories (PABL) (Supplementary Table 27).

Dental calculus and root samples were wrapped in aluminum foil, transferred to a sterile mortar and pestle, and crushed to a fine powder. Depending on availability, 12-80mg of sample was suspended in 1mL 0.5M EDTA (pH 8.0) and incubated overnight at room temperature under agitation. After centrifugation, the supernatant (EDTA-fraction) for all samples except G12, P1 and P2, was transferred to sterile 15mL tubes containing 9mL 8M urea, 0.1M Tris/HCl pH 8.0, mixed and ultrafiltered through an Amicon Ultra-4 centrifugal filter units with 10kDa NMWL in 4mL increments. For samples G12, P1 and P2, the EDTA fraction was dialyzed using Slide-A-Lyzer Dialysis Cassettes 2K MWCO (Pierce Biotechnology, Rockford, USA) against 1L ddH_2O for 24h, changing water three times in total. Dialyzed fractions were collected and buffered in 50 mM final concentration ammonium bicarbonate pH 7.5-8.0. EDTA-fractions for samples G12, P1 and P2 were stored at -20°C until reduction-alkylation-digestion was performed as previously described,[111] without adding Rapigest in this case, and were then purified using Stage-tips as reported below. For all samples the pellets obtained after centrifugation were then resuspended in 300µL lysis buffer (4% SDS, 0.1M DTT, 0.1M Tris/HCl, pH 8.0). Tooth root pellets were gelatinized by heating at 80˚C for two hours under agitation at 500 rpm. Dental calculus pellets were instead homogenized using a sterile micropestle and then heated at 95˚C for 10 minutes under agitation at 500 rpm. Following this step, the samples were then centrifuged to pellet insoluble minerals and cellular debris.

The supernatant (SDS-fraction) was mixed with 2 mL 8M urea and ultrafiltered using the unit previously used for the EDTA-fraction of the same sample or a new one for samples G12, P1 and P2. FASP protocol continued washing the fraction retained above ultrafilter with 2mL 8M urea, 0.1M Tris/HCl pH 8.0. Alkylation was achieved re-suspending in 500 µL of 50 mM 2-Chloroacetamide (CAA), 8M urea, 0.1M Tris/HCl pH 8.0 and incubating 20 min in the dark at room temperature. CAA was removed washing with 1 mL of 8M urea, 0.1M Tris/HCl pH 8.0 for two times, then urea was removed washing with 1 mL 50 mM ammonium bicarbonate, pH 7.5-8.0, followed by a second wash with 100µL of 50mM ammonium bicarbonate. The fraction retained above ultrafilter was re-suspended in 300µL of 50 mM ammonium bicarbonate pH 7.5-8.0 and mixed. One µL of solution was collected for protein quantification using a Qubit fluorometer (Invitrogen).

Protein digestion was started adding 4µL of 0.5µg/µL sequencing grade trypsin solution (Promega). After mixing pH was checked using pH strips and, if necessary, adjusted to 7.5-8.0. The ultrafiltration units were incubated at 37˚C overnight. The following morning one supplemental µg of fresh trypsin was added and digestion was extended for 6 additional hours. Ultrafiltration units were then transferred into new sterile 15mL tubes and centrifuged for 10 minutes to collect the digested peptides and 1µL of the filtrate was collected for Qubit protein quantification. An additional 500µL 0.05M ammonium bicarbonate pH 7.5-8.0 aliquot was

added to the filter, mixed, and centrifuged to elute remaining peptides. The filtrate was then transferred to a sterile 1.5 mL tube and acidified with 10% trifluoroacetic acid to a final concentration of 0.2-0.8% to reach a pH < 2. C-18 Empore (3M) solid phase extraction (SPE) Stage tips[111] were prepared in-house and sequentially conditioned with 150 µL methanol, 150 µL 80% acetonitrile solution (80% acetonitrile, 0.5% acetic acid, 19.5% ddH_2O), and 150 µL 0.5% acetic acid. The acidified peptides were then loaded into the stage tips and immobilized onto the C-18 filter by centrifugation. The filter was then washed with 150 µL 0.5% acetic acid, centrifuged until dry, and stored at -20˚C.

On the day of MS/MS analysis, the stage tips were placed into sterile collection tubes and eluted three times with 40 µL acetonitrile solution in increasing concentrations (40%, 60%, and 80% acetonitrile, 0.5% acetic acid in ddH_2O). The eluted peptides were then concentrated by centrifugal evaporation to a volume of < 4 µL and resuspended in a carrier solution according to sequencing center-specific protocols. At the FGCZ and York, samples were resuspended in 20 µL 3% acetonitrile solution (3% acetonitrile, 0.1% formic acid). At CPH, samples were resuspended in 10 µL 0.1% trifluoroacetic acid.

7.2 LC-ESI-high resolution MS/MS analysis

7.2.1 LTQ-Orbitrap Velos (FGCZ)

Samples were analyzed on an LTQ-Orbitrap VELOS mass spectrometer (Thermo Fischer Scientific, Bremen, Germany) coupled to an Eksigent-NanoLC-Ultra 1D plus HPLC system (Eksigent Technologies, Dublin (CA), USA). Solvent composition at the two channels was 0.2% formic acid, 1% acetonitrile for channel A and 0.2% formic acid, 100% acetonitrile for channel B. Peptides were loaded on a self-made tip column (75 µm × 80 mm) packed with reverse phase C18 material (AQ, 3 µm 200 Å, Bischoff GmbH, Leonberg, Germany) and eluted with a flow rate of 250 nl per min by a gradient from 0.8% to 4.8% of B in 2 min, 35% B at 57 min, 48% B at 60 min, 97% at 65 min. Full-scan MS spectra (300−1700 m/z) were acquired in the Orbitrap with a resolution of 30 000 at 400 m/z after accumulation to a target value of 1,000, 000. Higher energy collision induced dissociation (HCD) MS/MS spectra were recorded in data dependent manner in the Orbitrap with a resolution of 7500 at 400 m/z after accumulation to a target value of 100, 000. Precursors were isolated from the ten most intense signals above a threshold of 500 arbitrary units with an isolation window of 2 Da. Three collision energy steps were applied with a step width of 15.0% around a normalized collision energy of 40% and an activation time of 0.1 ms. Charge state screening was enabled excluding non-charge state assigned and singly charged ions from MS/MS experiments. Precursor masses already selected for MS/MS were excluded for further selection for 45 s with an exclusion window of 20 ppm. The size of the exclusion list was set to a maximum of 500 entries.

7.2.2 Q-Exactive Hybrid Quadrupole Orbitrap (CPR)

The LC-MS system consisted of an EASY-nLC™system (Thermo Scientific, Odense, Denmark) connected to the Q-Exactive (Thermo Scientific, Bremen, Germany) through a nano electrospray ion source. 5 uL of each peptide sample was auto-sampled onto and directly separated in a 15cm analytical column (75 µm inner diameter) in-house packed with 3µm C18 beads (Reprosil-AQ

Pur, Dr. Maisch) with a 130 minute linear gradient from 5% to 26% acetonitrile followed by a steeper linear 20 minute gradient from 26% to 48% acetonitrile. Throughout the gradients a fixed concentration of 0.5% acetic acid and a flow rate of 250 nL/min were set. A final washout and column re-equilibration added an additional 15 minutes to each acquisition. The effluent from the HPLC was directly electrosprayed into the mass spectrometer by applying 2.0 kV through a platinum-based liquid-junction. The Q-Exactive was operated in data-dependent mode to automatically switch between full scan MS and MS/MS acquisition. Software control was Tune version 2.0-1428 and Excalibur version 2.2.42, and the settings were adjusted for 'sensitive' acquisition. Briefly, each full scan MS was followed by up to 10 MS/MS events. The isolation window was set at 1.6 Th and a dynamic exclusion of 90 seconds was used to avoid repeated sequencing. Only precursor charge states above 1 and below 6 were considered for fragmentation. A minimum intensity threshold for triggering fragment MS/MS was set at 1e5. Full scan MS were recorded at resolution of 70,000 at m/z 200 in a mass range of 300-1700 m/z with a target value of 1e6 and a maximum injection time of 20 ms. Fragment MS/MS were recorded with a fixed ion injection time set to 120 ms through a target value set to 1e6 and recorded at a resolution of 35,000 with a fixed first mass set to 100 m/z.

7.2.3 MaXis UHR-Qq-TOF (PABL)

In the case of G12, an additional liquid IEF step was first performed using an Agilent 3100 OFFGEL Fractionator according to the protocol of the supplier. Briefly, the tryptic digest was loaded onto a rehydrated 12 cm long IPG gel strip with a linear pH gradient ranging from 3-10. The calculus extract (20 µl) was diluted with 340 µl of dH_20, to which 1.44 ml of Protein OFFGEL stock solution was added to give a final volume of 1.8 ml. 150 µl of sample solution was loaded into each well. The sample was focused with a maximum current of 50 µA and maximum voltage of 4000 V until 20 kVh was reached after approx. 24 h. Twelve separate peptide fractions were obtained. The recovered fractions (volumes between 100 and 150 µl) were acidified with 25 µl of 1% (v/v) TFA. Finally, peptide analysis was performed via LC-MS/MS, with each peptide fraction loaded on a separate run.

Samples were loaded onto a nano-Acquity UPLC system (Waters) equipped with a nanoAcquity Symmetry C_{18}, 5 µm trap (180 µm x 20 mm Waters) and a nanoAcquity BEH130 1.7 µm C_{18} capillary column (75 µm x 250 mm, Waters). The trap wash solvent was 0.1% (v/v) aqueous formic acid and the trapping flow rate was 10 µL/min. The trap was washed for 5 min before switching flow to the capillary column. The separation used a gradient elution of two solvents (solvent A: 0.1% (v/v) formic acid; solvent B: acetonitrile containing 0.1% (v/v) formic acid). The flow rate for the capillary column was 300 nL/min Column temperature was 60°C and the gradient profile was as follows: initial conditions 5% solvent B, followed by a linear gradient to 30% solvent B over 125 min, then a linear gradient to 50% solvent B over 5 min, followed by a wash with 95% solvent B for 10 min. The column was returned to initial conditions and re-equilibrated for 30 min before subsequent injections.

The nanoLC system was interfaced with a maXis LC-MS/MS System (Bruker Daltonics) with a Bruker nano-electrospray source fitted with a steel emitter needle (180 µm O.D. x 30 µm I.D., Thermo [Proxeon]). Positive ESI- MS & MS/MS spectra were acquired using AutoMSMS mode. Instrument control, data acquisition and processing were performed using Compass 1.3 SR3

software (microTOF control, Hystar and DataAnalysis, Bruker Daltonics). Instrument settings were: ion spray voltage: 1,400 V, dry gas: 4 L/min, dry gas temperature 160°C, ion acquisition range: *m/z* 50-2,200. AutoMSMS settings were: MS: 0.5 s (acquisition of survey spectrum), MS/MS (CID with N_2 as collision gas): ion acquisition range: *m/z* 300-1,500, 0.1 s acquisition for precursor intensities above 100,000 counts, for signals of lower intensities down to 1,000 counts acquisition time increased linear to 1s, the collision energy and isolation width settings were automatically calculated using the AutoMSMS fragmentation table: eight precursor ions, absolute threshold 1,000 counts, preferred charge states: 2 – 4, singly charged ions excluded. One MS/MS spectrum was acquired for each precursor, and former target ions were excluded for 30 s.

7.2.4 Conversion to Mascot generic format and H-Scoring

Tandem mass spectra were converted to the Mascot generic format (.mgf) using proteowizard version 2.2.3101 with the vendor peak picking option for MS level two. Corresponding .mgf files were further deisotoped and deconvoluted using the H-Scorer script.[68]

7.3 Bioinformatics Pipeline for Proteomic Data

7.3.1 Protein Modification and Damage Analysis

Proteins obtained from biological samples contain numerous post-translational modifications, and dental biofilm proteins in particular exhibit extensive degradation as a result of bacterial proteolytic activity. Additionally, proteins accumulate damage over time, a process that is particularly relevant for the study of archaeological proteins, and sample extraction preparation and analysis can also introduce artifacts. ProteinPilot v.4 (AB SCIEX, Framingham, MA, USA) was used to characterize protein modification and damage patterns in a subset of ancient and modern dental calculus extracts (Supplementary Table 28). Unlike Mascot, the ProteinPilot's Paragon algorithm allows for over 150 modifications to be searched simultaneously, allowing identification of common modifications. The results of this analysis were then used to select appropriate variable modifications for subsequent Mascot searching.

Using ProteinPilot v.4, Mascot generic format files were analyzed using the UniProt Knowledgebase Swiss-Prot database plus decoy (reversed) entries and common contaminants from the date 2011-01-11, selecting the biological modification focus and the urea-treatment option. The minimum confidence threshold for peptide assignment was set to the confidence level corresponding to a distinct peptide 5% local FDR level in each sample group. Peptide assignment rates were then compared between pooled modern and ancient samples. A 3.6-fold greater proportion of modern peptides were assigned compared to ancient ones, a finding that is consistent with higher expected damage rates in archaeological proteins compared to modern controls. Protein assignment rates at the 1% global FDR level were estimated at 1.7% (n=351) and 1.0% (n=157) in modern and ancient samples, respectively. Assigned peptides were then analyzed and compared across groups for accuracy of tryptic cleavage, frequency of amino acid modification, and types of modifications (Supplementary Figure 11).

Analysis of cleavage sites reveals that 89% of ancient peptides and 69% of modern peptides were fully tryptic (Supplementary Figure 11a). Peptides with missed cleavages, which can indicate incomplete protein denaturation during the extraction step, were more common in modern (13%) than in ancient samples (7%), as expected given that archaeological samples are unsurprisingly more fragmented and less likely to have well-preserved tertiary structure. Semi-tryptic peptides were detected at moderate levels of 11% and 29% for ancient and modern peptides, respectively, and in response we expanded the Mascot search space to accommodate semi-tryptic peptides. Semi-tryptic peptides may result from biofilm proteolytic activity or stochastic taphonomic processes. It is unclear why the proportion of semi-tryptic peptides is higher in modern than in ancient dental calculus. However, given that a smaller percentage of total spectra were assigned in the ancient samples compared to modern controls, this observation would be consistent with a greater accumulation over time of further chemical modifications at the N and C terminals of polypeptide residues generated by non-enzymatic cleavage during diagenesis. The combination of these two taphonomic processes would strongly affect identification of semitryptic peptides in ancient samples.

The proportion of peptides with at least one modified site was greater in ancient samples (50%) than in modern controls (40%) (Supplementary Figure 11b). When broken down by modification type, four modifications are observed at a normalized frequency of ≥ 5% in at least one sample group: asparagine deamidation, methionine oxidation, glutamine deamidation, and conversion of glutamine to pyro-glutamic acid. These modifications were also found to have the highest relative proportion of modified sites of possible sites in both ancient and modern samples (Supplementary Figure 11b). Consequently, these four modifications were selected as variable modifications for subsequent Mascot searching.

Ancient dental calculus samples clearly show elevated levels of asparagine deamidation, methionine oxidation, glutamine deamidation, and conversion of glutamine to pyro-glutamic acid at the N-terminus compared to modern dental calculus. While a proportion of these modifications in both ancient and modern samples may be attributable to sample preparation artifacts (e.g. oxidation during ESI spray), the large difference observed between ancient and modern samples likely reflects a greater degree taphonomic damage in the ancient samples. For example, asparaginyl and glutaminyl residues spontaneously deamidate over time at predictable rates that make them useful as a molecular clock in both living systems and archaeological specimens.[112] The higher frequency of asparagine and glutamine deamidation in the ancient dental calculus samples is therefore likely related to their greater age.

In addition to the four variable modifications listed above, acetylation of protein N-terminus and oxidation of proline were also added as variable modifications. N-terminus protein acetylation is a common modification found in human proteins, and proline hydroxylation (isobaric to proline oxidation), while uncommon in most proteins, is physiologic of collagen, the dominant protein in bone and dentine.

7.3.2 Protein Identification by Mascot searches and Scaffold filtering

Tandem Mass Spectra Interpretation

Mascot generic format MS/MS peak lists were submitted to Mascot (Matrix Science, London, UK; version 2.3.02) for searching. Selecting semi-trypsin as the proteolytic enzyme, Mascot was set up to search against a non-redundant, concatenated target/decoy protein database consisting of 4198561 forward and 4197958 reversed protein sequences that included all proteins available in UniProtKB/Swiss-Prot (v.20121031; total 1076779 sequences), all proteins available in the Human Oral Microbiome Database as of 2012/10/11 (total 4476028 sequences; http://www.homd.org/),[69] and all proteins available for Genbank genome accessions of bacteria and archaea in which the word "soil" appears in the metadata (total 2843972 sequences) as of 2012/02/22. Our concatenated database is available online (http://fgcz-s-021.uzh.ch/FASTA/p1043_all3DBsConcat_allDecoyed_db3_db4_fgczswissprot_forScaffold_20121029.fasta). For data generated on the LTQ Obitrap Velos and Q-Exactive Hybrid Quadrupole Obitrap instruments, Mascot was searched with a fragment ion mass tolerance of ± 0.8 Da; for data generated on the Q-TOF, Mascot was searched with a fragment ion mass tolerance of ± 0.1 Da. For Mascot search of all data, precursor mass tolerance was set at ± 10 ppm, and a maximum of 2 missed cleavages were allowed. Carbamidomethylation of cysteine was specified as a fixed modification, and as already mentioned, acetylation (Protein N-term), deamidation (N, Q), Gln→ pyro-Glu (N-term Q), oxidation (M), and oxidation (P) were specified in Mascot as variable modifications.

Peptide and Protein Identification

Scaffold software (version Scaffold 4.0.5, Proteome Software Inc., Portland, OR) was used to validate MS/MS based peptide and protein identifications. Mascot results for each extract were analyzed both individually and pooled by category (ancient human dental calculus, ancient fauna dental calculus, ancient human root, modern human dental calculus, negative control) using the MudPIT option. Peptide identifications were accepted if they could be established at greater than 95.0% probability as specified by the PeptideProphet algorithm, and protein identifications were accepted if they could be established at greater than 99.0% Protein Prophet probability and contained at least 2 identified peptides. Proteins that contained similar peptides and could not be differentiated based on MS/MS analysis alone were grouped to satisfy the principles of parsimony. Only proteins that met the above criteria after screening for potential contaminants (see below) were considered positively identified for further analysis. The amount of random matching was evaluated by performing the Mascot searches with databases containing decoy entries and checking how many decoy entries (proteins or peptides) passed the applied quality filters. Total FDR was estimated at 1.2% for 12,609 unique peptides and 0.1% for 589 unique proteins.

Prevention and Detection of Contaminants

Dental calculus protein extraction at the ZEM was carried out in a laboratory that had not been previously used for proteomic analysis. Because latex gloves have been found to be a source of protein contamination in previous studies[111] we only used nitrile gloves for sample preparation and analysis. Environmental contaminants, such as keratins and proteins commonly used in mass spectrometry facilities as standards and calibrants, were excluded from further investigation, and non-template extracts (negative controls) performed in parallel with the experimental samples were analyzed using multi-dimensional protein identification technology (MudPIT) to identify additional contaminants (Supplementary Table 29). MS runs analyzing blanks or fetuin-spiked samples were inserted between changes in types of samples (e.g., between ancient dental

calculus and root samples, and between ancient and modern dental calculus) to avoid sample carry-over contamination, and fetuin detected in any sample was discarded as a contaminant. Modern samples were always placed at the end of a run.

7.3.3 Protein analysis

The mass spectrometry proteomics data (.raw, .baf, .mgf, .dat, .xml, and .sf3 files) have been deposited to the ProteomeXchange Consortium (http://proteomecentral.proteomexchange.org) via the PRIDE partner repository[56] with the dataset identifier PXD000412, accessions 34605-34628.

Human
For ancient dental calculus, modern dental calculus, and ancient tooth roots, proteins assigned by Scaffold to members of the primate lineage (n=108) were manually validated (Source File for Figure 3). Eighty-nine of these proteins were assigned to humans alone, while 19 were conserved among primates alone. Proteins conserved among Eukaryotes outside the primate lineage were excluded from human analysis (see Dietary protein section below). Because there is neither a reasonable expectation of other primates in our archaeological samples nor a foreseeable possibility of non-human primate contamination, all proteins assigned exclusively to the primate lineage were treated as human in subsequent analyses.

Entrez, UniProt, GO, and KEGG metadata for each human protein was retrieved using the GeneCards v.3 GeneALaCart tool[70] for batch queries (http://www.genecards.org/). This metadata was then used to manually classify each protein into one of six arbitrary categories: innate immune system, adaptive immune system, blood coagulation, digestion, structure and support, and other. In cases of ambiguity, additional information was obtained from peer-reviewed publications in the NCBI PubMed database.

Protein interaction information and GO enrichment for proteins identified in ancient dental calculus was obtained from STRING 9.0[37] (http://string-db.org/) in protein mode. Network display was set to evidence view with default parameters using all active prediction methods at medium confidence (0.400). GO enrichment for molecular function, cellular component, and biological process was calculated against a genome background with FDR correction of *p*-values.

Bacteria
Four hundred seventy-three bacterial proteins were recovered from all four ancient human calculus samples (G12, B17, B61, B78) and from both modern calculus samples (P1, P2), but no bacterial proteins were recovered from ancient root samples (G12, B17, B61, B78). Proteins assigned by Scaffold to pathogens found in the PATRIC (Pathosystems Resource Integration Center; http://www.patricbrc.org/) database were manually checked for putative virulence, antibiotic resistance, mobile element, plasmid, and phage proteins.

In order to evaluate the functional profiles of bacterial proteins in ancient and modern dental calculus, peptides assigned by Scaffold to bacterial proteins were binned into two groups by length (Group 1: <15 residues; Group 2: >15 residues) and submitted to protein BLAST for

sequence matching using the NCBI database (http://blast.ncbi.nlm.nih.gov/Blast.cgi) with the following criteria: for Group 1 peptides an expect value of 20000 was used and PAM30 was selected as the Score Matrix; for Group 2 peptides an expect value of 1000 was used and BLOSUM62 was selected as the Score Matrix. The resulting BLASTp files were then parsed using MEGAN metagenomic software and analyzed for protein function using SEED hierarchy[72].

Despite variation in both the number of bacterial peptides identified in each dental calculus sample, as well as the number of assigned functional classifications, overall protein functional profiles were relatively consistent among ancient and modern dental calculus (Supplementary Figure 10). All dental calculus samples exhibit a large proportion of proteins involved in carbohydrate-related functions, protein metabolism, and virulence, disease, and defense. Together, these top three functions account for more than 50% of all bacterial protein functions in both ancient and modern dental calculus.

Diet

Eukaryotic proteins shared by primates and non-primates, as well as non-primate assigned proteins that were identified in ancient or modern dental calculus, were evaluated as potential dietary indicators. Nucleophosmin (NPM), nuleoside diphosphate kinase A (NDKA), protein DJ-1 (PARK7), histone (H2A1), and actin peptides were identified in dental calculus, but these peptide sequences were too conserved among diverse animal taxa to determine the species of origin or to exclude humans as the protein source. Four peptides matching highly conserved regions of the chloroplast protein GAPDH (glyceraldehyde 3-phosphate dehydrogenase) were identified in ancient dental calculus. Although possibly dietary in origin, these sequences are found in diverse members of Viridiplantae, from common crops to green algae, and thus are relatively uninformative. Bovine milk protein β-lactoglobulin was identified in modern dental calculus only, and is likely an authentic dietary protein.

Database bias is clearly a limiting factor in protein-based dietary analyses. With 133,845 curated protein entries, humans have excellent coverage in the UniProt KB database. Putative Dalheim dietary items, by contrast, are less well represented in the database: e.g., *Sus* spp. (33,119), *Bos taurus* (32,738), *Ovis aries* (3,944), *Triticum* spp. (7,761), and *Brassica* spp. (5,824). Thus, poorly represented dietary items are likely to be missed during protein assignment, or, if some of the constituent peptides are conserved, to be incorrectly assigned to another taxon. To test this bias, we analyzed ancient tooth samples from cattle (sample F5) and sheep (sample F1) in parallel with ancient and modern human samples as controls. After excluding contaminants and collagens (which generally show poor taxonomic discrimination), all proteins from the faunal samples were assigned to Eukaryota. For the cattle sample, 16 proteins were assigned to *Bos taurus* and 7 proteins were assigned to other taxa (mouse, rat, pig, rabbit, human); of the mis-assigned proteins, 5 have no *Bos taurus* coverage in the UniProt KB database. For the sheep sample, 5 proteins were assigned to *Ovis aries*, while 9 were assigned to other taxa (goat, cow, pig, mouse, human); all 9 of the mis-assigned proteins have no *Ovis aries* coverage in the UniProt KB database. Thus, database representation impacts the detectability of potential dietary items. In light of the fact that many important dietary taxa are poorly represented in the database, any dietary protein finds can be assumed to be an underestimate.

8. References

73 van Klinken, G. J. Bone collagen quality indicators for paleodietary and radiocarbon measurements. *J Archaeol Sci* **26**, 687-695 (1999).

74 Dissing, J., Kristinsdottir, M. A. & Friis, C. On the elimination of extraneous DNA in fossil human teeth with hypochlorite. *J Archaeol Sci* **35**, 1445-1452 (2008).

75 Hofmann, M. I., Boni, T., Alt, K. W., Woitek, U. & Ruhli, F. J. Paleopathologies of the vertebral column in medieval skeletons. *Anthropologischer Anzeiger* **66**, 1-17 (2008).

76 Pieper, R. *Kloster Dalheim: Eine kurze Geschichte*. (Landschaftsverband Westfalen-Lippe, 2003).

77 White, D. J. Dental calculus: recent insights into occurrence, formation, prevention, removal and oral health effects of supragingival and subgingival deposits. *Eur J Oral Sci* **105**, 508-522 (1997).

78 Torrence, R. B., H. *Ancient starch research*. (Left Coast Press, Inc., Walnut Creek, CA, 2006).

79 Piperno, D. R. *Phytoliths: A comparative guide for archaeologists and paleoecologists*. (Altamira Press, 2006).

80 Moore, P. D. W., J. A.; Collinson, M. E. *Pollen Analysis*. 2 edn, (Blackwell Scientific, 1991).

81 Bergfjord, C. & Holst, B. A procedure for identifying textile bast fibres using microscopy: flax, nettle/ramie, hemp and jute. *Ultramicroscopy* **110**, 1192-1197 (2010).

82 Mould, Q., Carlisle, Ian, Cameron, Esther Anita, York Archaeological Trust. *Leather and Leatherworking in Anglo-Scandinavian and Medieval York*. Vol. 17 (Council for British Archaeology, 2003).

83 Tsuda, H. & Arends, J. Raman spectra of human dental calculus. *Journal of dental research* **72**, 1609-1613 (1993).

84 Bertoluzza, A. *et al.* Preliminary results in dating human skeletal remains by Raman spectroscopy. *J Raman Spectrosc* **28**, 185-188 (1997).

85 Morris, M. D. & Mandair, G. S. Raman assessment of bone quality. *Clinical orthopaedics and related research* **469**, 2160-2169 (2011).

86 Awonusi, A., Morris, M. D. & Tecklenburg, M. M. Carbonate assignment and calibration in the Raman spectrum of apatite. *Calcified tissue international* **81**, 46-52 (2007).

87 Thomas, D. B., McGoverin, C. M., Fordyce, R. E., Frew, R. D. & Gordon, K. C. Raman spectroscopy of fossil bioapatite: A proxy for diagenetic alteration of the oxygen isotope composition. *Palaeogeogr Palaeocl* **310**, 62-70 (2011).

88 Tramini, P., Pelissier, B., Valcarcel, J., Bonnet, B. & Maury, L. A Raman spectroscopic investigation of dentin and enamel structures modified by lactic acid. *Caries research* **34**, 233-240 (2000).

89 Ho, S. P. *et al.* Structure, chemical composition and mechanical properties of human and rat cementum and its interface with root dentin. *Acta biomaterialia* **5**, 707-718 (2009).

90 Hamilton, I. A. in *Oral Bacterial Ecology* (ed H.K. Kuramitsu, Ellen, R.P.) 219-275 (Horizon Scientific Press, 2000).

91 Rohland, N., Siedel, H. & Hofreiter, M. A rapid column-based ancient DNA extraction method for increased sample throughput. *Molecular ecology resources* **10**, 677-683 (2010).

92 Alonso, A. *et al.* Real-time PCR designs to estimate nuclear and mitochondrial DNA copy number in forensic and ancient DNA studies. *Forensic science international* **139**, 141-149 (2004).
93 Quail, M. A. *et al.* Optimal enzymes for amplifying sequencing libraries. *Nature methods* **9**, 10-11 (2012).
94 Ginolhac, A., Rasmussen, M., Gilbert, M. T. P., Willerslev, E. & Orlando, L. mapDamage: testing for damage patterns in ancient DNA sequences. *Bioinformatics* **27**, 2153-2155 (2011).
95 Lindgreen, S. AdapterRemoval: easy cleaning of next-generation sequencing reads. *BMC research notes* **5**, 337 (2012).
96 Walters, W. A. *et al.* PrimerProspector: de novo design and taxonomic analysis of barcoded polymerase chain reaction primers. *Bioinformatics* **27**, 1159-1161 (2011).
97 Horz, H. P., Vianna, M. E., Gomes, B. P. & Conrads, G. Evaluation of universal probes and primer sets for assessing total bacterial load in clinical samples: general implications and practical use in endodontic antimicrobial therapy. *Journal of clinical microbiology* **43**, 5332-5337 (2005).
98 Cole, J. R. *et al.* The Ribosomal Database Project: improved alignments and new tools for rRNA analysis. *Nucleic acids research* **37**, D141-145 (2009).
99 DeSantis, T. Z. *et al.* Greengenes, a chimera-checked 16S rRNA gene database and workbench compatible with ARB. *Applied and environmental microbiology* **72**, 5069-5072 (2006).
100 Caporaso, J. G. *et al.* QIIME allows analysis of high-throughput community sequencing data. *Nature methods* **7**, 335-336 (2010).
101 Contreras, M. *et al.* The bacterial microbiota in the oral mucosa of rural Amerindians. *Microbiology* **156**, 3282-3287 (2010).
102 Liu, B. *et al.* Deep sequencing of the oral microbiome reveals signatures of periodontal disease. *PloS one* **7**, e37919 (2012).
103 Segata, N. *et al.* Metagenomic microbial community profiling using unique clade-specific marker genes. *Nature methods* **9**, 811-814 (2012).
104 Stewart, F. J., Ulloa, O. & DeLong, E. F. Microbial metatranscriptomics in a permanent marine oxygen minimum zone. *Environmental microbiology* **14**, 23-40 (2012).
105 Belstrøm, D. *et al.* Differences in bacterial saliva profile between periodontitis patients and a control cohort. *Journal of Clinical Periodontology* (2013).
106 Kumar, P. S. *et al.* Changes in periodontal health status are associated with bacterial community shifts as assessed by quantitative 16S cloning and sequencing. *J Clin Microbiol* **44**, 3665-3673 (2006).
107 Bouhss, A., Trunkfield, A. E., Bugg, T. D. & Mengin-Lecreulx, D. The biosynthesis of peptidoglycan lipid-linked intermediates. *FEMS microbiology reviews* **32**, 208-233 (2008).
108 Derrien, M. *et al.* Mucin-bacterial interactions in the human oral cavity and digestive tract. *Gut microbes* **1**, 254-268 (2010).
109 Zuger, J., Luthi-Schaller, H. & Gmur, R. Uncultivated Tannerella BU045 and BU063 are slim segmented filamentous rods of high prevalence but low abundance in inflammatory disease-associated dental plaques. *Microbiology* **153**, 3809-3816 (2007).

110 Whittle, G., Hamburger, N., Shoemaker, N. B. & Salyers, A. A. A bacteroides conjugative transposon, CTnERL, can transfer a portion of itself by conjugation without excising from the chromosome. *Journal of bacteriology* **188**, 1169-1174 (2006).
111 Cappellini, E. *et al.* Proteomic analysis of a pleistocene mammoth femur reveals more than one hundred ancient bone proteins. *J Proteome Res* **11**, 917-926 (2012).
112 van Doorn, N. L., Wilson, J., Hollund, H., Soressi, M. & Collins, M. J. Site-specific deamidation of glutamine: a new marker of bone collagen deterioration. *RCM* **26**, 2319-2327, doi:10.1002/rcm.6351 (2012).